NATIONAL OPTICAL ASTRONOMY OBSERVATORIES

Preprint Series

NOAO Preprint No. 837

CEPHEID CALIBRATION OF THE PEAK BRIGHTNESS OF SNe Ia. IX. SN 1989B IN NGC 3627

A. SAHA
(National Optical Astronomy Observatories)

ALLAN SANDAGE
(The Observatories of the Carnegie Institution of Washington)

G.A. TAMMANN, LUKAS LABHARDT
(Astronomisches Institut der Universität Basel)

and

F.D. MACCHETTO, N. PANAGIA
(Space Telescope Science Institute)

To Appear In: The Astrophysical Journal

May 1999

Submitted to the Astrophysical Journal, Part I

Cepheid Calibration of the Peak Brightness of SNe Ia. IX. SN 1989B in NGC 3627[1]

A. Saha
National Optical Astronomy Observatories
950 North Cherry Ave., Tucson, AZ 85726

Allan Sandage
The Observatories of the Carnegie Institution of Washington
813 Santa Barbara Street, Pasadena, CA 91101

G.A. Tammann, Lukas Labhardt
Astronomisches Institut der Universität Basel
Venusstrasse 7, CH-4102 Binningen, Switzerland

and

F.D. Macchetto[2], N. Panagia[2]
Space Telescope Science Institute
3700 San Martin Drive, Baltimore, MD 21218

ABSTRACT

Repeated imaging observations have been made of NGC 3627 with the *Hubble Space Telescope* in 1997/98, over an interval of 58 days. Images were obtained on 12 epochs in the $F555W$ band and on five epochs in the $F814W$ band. The galaxy hosted the prototypical, "Branch normal", type Ia supernova SN 1989B. A total of 83 variables have been found, of which 68 are definite Cepheid variables with periods ranging from 75 days to 3.85 days. The de-reddened distance modulus is determined to be $(m - M)_0 = 30.22 \pm 0.12$ (internal uncertainty) using a subset of the Cepheid data whose reddening and error parameters are secure.

The photometric data of Wells et al. (1994), combined with the Cepheid data for NGC 3627 give $M_B(\max) = -19.36 \pm 0.18$ and $M_V(\max) = -19.34 \pm 0.16$ for SN 1989B. Combined with the previous six calibrations in this program, plus two additional calibrations determined by others gives the mean absolute magnitudes at

---

[1]Based on observations with the NASA/ESA *Hubble Space Telescope*, obtained at the Space Telescope Science Institute, operated by AURA, Inc. under NASA contract NAS5-26555.

[2]Affiliated to the Astrophysics Division, Space Sciences Deptartment of ESA.

maximum of $\langle M_B \rangle = -19.48 \pm 0.07$ and $\langle M_V \rangle = -19.48 \pm 0.07$ (Table 5) for "Branch normal" SNe Ia at this interim stage in the calibration program.

Using the argument by Wells et al. (1994) that SN 1989B here is virtually identical in decay rate and colors at maximum with SN 1980N in NGC 1316 in the Fornax cluster, and that such identity means nearly identical absolute magnitude, it follows that the difference in the distance modulus of NGC 3627 and NGC 1316 is 1.62 ± 0.03 mag. Thus the NGC 3627 modulus implies that $(m - M)_0 = 31.84$ for NGC 1316.

The second parameter correlations of $M(\max)$ of blue SNe Ia with decay rate, color at maximum, and Hubble type are re-investigated. The dependence of $\langle M(\max) \rangle$ on decay rate is non-linear, showing a minimum for decay rates between $1.0 < \Delta m_{15} < 1.6$. Magnitudes corrected for decay rate show no dependence on Hubble type, but a dependence on color remains. Correcting both the fiducial sample of 34 SNe Ia with decay-rate data and the current eight calibrating SNe Ia for the correlation with decay rate as well as color gives

$$H_0 = 60 \pm 2 \text{ (internal) km s}^{-1} \text{ Mpc}^{-1},$$

in both B and V. The same value to within 4% is obtained if only the SNe Ia in spirals (without second parameter corrections) are considered.

The correlation of SNe Ia color at maximum with $M(\max)$ cannot be due to internal absorption because the slope coefficients in B, V, and I with the change in magnitude are far from or even opposite to the canonical reddening values. The color effect must be intrinsic to the supernova physics. "Absorption" corrections of distant blue SNe Ia will lead to incorrect values of H_0.

The Cepheid distances used in this series are insensitive to metallicity differences (Sandage, Bell, & Tripicco 1999). The zeropoint of the P-L relation is based on an assumed LMC modulus of $(m - M)_0 = 18.50$. As this may have to be increased by $0\overset{m}{.}06$ to $0\overset{m}{.}08$, all distances in this paper will follow and H_0 will decrease by 3 – 4%.

Subject headings: Cepheids — distance scale — galaxies: individual (NGC 3627) — supernovae: individual (SN 1989B)

1. Introduction

This is the ninth paper of a series whose purpose is to obtain Cepheid distances to galaxies that have produced supernovae of type Ia (SNe Ia), thereby calibrating their absolute magnitudes at maximum light. The Hubble diagram for SNe Ia that are not abnormal in either their intrinsic colors or their spectra at maximum (Branch, Fisher, & Nugent 1993) is exceedingly tight (Sandage & Tammann 1993; Tammann & Sandage 1995; Saha et al. 1997 ; Parodi et al. 1999) even before second-order corrections for light curve decay rate or color (Hamuy et al. 1995, 1996a, b; Riess,

Press, & Kirshner 1996) are applied. Hence, the absolute magnitude calibrations lead directly to a good estimate of the global value of the Hubble constant because the SNe Ia Hubble diagram is defined at redshifts that are well beyond any local velocity anomalies in the Hubble flow.

The previous papers of this series concern Cepheids in IC 4182 for SN 1937C (Sandage et al. 1992, Paper I; Saha et al. 1994, Paper II), NGC 5253 for the two SNe Ia 1895B and 1972E (Sandage et al. 1994, Paper III; Saha et al. 1995, Paper IV), NGC 4536 for SN 1981B (Saha et al. 1996a, Paper V); NGC 4496A for SN 1960F (Saha et al. 1996b, Paper VI); NGC 4639 for SN 1990N (Sandage et al. 1996, Paper VII; Saha et al. 1997, Paper VIII).

The purpose of this paper is to set out the data for the discovery and photometry of Cepheids in NGC 3627, the parent galaxy of the type Ia SN 1989B. This case, together with the new SN Ia 1998bu in NGC 3368 for which Tanvir et al. (1995) have a Cepheid distance, and the new Cepheid distance of NGC 4414 (Turner et al. 1998), parent galaxy to SN 1974G, and the compilation of the extant photometric data on SN 1998bu (Suntzeff et al. 1998) and on SN 1974G (Schaefer 1998), now increase the number of SNe Ia calibrators from seven in Sandage et al. (1996) and Saha et al. (1997) to nine here. It will be recalled that we have used the absolute magnitude of SN 1989B in two previous discussions (Sandage et al. 1996; Saha et al. 1997) but based on the then unproven premise that the Tanvir et al. (1995) Cepheid distance to NGC 3368 would be the same as the distance to NGC 3627, as both galaxies are in the loose Leo association.

SN 1989B was discovered by visual inspection of NGC 3627 by Evans (1989) on January 30, 1989 which was 7 days before maximum light in B. A detailed light curve in $UBVRI$ and a determination of the reddening of $E(B-V) = 0\overset{m}{.}37 \pm 0\overset{m}{.}03$ was made by Wells et al. (1994), following the earlier analysis by Barbon et al. (1990). The magnitudes at maximum corrected for the extinction are $B(\max) = 10\overset{m}{.}86 \pm 0\overset{m}{.}13$ and $V(\max) = 10\overset{m}{.}88 \pm 0\overset{m}{.}10$.

The parent galaxy NGC 3627 (M 66) is one of the brightest spirals (Sb(s)II.2) in the complicated region of the Leo group, first isolated by Humason et al. (1956, Table XI) where 18 possible members were identified including NGC 3627 and NGC 3368 (M 96). Both galaxies are illustrated in the Hubble Atlas (Sandage 1961, panels 12 and 23), and the Carnegie Atlas (Sandage & Bedke 1994, Panels 118, 137, and S14).

De Vaucouleurs (1975) has divided the larger Leo group complex into three groups. G9 in his Table 3 is a spiral–dominated subgroup near NGC 3627 (M 66). His G11 is dominated by NGC 3368 (M 96), parent to SN 1998bu and contains NGC 3351, for which a Cepheid distance is also available (Graham et al. 1997). The agreement of the Cepheid distances of NGC 3368 and NGC 3351 to within $0\overset{m}{.}36 \pm 0\overset{m}{.}25$ is satisfactory. The smaller group G49 surrounds NGC 3607. The division into three subgroups is supported by the three-dimensional hierarchical clustering analysis of Materne (1978). A catalog of 52 possible members of the subgrouping in the field of NGC 3368, NGC 3379, and NGC 3384 is given by Ferguson & Sandage (1990).

Because of the complication of three subgroups rather than a well defined single group, we have never been totally convinced that the distance to NGC 3627, required to calibrate SN 1989B,

could be taken to be that of the Cepheids in NGC 3368 from Tanvir et al. (1995), although we analyzed our calibration data in Papers VII and VIII on that premise. This assumption is now no longer necessary with the discovery and analysis of Cepheids in NGC 3627.

Figure 1 shows a ground-based image of NGC 3627 made from the Mount Wilson 100-inch Hooker blue plate (E40) that was used in the Hubble Atlas and for one of the frames of the Carnegie Atlas. The position of the four WFPC2 chips of the *HST* is superposed to show our search area for the Cepheids. The position of SN 1989B is marked, taken from the photographs in Barbon et al. (1990).

Figure 2 is a color composite *HST* montage of stacked frames. The dust lanes are striking both here and in Fig. 1. The extinction clearly varies over short scales on the image. This forewarns about the importance of differential extinction to the Cepheids, requiring good color information for them to obtain a reliable true modulus. The extinction in NGC 3627 is more severe than in any galaxy of our six previous calibrations in Papers I–VIII of the series.

The journal of the *HST* observations and the photometry of the master template frame are in the next section. The identification and classification of the variables are in § 3. The apparent period-luminosity relations, the analysis of the severe absorption problem and how we have corrected for it, the resulting distance modulus, and the absolute magnitude at maximum for SN 1989B are in § 4. In § 5 we combine the data with our six previous calibrators, as well as SN 1974G in NGC 4414 and SN 1998bu in NGC 3368 from external sources. This paper provides a direct Cepheid distance to NGC 3627 and removes the uncertainty, thereby strengthening the weight of SN1989B in the overall calibration. A first value of H_0 is given. A discussion of the second-parameter corrections and their effect on H_0 is in the penultimate section § 6.

2. Observations and Photometry

2.1. The Data

Repeated images of the field in NGC 3627, shown in Fig. 2, were obtained using the WFPC2 (Holtzman et al. 1995a) on the *HST* between November 1997 and January 1998. There are 12 discrete epochs in the $F555W$ passband, and 5 epochs in the $F814W$ passband, spanning a period of 58 days. The duration of this period is constrained by the time window during which this target can be observed with *HST* without altering the field orientation. This window was further curtailed due to logistics for accommodating a campaign with the NICMOS camera, for which a change of the telescope focus was necessary, thus rendering the telescope useless for other kinds of observations.

The epochs were spaced strategically over this period to provide maximum leverage on detecting and finding periods of Cepheid variables over the period range 10 to 60 days. Each epoch in each filter was made of two sub-exposures taken back-to-back on successive orbits of the

spacecraft. This allows the removal of cosmic rays by an anti-coincidence technique. The images from various epochs were co-aligned to within 3–4 pixels on the scale of the PC chip, which is 1–2 pixels on the scale of the other three wide-field chips. The journal of observations is given in Table 1.

2.2. Photometry

The details of processing the images, combining the sub-exposures for each epoch while removing cosmic rays and performing the photometry with a variant of DoPHOT (Schechter et al. 1993) optimized for WFPC2 data has been given in Saha et al. (1996a) and need not be repeated here. The data reduction procedure is identical to that described in Paper V, with the one exception of a change in the definition of the "partial aperture". Instead of the 9×9 pixel aperture, a circular aperture of 5 pixel radius was used, and the local background is defined as the value for which the aperture growth curve is flat from 6 to 8 pixels. The details of these changes are given in Stetson et al. (1998) in their § 2.2. This change produces no known systematic differences, but improves the S/N with which aperture corrections are measured.

In keeping with the precepts in Paper V, the measurements in any one passband are expressed in the magnitude system defined by Holtzman et al. (1995b) that is native to the WFPC2. These are the $F555W$ and $F814W$ "ground system" magnitudes calibrated with HST "short" exposure frames. The issue of the discrepancy of the photometric zero-points for the "long" and "short" WFPC2 exposures, originally found by Stetson (1995) is described in some detail in Paper V. In any eventual accounting for this zero-point correction, one must *add* $0\overset{\mathrm{m}}{.}05$ in *both* passbands to the Holtzman et al. (1995b) calibration whenever the exposures are longer than several hundred seconds. The cause of this zero-point difference is not fully understood at the time of this writing, and, as in previous papers of this series, we continue to present the basic photometry (Tables 3 and 4) on the "uncorrected" Holtzman et al. (1995b) "short exposure" calibration. And, because all of our WFPC2 observations have exposure times that are "long", we make the $0\overset{\mathrm{m}}{.}05$ adjustment only at the resulting distance modulus of NGC 3627 (cf. § 4.2.2.). Correspondingly the distance moduli in Table 5 are corrected to the 'long' calibration scale by $0\overset{\mathrm{m}}{.}05$, except the moduli of IC 4182 and NGC 5253 which were observed with the older WF/PC.

3. Identification and Classification of the Variable Stars

Armed with measured magnitudes and their reported errors at all available epochs for each star in the object list, the method described by Saha & Hoessel (1990) was used to identify variable stars. The details specific to WFPC2 data have been given in various degrees of detail in Papers V, VI, and VIII.

All variable stars definitely identified are marked in Fig. 3. However, some of the identified

variables cannot be seen in Fig. 3 because of their extreme faintness and/or because of the large variation in surface brightness over the field. Hence, to complement these charts, we set out in Table 2 the X and Y pixel positions for all variable stars as they appear in the images identified in the *HST* data archive as U3510701R and U3510702R.

The photometry on the Holtzman et al. (1995b) "short exposure" calibration system for the final list of 83 variable stars is presented in Table 3 for each epoch and each filter. The periods were determined with the Lafler-Kinman algorithm (1965) by using only the $F555W$ passband data. Aliassing is not a serious problem for periods between 10 and 58 days because the observing strategy incorporated an optimum timing scheme as before in this series.

The resulting light curves in the $F555W$ passband, together with periods and mean magnitudes (determined by integrating the light curves, converted to intensities, and then converting the average back to magnitudes, and called the "phase-weighted intensity average" in Saha & Hoessel 1990), are shown in Fig. 4, plotted in the order of descending period.

Four objects, C2-V23, C2-V25, C2-V36, and C2-V37 are definitely variable but are unlikely to be Cepheids. They may be periodic with periods greater than the time spanned by our 12 epochs, or they may be transient variables such as novae. They are plotted in Fig. 4 with periods set artificially at 100 days (much larger than the observing time base of 58 days) for the purpose of visualization. Four obvious objects, C1-V1, C2-V38, C4-V3, and C4-V14 have periods that are just a little larger than the observing time base. Best guesses of the periods have been made from the light curve shapes. As the periods of these variables are not definitive, they should be used with caution in deriving distances. The remaining variables have light curves and periods that are consistent with being Cepheids.

The available data for the variables in $F814W$ were folded with the ephemerides derived above using the $F555W$ data. The results are plotted in Fig. 5. The long-period variables, transient variables, and long-period Cepheids (as discussed above) are shown with the same assigned ephemerides as in Fig. 4. Not all the variables discovered from the $F555W$ photometry were found in the $F814W$ images. The fainter variables, either because they are intrinsically faint or else appear faint due to high extinction, may not register clearly on the $F814W$ frames which do not reach as faint a limiting magnitude as those in $F555W$. Since photometry of such objects was obviously impossible in $F814W$, these variables are dropped from Fig. 5 and also from further analysis. Only the 68 variables from the $F555W$ frames that were recovered in at least one of the $F814W$ epochs are considered further.

The mean magnitudes in $F814W$ (integrated as intensities over the cycle) were obtained from the procedure of Labhardt, Sandage, & Tammann (1997) whereby each $F814W$ magnitude at a randomly sampled phase is converted to a mean value $\langle F814W \rangle$ using amplitude and phase information from the more complete $F555W$ light curves. Note that each available observation of $F814W$ can be used independently to derive a mean magnitude. Hence, the scatter of the individual values about the adopted mean $F814W$ value is an *external* measure of the uncertainty

in determining $\langle F814W \rangle$. This value is retained as the error in $\langle F814W \rangle$, and propagated in the later calculations.

The prescription given in Paper V for assigning the light-curve quality index QI (that ranges from 0 to 6) was used. In this scheme, two points are given for the quality of the $F555W$ light curves, two points for the evenness in phase coverage of the five $F814W$ observation epochs, and three points for the amplitude and phase coherence of the $F814W$ observations compared with the $F555W$ light curve. Hence, a quality index of 6 indicates the best possible light curve quality. A quality index of 2 or less indicates near fatal flaws such as apparent phase incoherence in the two passbands. This is generally the indication that object confusion by crowding and/or contamination by background is likely.

Table 4 lists the characteristics of the 68 objects whose light curves in $F555W$ are consistent with those of Cepheids, and for which an $F814W$ measurement exists for at least one epoch. The $F555W$ and $F814W$ instrumental magnitudes of Table 3 have been converted to the Johnson V and Cousins (Cape) I standard photometric system by the color equations used in Papers V to VIII of this series, as set out in equations (2) and (3) of Paper V, based on the transformations of Holtzman et al. (1995b).

The magnitude scatter $\sigma_{\langle V \rangle}$ in Table 4 is based on the estimated measuring errors in the photometry of the individual epochs. The determination of the scatter $\sigma_{\langle I \rangle}$ is described above. The quality index discussed above is also listed. Other columns of Table 4 are explained in the next section.

4. The Period-Luminosity Relation and the Distance Modulus

4.1. The P-L Diagrams in V and I

As in the previous papers of this series we adopt the P-L relation in V from Madore & Freedman (1991) as

$$M_V = -2.76 \log P - 1.40 , \quad (1)$$

whose companion relation in I is

$$M_I = -3.06 \log P - 1.81 . \quad (2)$$

The zeropoint of equations (1) and (2) is based on an adopted LMC modulus of 18.50.

The P-L relations in V and I for the 68 Cepheids in Table 4 are shown in Fig. 6. The filled circles show objects with periods between 20 and 58 days that have a quality index of 4 or higher. These are the best observed Cepheids. No selection based on color has been made here, hence the

total range of differential extinction values is contained in the data as plotted, explaining part of the large scatter.

The continuous line in each of the two panels shows equations (1) and (2) as the ridge-line relation using an apparent distance modulus of 30.2. The faint dashed upper and lower envelope lines indicate the expected scatter about the mean due to the intrinsic width of the Cepheid instability strip in the HR diagram (Sandage & Tammann 1968).

The large observed scatter of the data outside these envelope lines are due to the combination of (1) measuring and systematic errors due to background and contamination, (2) the random error of photon statistics, and (3) the large effects of the variable extinction evident from Fig. 2. Any modulus inferred directly from Fig. 6 would be unreliable. No matter how the lines defining the P-L strip are shifted vertically in the two panels of Fig. 6, a large fraction of the points of the total sample will remain outside the boundaries of the instability strip. Analysis of the scatter is the subject of the next two subsections.

4.2. Deriving the Distance Modulus

4.2.1. A Preliminary Analysis of the P-L Relation

Inspection of Fig. 6 reveals that the deviations from the ridge-lines in V and I of individual Cepheids are correlated. Stars that deviate faintward in V also generally deviate faintward in I and vice versa. This, of course, is a signature of variable extinction, but it can also be caused if the *systematic* measuring errors are correlated due, for example, to confusion or to errors in the compensation for background contamination that are not independent in the V and I passbands. To explore these possibilities and to correct for them we use the tools developed in Paper V and used again in Papers VII and VIII.

For each Cepheid we calculate the apparent distance moduli separately in V and in I from the P-L relations of equations (1) and (2) and the observed $\langle V \rangle$ and $\langle I \rangle$ magnitudes from Table 4. These apparent distance moduli, called U_V and U_I in columns (7) and (8) of Table 4, are calculated by

$$U_V = 2.76 \log P + 1.40 + \langle V \rangle , \tag{3}$$

and

$$U_I = 3.06 \log P + 1.81 + \langle I \rangle . \tag{4}$$

They are the same as equations (6) and (7) of Paper V.

If the differences between the V and I moduli are due solely to reddening, and if the dependence of the reddening curve on wavelength is the normal standard dependence as in the Galaxy, then the true modulus U_T is given by

$$U_T = U_V - R'_V \cdot (U_V - U_I) , \tag{5}$$

where R is the ratio of total to selective absorption, $A_V/E(V-I)$. This is equation (8) of Paper V. However, equation (5) is valid only if the difference between U_V and U_I is due to extinction, not to correlated measuring errors, in which case the value of R would *not* be given by the normal extinction curve where $A_V/A_I = 1.7$ and the ratio of absorption to reddening is $R'_V = A_V/E(V-I) = 2.43$ (Scheffler 1982). Such coupled errors clearly exist (based on Fig. 7 later where the slope of the U_V vs. U_I correlation is closer to 1 than to the required slope of $A_V/A_I = 1.7$ if the correlation were to be due entirely to differential extinction rather than to measuring errors). Hence, the interpretation of the values calculated from equations (3), (4), and (5) is considerably more complicated than would be the case in the absence of the correlated systematic measuring errors. Nevertheless, in the initial pass at the data to derive the true modulus, we use equations (3) to (5) as a first approximation. The second approximation, based on knowledge gained by the methods of this section, is in the next section 4.2.2.

The values of U_T are listed in column 9 of Table 4. These would be the true moduli, as corrected for normal extinction, assuming that there are no systematic measuring errors. The total rms uncertainty for each U_T value is listed in column 10. This uncertainty includes contributions from the estimated random measuring errors in the mean V and I magnitudes, (in columns 4 and 6), as propagated through the de-reddening procedure, as well as the uncertainty associated with the intrinsic width of the P-L relation, i.e. a given Cepheid may not be on the mean ridge-line of the P-L relation. The de-reddening procedure amplifies the measuring errors. Therefore many Cepheids are needed to beat down these large errors (notice the very large values in column 10) in any final value of the modulus. The values shown in column 10 of Table 4 were calculated using equations 9, 10 and 11 of Paper V, and correspond to σ^2_{tot} as defined in Paper V. However, note that equation (11) in Paper V should be :

$$\sigma^2_{width} = (R'_V - 1)^2 \cdot \rho^2_V + {R'_V}^2 \cdot \rho^2_I \, .$$

Our records show that while this equation was given incorrectly in Paper V, the calculations were done with the correct relation.

Various arithmetics done on the U_T values in column 9 of Table 4 give the first indication of the true modulus. Consider first all Cepheids of all quality indices, but excluding C1-13 and C3-V15 because of their extreme values of U_T. The 66 Cepheids in this sample give $\langle U_T \rangle = 29.90 \pm 0.08$ (the error estimate is based on the adopted rms of a single Cepheid of $0\overset{m}{.}646$). Restricting the sample to only those Cepheids with good to excellent data defined by a quality index of 4 or higher gives a subsample of 41 Cepheids for which $\langle U_T \rangle = 30.09 \pm 0.085$ (error based on an rms of $0\overset{m}{.}535$). Note that the 3-sigma upper and lower limits on the true modulus from this arithmetic are 30.34 and 29.83. These are therefore very strong upper and lower limits on the true distance modulus of NGC 3627.

These are the best values we can derive without making cuts in the data according to period, QI, and/or color that would select the bluest and least reddened, and that would be least affected by selection bias at the low-period end. We consider now such subsamples, first using cuts in

period and QI, but not yet in color which follows in the next section.

A plot of U_T vs. period (not shown) reveals a trend that objects with the shortest periods yield smaller U_T moduli. This result has been seen by us in the previously analyzed galaxies, and by other investigators analyzing similar data in yet other galaxies. It is due to a combination of selection bias at the short-period end (Sandage 1988) as well as non-symmetrical observational bias in measuring colors near the faint limit, skewing U_T via the color effect in equation (5). We note that this trend disappears once periods are restricted to longer than 25 days. We also note that the variation of U_T with Quality Index is not as acute for these data as we have seen in previous cases. A likely reason is that I magnitudes were obtained at five epochs, while in all except one of our previous papers fewer epochs were available. At any rate there is no compelling trend in U_T once the sample is restricted to objects with QI ≥ 3.

Using the sample of 27 Cepheids that have periods ≥ 25 days but shorter than the baseline of 58 days, and that have QI ≥ 3, and weighting the individual U_T values by $(1/\mathrm{rms})^2$, gives the mean de-reddened modulus of $(m - M)_0 = 30.04 \pm 0.12$. If we make more restrictive cuts by accepting only objects with QI ≥ 4, and then ≥ 5, and then 6, (with the same period cuts as above), we obtain respectively weighted mean "true" moduli of 29.99 ± 0.13, 30.10 ± 0.15, and 30.07 ± 0.18. This shows the general stability of the result. For the unweighted average of the 27 Cepheids we obtain $(m - M)_0 = 30.10 \pm 0.14$. Due to the fact that the P-L relations in V and I have non-negligible width at a constant period, a Cepheid that is *intrinsically* redder and fainter will, on the average, carry *larger* measuring errors. This can contribute to systematically underestimating the distance when individual U_T's are weighted as above. The unweighted solution is therefore preferred, since the uncertainties are similar.

We note again that the U_T values so derived depend on the assumption that the differences between U_V and U_I are due to reddening alone, in the absence of appreciable systematic and correlated measuring errors, or when the errors for $U_V - U_I$ *are distributed symmetrically.* If equation (5) is used for Cepheids *where correlated and/or asymmetrical errors in V and I dominate over differential reddening*, thereby producing a ratio of the V-to-I errors that is different from 2.43, the U_T derived via equation (5) *will be in error.*

In particular, several Cepheids which were discovered in V are too faint in I to be measured, as already mentioned. This introduces a selection effect that biases against Cepheids with bluer colors. The effect is most pronounced at short periods where the *intrinsic* colors are bluest. This effect gives an asymmetrical distribution of errors in $U_V - U_I$ in the sense that it makes the de-reddened modulus *too small.*

In Paper V we devised a method to test for the presence of differential extinction or for the fact that the scatter about the P-L relation is due predominantly to measuring errors, or a combination of both. The method, shown in Fig. 11 of Paper V for NGC 4536 and explained in the Appendix there, was used in Paper VI for NGC 4496A (Fig. 9 there) and in Paper VIII for NGC 4639 (Fig. 7 there). The method is to plot the difference in the apparent$V$ and I moduli for

any given Cepheid as ordinate against the apparent V modulus as abscissa. If there is a systematic trend of the data along a line of slope $dU_V/d(U_V - U_I) = 2.43$, then equation (5) applies and there is clearly differential reddening. If, on the other hand, there is a general scatter with no trend, that scatter is dominated by measuring errors. While in the latter case true differential extinction can be hidden by measuring errors, trying to correct for putative reddening will result in interpreting any asymmetry in the error distribution as specious extinction. In two of the three previous cases, NGC 4536 (Paper V), and NGC 4496A (Paper VI) there is no trend along a differential reddening line. In the third case of NGC 4639 (Paper VIII), there is a slight trend but also large scatter showing that the spread of points appears to be due to a mixture of measurement errors as well as from differential extinction.

The diagnostic diagram just described is shown for the NGC 3627 data from Table 4 in Fig. 7. The filled circles show Cepheids with periods between 25 and 58 days. The solid line indicates the reddening vector for the P-L ridge line, if the true (de-reddened) distance modulus is 30.05 which is close to the mean derived earlier in this section. The dashed lines show the bounds due to the intrinsic dispersion of the P-L relation as explained in Paper V. The slope of the lines is $A_V/E(V - I) = 2.43$ as before.

There is only marginal evidence from Fig. 7 for a general trend along the solid line. The spread of points clearly spills outside these bounds, indicating that a very significant fraction of the scatter is due to measuring errors and related biasses. If such errors are distributed symmetrically, equation (5) will yield the correct answer, but if there are correlated errors in V and I, or if there are selection effects that depend on color, using equation (5) will introduce errors. Note that the scatter of points is skewed along a direction orthogonal to the reddening vector: the lower right side appears to be more sparsely filled, indicating a possible selection effect. A more detailed inspection of the spread in Fig. 7 shows that the largest scatter occurs in the reddest Cepheids, using the $(\langle V\rangle - \langle I\rangle)$ colors computed from columns (3) and (5) of Table 4. This implies that the reddest Cepheids are so more because of skewed measurement errors than due to bona-fide reddening. This is not to deny the presence of differential reddening, but an acknowledgement that equation (5) alone is not adequate for obtaining a bias free result. We proceed by making an additional restriction of the data by color. Note that such a restriction used in conjunction with equation (5) does not introduce a procedural bias in the distance modulus.

4.2.2. The Distance Modulus By Restricting The Data By Color

A plot (not shown) of the color-period relation from the data in Table 4 shows a distinctive separation into two major color groups, one close to the intrinsic $(\langle V\rangle_0 - \langle I\rangle_0)$-period relation known for unreddened Cepheids in the Galaxy, LMC, and SMC as summarized in Sandage, Bell, & Tripicco (1999) from data by Dean, Warren, & Cousins (1978), Caldwell & Coulson (1985), and Fernie (1990). The other group of Cepheids with $(\langle V\rangle - \langle I\rangle)$ colors larger than 1.15 are far removed from the intrinsic domain in the color-period plot. They are also the Cepheids that show

the largest deviation faintward in the P-L relations of Fig. 6. Excluding these as the Cepheids with the largest reddening leaves a subsample of 29 Cepheids (the blue group) with $QI \geq 3$, and with $1.15 < \log P < 1.76$. We also have excluded C1-V13 because it is obviously an outlier. C1-V1, although blue, is excluded because its proposed period of 75 days is outside the baseline of 58 days.

Figure 8 shows again that differential reddening is not the major factor in the scatter of the P-L relation, where U_V is plotted vs. U_I for the 29 blue Cepheids of the subsample.

There is a clear correlation of U_V and U_I, but the slope is not $A_V/A_I = 1.7$ as required if the Cepheids below the ridge lines of Fig. 6 were fainter because of a larger differential extinction. Rather, the slope near 1 in Fig. 8 can only be due to *correlated measuring errors* as we suspected in the last section. Of course, a part of the correlation must also be due to reddening, if for no other reason than the obvious dust pattern in Fig. 1 and 2.

Figure 9 shows the P-L relations for the subset of the 29 bluest Cepheids. The scatter is markedly reduced from that in Fig. 6, showing that the color cut has produced a subset with the smallest extinction and/or measuring error.

We use the U_V and U_I apparent moduli in Table 4 calculated from equations (3) and (4) of § 4.2.1, and calculate mean values $\langle U_V \rangle$ and $\langle U_I \rangle$ using the 29 Cepheids of this subset. Assuming that the measuring errors for this sample are random and that they cancel in the mean permits the premise that the *difference* in the mean apparent moduli in the V and I passbands *is* now due to reddening. Multiplying the mean modulus difference by $A_V/E(V-I) = 2.43$ then gives A_V, which when subtracted from $\langle U_V \rangle$ gives the true modulus. This, of course, is what equation (5) does automatically, hence we need only analyze the U_T values in Table 4 for the 29 Cepheid subsample.

The weighted mean $\langle U_T \rangle_W$ for the subset of 29 Cepheids gives $\langle U_T \rangle = 30.12 \pm 0.11$. The individual U_T values are plotted vs. $\log P$ in Fig. 10. As noted in the last section and seen in Fig. 10, there is a tendency for the shortest period Cepheids to have the smallest individual moduli. Making the period cut at $\log P > 1.25$ removes the tendency and gives

$$\langle U_T \rangle_W = 30.17 \pm 0.12 \,, \tag{6}$$

as the weighted mean from the 25 Cepheids with $1.25 < logP < 1.78$, which we adopt. The unweighted mean is $\langle U_T \rangle = 30.24 \pm 0.09$.

Justification for our restriction to the subsample of 25 Cepheids is given in Fig. 11 which is the diagnostic diagram of Fig. 7 but using only this subsample. Plotted are again the individual apparent moduli U_V vs. the difference between the individual V and I apparent moduli.

Figure 11 is much cleaner than Fig. 7, and the data points now scatter nearly symmetrically about the differential reddening line.

Applying, as in previous papers of this series, the correction for the "long" vs. "short"

exposure effect of $0^m.05$ to equation (6), the de-reddened modulus of NGC 3627 is

$$(m - M)_0 = 30.22 \pm 0.12 \ , \tag{7}$$

which we adopt.

5. The Absolute Magnitude at Maximum of SN 1989B Added to Previous Calibrators; the Present Status of the Calibration

The light curves in the *UBVRI* passbands of SN 1989B are well determined near maximum light, giving $B_{\rm max} = 12.34 \pm 0.05$, and $V_{\rm max} = 11.99 \pm 0.05$ (Wells et al. 1994). These authors have also determined the reddening of SN 1989B itself to be $E(B-V) = 0.37 \pm 0.03$. Hence, the de-reddened magnitudes at maximum light are $B^0_{\rm max} = 10.86 \pm 0.13$ and $V^0_{\rm max} = 10.88 \pm 0.10$. The absolute magnitudes at maximum for SN 1989B are

$$M^0_B(\max) = -19.36 \pm 0.18 \ , \tag{8}$$

and

$$M^0_V(\max) = -19.34 \pm 0.16 \ , \tag{9}$$

based on equation (7) and on the Cepheid zero points of equations (1) and (2).

These values are combined in Table 5 with our previous calibrations of the six SNe Ia from Papers I–VII of this series. In addition, two new values are included from data for SN 1974G in NGC 4414 (Turner et al. 1998; Schaefer 1998), and SN 1998bu in NGC 3368 (M 96) whose distance modulus is by Tanvir et al. (1995) with photometry of the SN reported by Suntzeff et al. (1998). All Cepheid distances from the WFPC2 are corrected by $0^m.05$ for the short vs. long exposure photometric zeropoint difference (Stetson 1995; Saha et al. 1996a).

Neglecting the listed M_B of SN 1895B, which is the most uncertain of the group, and because it is not absolutely certain whether it was spectroscopically normal at all phases, gives the straight mean values of $\langle M_B \rangle = -19.49 \pm 0.03$ and $\langle M_V \rangle = -19.49 \pm 0.03$. We adopt the *weighted* means, giving the mean calibration without any second parameter corrections for decay rate (see § 7) as

$$\langle M_B(\max) \rangle = -19.49 \pm 0.07 \ , \tag{10}$$

and

$$\langle M_V(\max) \rangle = -19.48 \pm 0.07 \tag{11}$$

on the Cepheid distance scale of equations (1) and (2). Inclusion of SN 1895B would give $\langle M_B \rangle = -19.54 \pm 0.06$ for the straight mean and $\langle M_B \rangle = -19.52 \pm 0.07$ for the weighted mean.

We have been criticized for using calibrators such as SN 1960F and SN 1974G, for which the photometry is more uncertain than others. We should point out that the net worth is not

just the uncertainty in the photometry of the supernova, but the combined uncertainty with that of the Cepheid distance determination. Given the range of uncertainties in the Cepheid distance determinations (which depend on distance/faintness, crowding, etc), even photometric uncertainties considerably worse than for SN 1960F can be tolerated if the Cepheid determinations are as good as they are for its host galaxy NGC 4496A. In addition, we weight the contribution of individual calibrators by the inverse variance from the combined uncertainty of distance and supernova photometry, a procedure consistent with Bayesian inference. Thus even bona-fide 'poor' cases like SN 1974G (which has also a relatively poor Cepheid distance to its host galaxy NGC 4414), enter only with appropriately lowered weight.

Equations (10) and (11), based now on eight calibrators (neglecting SN 1895B), are similar to equations (12) and (13) of Paper VIII (Saha et al. 1997) based there on six calibrators (again neglecting SN 1895B). Equation (10) here is $0\overset{m}{.}03$ fainter than in Paper VIII. Equation (11) here is identical with that of Paper VIII. Because of the similarity of the equations (10) and (11) here with equations (12) and (13) in Paper VIII, the interim value of the Hubble constant, sans decay-rate corrections, for this stage of our *HST* experiment is nearly identical with the values set out in Table 7 of Paper VIII. The means of all values in that table, depending on how the SNe Ia Hubble diagram is divided between *spirals* observed before and after 1985, and/or with redshifts larger or smaller than $\log v_{220} = 3.8$, and using equation (10) here rather than equation (12) of Paper VIII, are then

$$\langle H_0(B) \rangle = 58 \pm 2 \ \text{(internal)} \, \text{km} \ \text{s}^{-1} \ \text{Mpc}^{-1} \ , \tag{12}$$

and

$$\langle H_0(V) \rangle = 59 \pm 2 \ \text{(internal)} \, \text{km} \ \text{s}^{-1} \ \text{Mpc}^{-1} \ . \tag{13}$$

6. The Hubble Diagram of SNe Ia and the Value of H_0 if Second Parameter Corrections are Made

The Hubble diagram for blue SNe Ia with $(B_{\rm max} - V_{\rm max}) < 0.20$, based on many sources, historical as well as modern, was given in Paper VIII (Saha et al. 1997, Fig. 10). When calibrated with the SNe absolute magnitudes, this diagram gives the Hubble constant directly. The details of the sample are being published in a paper by Parodi et al. (1999), and we make use of these data in this section to calibrate again correlations of absolute magnitudes of SNe Ia with the often adopted second parameters of decay rate of the light curve, color of the SNe at maximum, and galaxy type.

The precept adopted in the early papers of this series was that by restricting both our calibrator SNe Ia and the Hubble diagram of SNe Ia to "Branch normal" events (Branch, Fisher, & Nugent 1993), we have selected a homogeneous sample of SNe Ia for which any systematic variation of absolute magnitude among the sample will be small enough to be neglected to first order at the 10% level (Cadonau et al. 1985; Leibundgut et al. 1991b; Sandage & Tammann

1993; Tammann & Sandage 1995). In the meantime, thanks to the observational program of the Calan/Tololo Chilean consortium (Hamuy et al. 1995; 1996a, b) and the theoretical insights of variations in the pre-explosion conditions of the progenitors (cf. von Hippel et al. 1997, Höflich 1998, Nadyozhin 1998 for summaries), it has become clear that there is in fact a *continuous* variation of SNe Ia properties, including absolute magnitude, that can be detected from observed second- parameter properties and which can now be accounted for even at this $< 10\%$ level.

The most apparent of these second parameters is the change in the shape of the light curve, quantified by the rate of decay from maximum light (Rust 1974; de Vaucouleurs & Pence 1976; Pskovskii 1977, 1984; Phillips et al. 1987; Barbon et al. 1990; Branch, & Tammann 1992; Hamuy et al. 1996a, b). Phillips (1993) derived a very steep relation between decay rate and absolute magnitude using distances determined by a variety of methods and including also very red SNe Ia. A much flatter dependence was found by Tammann & Sandage (1995) for blue SNe Ia using more reliable relative distances from recession velocities. The flatter slope was confirmed for only the blue SNe Ia by the subsequent extensive Calan/Tololo data (Hamuy et al. 1996a, b; Saha et al. 1997).

A detailed discussion of the second order corrections to the SNe Ia distance scale depending on second and third parameter correlations is the subject of the accompanying paper by Parodi et al. (1999) where it is shown that besides the decay rate, color at maximum is also a principal second parameter, confirming a similar result by Tripp (1998).

The Parodi et al. paper lists relative kinematic absolute magnitudes as if the local Hubble redshift-to-distance ratio is the same for redshifts smaller than $10,000\,\mathrm{km\ s^{-1}}$ as for the remote H_0 for $v > 10,000\,\mathrm{km\ s^{-1}}$, neglecting the evidence set out in Paper VIII (Saha et al. 1997, § 8; cf. also Zehavi et al. 1998) that the local value may be 5% to 10% larger than the global value.

This possible change of the Hubble ratio outward, decreasing with distance by $\leq 10\%$ for v out to $10,000\,\mathrm{km\ s^{-1}}$, is also consistent with other external data on first ranked cluster galaxies (Lauer & Postman 1994; Tammann 1998a). The suggestion is also consistent with the derived shallow slope of $d\log v/dm = 0.192$ of the local ($v < 10,000\,\mathrm{km\ s^{-1}}$) Hubble diagram by Parodi et al. (1999, their eqs. 7 and 8) rather than 0.200 required if H_0 did not vary with distance.

In the analysis of this section we consider the consequences of a variable H_0 decreasing outward, that is required to give a slope of 0.192 to the Hubble diagram locally, and then carry again the analysis of the second parameter effects of decay rate, color, and galaxy type using the derived kinematic absolute magnitudes.

6.1. Kinematic Absolute Magnitudes Using a Variable Hubble Constant with Local Distance for $v < 10,000\,\mathrm{km\ s^{-1}}$

We accept the premise that the slope of the Hubble diagram for redshifts smaller than $10,000\,\mathrm{km\ s^{-1}}$ is 0.192 (Parodi et al. 1999). If we adopt an arbitrary global (remote field) value of $H_0 = 55$ (to be adjusted later by our calibrators in Table 5), then, by an obvious calculation, the variation of H_0 in the distance interval of $1000 < v < 10,000$ is well approximated (within 1%) by

$$H_0(v) = -5.39 \log v + 76.50\ . \tag{14}$$

This gives $H_0 = 60.3$ at $v = 1000\,\mathrm{km\ s^{-1}}$ and $H_0 = 54.9$ at $v = 10,000\,\mathrm{km\ s^{-1}}$.

Equation (14) has been used to recalculate the absolute magnitudes of all SNe Ia in the fiducial sample in Table 1 of Parodi et al. (1999) for which $\log v < 4.00$. $H_o = 55$ has been assumed for $\log v > 4.00$. The results are set out in Table 6 which is divided into three parts according to Hubble type to better understand the type dependence of the Hubble diagram seen in Fig. 10 of Paper VIII (Saha et al. 1997). The first section of Table 6 lists the SNe in late type spirals (T of 3 and greater, meaning Sb to Im types). The second section for $T = 1$ and 2 are for Sa and Sab parent galaxies. The third section lists parent galaxy T types of 0 and smaller (E and S0).

Columns (1) through (6) repeat data from Table 1 of Parodi et al. (1999) with magnitudes at the respective maxima denoted by B_0, V_0, and I_0. The redshifts in column (3) are corrected for peculiar motions. For $v < 3000\,\mathrm{km\ s^{-1}}$ the redshifts, reduced to the frame of the centroid of the Local Group (Yahil, Tammann, & Sandage 1977), were then corrected again to the frame of the Virgo cluster using the self-consistent Virgocentric infall model with the local infall vector (actually retarded expansion of the Local Group relative to Virgo) of $220\,\mathrm{km\ s^{-1}}$ (Kraan-Korteweg 1986a, b). For $v > 3000\,\mathrm{km\ s^{-1}}$ an additional correction of $630\,\mathrm{km\ s^{-1}}$ relative to the CMB frame due to the CMB dipole anisotropy (Boughn et al. 1981; Wilkinson 1984) was applied according to the model of Tammann & Sandage (1985, their Fig. 2). For more distant galaxies we have adopted the corrected velocities from Hamuy et al. (1996a). The sources for the photometry in columns (4) to (6) are listed in Parodi et al. (1999). The magnitudes are corrected for Galactic absorption (Burstein & Heiles 1984).

Column (7) is the adopted local value of H_0 calculated from equation (14) for $\log v < 4.00$, and using $H_0 = 55$ for larger redshifts. The resulting distance moduli are in column (8). The corresponding absolute magnitudes are in columns (9) to (11). The decay rates $\Delta m_{15}(B)$ in column (12) are from the sources listed by Parodi et al. (1999).

The data for the eight calibrators in Table 5, except for the observed apparent magnitudes, are not shown in Table 6 because their absolute distance moduli are on the Cepheid system, not based on redshifts.

The means of columns (9) to (11) for the absolute magnitudes in B, V, and I are shown at the foot of each of the three sections of Table 6. The systematic progression, becoming fainter for

the earlier galaxy types, is evident and is significant at the 2-sigma level. It is this difference that causes the separation of the ridge lines in the Hubble diagram of spirals and E and S0 galaxies seen in Fig. 10 of Saha et al. (1997).

However, this is not a type dependence per se. Note in column 12 that the mean decay rates, shown at the foot of each section, differ significantly between the three sections of Table 6. The decay rates are much longer for the E to S0 types, averaging $\langle \Delta m_{15}(B) \rangle = 1.44 \pm 0.04$ for these early Hubble types, compared with $\langle \Delta m_{15}(B) \rangle = 1.03 \pm 0.03$ for the spirals in the first section of Table 6.

Because the decay rate itself is correlated with absolute magnitude (next section), the *apparent* dependence of $\langle M(\mathrm{max}) \rangle$ on Hubble type is in fact due to the decay rate correlation. This, of course, is a clue as to differences in the progenitor mass of the pre-SNe Ia as a function of Hubble type, and goes to the heart of the physics of the phenomenon (eg. Nadyozhin 1998). In any case, the apparent correlation of $\langle M \rangle$ with Hubble type disappears when the decay rate corrections of the next section are applied.

Said differently, the *apparent* dependence of mean absolute magnitude with Hubble type is due to the difference in mean decay rate between early type galaxies (E to S0 types) and late type spirals (the first section of Table 6), together with the dependence of decay rate on absolute magnitude at maximum (Fig. 12 in the next section).

6.2. The Decay Rate Dependence

The absolute magnitudes in columns (9) to (11) of Table 6 are plotted in Fig. 12. It is clear that there is a relation of decay rate with (kinematic) absolute magnitude (Phillips 1993), but that the relation is strongly non-linear. There is a clear plateau between abscissa values of decay rates that are greater and smaller than 1.0 to 1.5. In this plateau region, the absolute magnitude is nearly independent of the decay rate.

Figure 12 shows the correlations of columns (9), (10), and (11) (of Table 6) with the decay rate in column (12). The correlation with absolute magnitude for small and for large $\Delta m_{15}(B)$ is obvious. Nevertheless, the correlation is clearly non-linear. There is a central region ($1.0 < \Delta m_{15}(B) < 1.5$) where the correlation is weak. This is the core of the "Branch normal" majority of SNe Ia, comprising 95% of the observed SNe Ia (only 1 in 20 of the local SNe Ia discoveries are "Branch abnormal"; see Branch, Fisher, & Nugent 1993). It is only when the few known abnormal SNe Ia are added to the "Branch normal", i.e. blue SNe Ia, that they show a wide variation in luminosity.

Consider now the apparent correlation of $\langle M_{\mathrm{max}} \rangle$ with Hubble type, shown in Fig. 10 of Saha et al. (1997, Paper VIII). It is of central physical interest how the Hubble type of the parent galaxy can produce slow-decay rate SNe Ia in E galaxies, and faster-decay rate SNe Ia in

later-type galaxies. One supposes that the mass of the pre-SNe Ia stars must be a function of chemical evolution in any given parent galaxy, causing the change in the character of the SNe Ia explosion with Hubble type (Nadyozhin 1998). Nevertheless, this is an astrophysical problem, not an astronomical problem of how to use the data to determine reliable distances. It suffices here to note that the type dependence on $\langle M_{\rm max} \rangle$ disappears when the correction, now described for decay rate (Fig. 12), is applied.

The correlation of decay rate $\Delta m_{15}(B)$ with absolute magnitudes in B, V, and I in Fig. 12 is striking, confirming Pskovskii's (1977, 1984) initial suggestions. But again, the correlations are much less steep than suggested by Phillips (1993) and by Hamuy et al. (1996b, their Fig. 2), especially in the region of the "Branch normal" SNe Ia with $0.95 < \Delta m_{15}(B) < 1.3$ where there is no strong correlation.

Hamuy et al. (1994a) distinguish between the slope of the decay-rate correlation with $M(\max)$ obtained from using TF, PN and SBF distances to nearby SNe Ia (as originally done by Phillips 1993), versus that from using relative distances from redshifts at intermediate distances. The latter sample gives a shallower slope than that of Phillips. By restricting to a Branch normal sample, the slope is further reduced.

In Fig. 12 we have fitted cubic polynomials to the data contained in Table 6 for the correlations of absolute magnitudes in B, V, and I in columns (9) to (11) with $\Delta m(B)_{15}$ in column (12). Denote the correction to M_i for decay rate by y_i, such that the "corrected" absolute magnitude, reduced to $\Delta m_{15}(B) = 1.1$, is defined by

$$M_i^{15} = M_i(\text{ Table 6}) - y_i \ .$$

The correlations in Fig. 12, based on the decay-rate data and absolute magnitude data in Table 6, give the following cubic corrections for decay rate vs. absolute magnitude in B, V, and I. The lines drawn in Fig. 12 are calculated from these equations. We reduce all data to $\Delta m_{15}(B) = 1.1$, and therefore define $x = \Delta m_{15}(B) - 1.1$.

$$y_B = 0.693x - 1.440x^2 + 3.045x^3, \tag{15}$$

$$y_V = 0.596x - 2.457x^2 + 4.493x^3, \tag{16}$$

$$y_I = 0.360x - 2.246x^2 + 4.764x^3. \tag{17}$$

Note that these polynomials are not well constrained outside the range of $\Delta m(B)_{15}$ spanned by the SNe Ia in this sample. In particular, the upturn for very slow declining SNe Ia is uncertain. However, the cubic characterization given here is adequate for the present arguments and calculations: it is not used in a region where it is ill constrained.

The corrections for decay rate, y_i, from equations (15) to (17), have been applied to columns (9) to (11) of Table 6 to obtain absolute magnitudes freed from the $\Delta m(B)_{15}$ parameter effect. The arithmetic is not shown but the mean corrected magnitudes $\langle M_i^{15} \rangle$, still binned into the three

morphological groups of Table 6 are listed in the first four lines of Table 7. The corresponding mean magnitudes $\langle M_B^{15} \rangle$ and $\langle M_V^{15} \rangle$ of the eight calibrators from Table 5 are shown in the last line. No mean value$\langle M_I^{15} \rangle$row is shown in the last line because too few calibrators have known $I_{\max}$.

Table 7 permits two conclusions:

(1) The type dependence shown in Fig. 10 of Paper VIII between E galaxies and spirals has now disappeared to within one sigma differences after the Δm_{15} corrections are applied.

(2) Comparing the $\langle M_B^{15} \rangle$ and $\langle M_V^{15} \rangle$ values in the fourth line (the total sample) with the corrected values of the calibrators in the fifth line shows the statistical difference of $0\overset{\mathrm{m}}{.}14 \pm 0\overset{\mathrm{m}}{.}058$ in B and $0\overset{\mathrm{m}}{.}15 \pm 0\overset{\mathrm{m}}{.}076$ in V between the fiducial sample and the Table 5 calibrators. Because the absolute magnitudes of the fiducial sample are based on $H_0 = 55$, these data, corrected for decay rate, give

$$H_0(B)(\text{ decay rate}) = 58.8 \pm 2\,\text{km s}^{-1}\ \text{Mpc}^{-1}\,, \tag{18}$$

and

$$H_0(V)(\text{ decay rate}) = 59.1 \pm 2\,\text{km s}^{-1}\ \text{Mpc}^{-1}\,. \tag{19}$$

It is shown in Parodi et al. (1999), that the effect of the decline rate correction taken alone, is to increase H_0 by 7%. This correction depends on the extent to which the decline rate distribution is different for the calibrating and distant samples of SNe Ia.

6.3. The Color Dependence

Figure 13 shows that there is still a dependence of the corrected M_i^{15} magnitudes on color that is not removed by the Δm_{15} corrections, contrary to the removal of the dependence on Hubble type. The symbols are the same as in Fig. 12.

The ordinates are the kinematic ($H_0 = 55$) absolute magnitudes, M_i^{15}, based on variable local values of H_0 and the decay rate corrections from the last subsection. The abscissa is the observed $(B_0 - V_0)$ color that can be derived from columns (4) and (5) of Table 6.

The equations for the least squares solutions for the lines are,

$$M_B^{15} = 1.712 \cdot (B_0 - V_0) - 19.648\,, \tag{20}$$

$$M_V^{15} = 0.587 \cdot (B_0 - V_0) - 19.562\,, \tag{21}$$

and

$$M_I^{15} = -0.216 \cdot (B_0 - V_0) - 19.312\,. \tag{22}$$

Figure 14 is the same as Fig. 13 but with $(V_0 - I_0)$ colors derived from columns (10) and (11) of Table 6. The least squares solutions for the lines are

$$M_B^{15} = 0.257 \cdot (V_0 - I_0) - 19.540\,, \tag{23}$$

$$M_V^{15} = -0.260 \cdot (V_0 - I_0) - 19.621\,, \tag{24}$$

and

$$M_I^{15} = -1.115 \cdot (V_0 - I_0) - 19.607\,. \tag{25}$$

The immediate consequence of equations (20) to (25) is that these color dependencies *are not due to reddening and absorption* because the slope coefficients in B and V, nor their ratios, conform to the canonical normal interstellar values of $A_B/E(B-V) = 4$, $A_V/E(B-V) = 3$, and $A_I/E(B-V) = 1.76$, and $A_B/E(V-I) = 3.2$, $A_V/E(V-I) = 2.4$, and $A_I/E(V-I) = 1.4$ (Scheffler 1982). If, for example, the variation of absolute magnitude with color index from SN to SN were due entirely to absorption and reddening, then the slope coefficients in the correlations of Fig. 13, (Eqs. 20 to 22) would have to be $dM_B/E(B-V) = 4$, $dM_V/E(B-V) = 3$, and $dM_I/E(B-V) = 1.76$, based on $A_V/A_I = 1.7$. Not only are the coefficients for B and V in equations (20) and (21) very different from these requirements for reddening, but even the sign of the variation in I with $(B-V)$ is negative. This is impossible if the cause is internal reddening with its corresponding dimming.

The situation is even more decisive from equations (23) to (25) using $(V-I)$ colors in Fig. 14. From E(V-I)/E(B-V) = 1.25 (Eq. 1 of Dean, Warren, & Cousins 1978), the predictions are $dM_B/E(V-I) = 3.2$, $dM_V/E(V-I) = 2.4$, and $dM_I/E(V-I) = 1.41$. These are not only far different from the coefficients in equations (23) to (25), but again the sense of the observed correlation in equations (24) and (25) belies a reddening/extinction explanation. *Brighter* magnitudes for redder colors are not possible for any known reddening and absorption law.

The conclusion is that the correlations in Figs. 13 and 14 are due to intrinsic properties internal to the physics of the SNe themselves rather than to reddening and absorption. Hence, any corrections to the absolute magnitudes based solely on assumed absorption-to-reddening ratios for normal extinction are most likely to be incorrect.

Nevertheless, the correlations in Figs. 13 and 14 are definite, and can be used to further reduce the absolute magnitudes to some fiducial value of observed color. We thus reduce to a fiducial color of $(B_0 - V_0) = 0.00$ as a second parameter, in addition to the decay-rate parameter, in agreement with Tripp (1998).

Our approach is different in principle from that of Phillips et al. (1999), where they assert that the color range at given decline rate is due to reddening, and proceed accordingly. Our conclusion from the above analysis is that for our sample of SNe Ia, with $(B_{\rm max} - V_{\rm max}) < 0.20$, the color spread at given decline rate is intrinsic in nature, since correlation of the peak brightness with the residual color for this sample is different from what is expected from reddening.

Applying the color-term corrections of equations (20) and (21) to the M_B and M_V magnitudes of Table 6, and taking the mean values over the complete sample of 34 SNe Ia in Table 6 where the decay rates are known, gives

$$\langle M_B^{\rm corr}\rangle = \langle M_B^{15} + \text{ color term}\rangle = -19.64 \pm 0.026\,, \tag{26}$$

and

$$\langle M_V^{\rm corr}\rangle = \langle M_V^{15} + \text{ color term}\rangle = -19.61 \pm 0.026\,. \tag{27}$$

These magnitudes are calculated with variable H_0 following the precepts of §6.1 and reduced to $\Delta m_{15} = 1.1$ and $(B_0 - V_0) = 0.00$.

For the calibrators in Table 5 one finds in analogy

$$\langle M_B^{\rm corr}\rangle = -19.45 \pm 0.060\,, \tag{28}$$

and

$$\langle M_V^{corr}\rangle = -19.44 \pm 0.079\,. \tag{29}$$

Comparison of equations (28) and (29) with equations (26) and (27) shows that the $H_0 = 55$ assumption must be changed to accommodate the differences of $0\overset{\rm m}{.}19 \pm 0\overset{\rm m}{.}08$ in B and $0\overset{\rm m}{.}17 \pm 0\overset{\rm m}{.}09$ in V. They require the global value of H_0, now fully corrected for the three effects of (1) the change of H_0 outward, (2) the light curve decay rate, and (3) the color variation with $M(\max)$, to be

$$H_0(B) = 60.2 \pm 2\,\text{km s}^{-1}\ \text{Mpc}^{-1}\,, \tag{30}$$

and

$$H_0(V) = 59.6 \pm 2\,\text{km s}^{-1}\ \text{Mpc}^{-1}\,. \tag{31}$$

These values are only 2% higher than equations (18) and (19) which use only the decay-rate correction, and 1% to 4% higher than equations (12) and (13) which are weighted towards SNe Ia in spirals.

Other authors have adopted $\langle M(\max)\rangle$ values that differ from those in equations (10) and (11) for the calibrator absolute magnitudes. For example, Kennicutt, Mould, & Freedman (1998), and Freedman (1999) have discarded several of our calibrators, and added two that are not based on direct Cepheid distances to the host galaxy. They have consequently derived a fainter mean absolute B magnitude than in equation (10). Specifically, they assume that the distances of the early-type galaxies NGC 1316 and NGC 1380 in the Fornax cluster, parent galaxies to SN 1980N and SN 1992A, are identical with that of the spiral NGC 1365 for which there is a Cepheid distance. Suntzeff et al. (1998) have also considered the questionable SN 1980 and SN 1992A as possible calibrators.

However, there are reasons to suspect that NGC 1365 is in the foreground of the Fornax cluster (Sandage, Tammann, & Saha 1999), and therefore that the precept of the fainter calibration used by Kennicutt, Mould, & Freedman (1998), calibrating the two Fornax SNe Ia via NGC 1365,

is not correct. The evidence is that Wells et al. (1994) have demonstrated that the multi-color light curves of SN 1989B in NGC 3627 and SN 1980N in NGC 1316 are virtually identical, and in fact establish the reddening and extinction to SN 1989B by comparing the magnitude shifts in different passbands relative to SN 1980N. Asserting then that SN 1980N has the same peak brightness as SN 1989B yields the distance modulus difference of $1\overset{m}{.}62 \pm 0\overset{m}{.}03$ (Wells et al. 1994). There is additional uncertainty of ± 0.17 to allow for scatter in the difference in peak brightness of two SNe Ia with the same decline rate. With our modulus of $(m - M)_0 = 30.22 \pm 0.12$ (Eq. 7) for SN 1989B, the derived modulus of NGC 1316, host to SN 1980N, is 31.84 ± 0.21. This is $0\overset{m}{.}5$ more distant than the Cepheid distance of NGC 1365 (Madore et al. 1998), but is close to the value found for the early-type galaxies of the Fornax cluster by independent methods (Tammann 1998b). In any case the implication of Kennicutt, Mould, & Freedman (1998) and Freedman (1999) that the two SNe Ia 1989B and 1980N differ by $0\overset{m}{.}5$ in luminosity, which is based on the unproved assertion that NGC 1365 and NGC 1316 are at the same distance, is not credible.

The further consequence of the precept of equating the Cepheid distance of NGC 1365 to that of the unknown distance to NGC 1316 and NGC 1380 is that the decay-rate absolute magnitude relation which Freedman (1999) deduce using their faint absolute magnitudes of the two Fornax SNe Ia is steeper than that in Fig. 12 by an amount that compromises their conclusions concerning H_0, explaining their abnormally high value of $H_0 \approx 73$.

7. Summary and Conclusions

(1) Comparison of 12 epoch *HST* frames in the $F555W$ band and five epoch frames in the $F814W$ band has isolated 68 definite Cepheid variables with periods between 3 and ~ 75 days in the dust-rich galaxy NGC 3627 in the Leo Group.

(2) The adopted true modulus of $(m - M)_0 = 30.22 \pm 0.12$ that results from analysis of various subsamples of the data according to the degree of internal absorption, agrees well with the distance moduli of $(m - M)_0 = 30.37 \pm 0.16$ for NGC 3368 (parent of SN 1998bu) (Tanvir et al. 1995) and $(m - M)_0 = 30.01 \pm 0.19$ for NGC 3351 (Graham et al. 1997), showing that the extended Leo Group in fact exists (Humason et al. 1956, Table XI).

(3) Combining the NGC 3627 Cepheid modulus of $(m - M)_0 = 30.22$ with the photometry of Wells et al. (1994) for the daughter SN Ia SN 1989B (corrected for extinction) gives the absolute magnitudes in B and V at maximum light of $M_B = -19.36 \pm 0.18$, and $M_V = -19.34 \pm 0.16$ for SN 1989B as listed in Table 5.

(4) Combining these absolute magnitudes with those for the previous six calibrators determined in previous papers of this series, and with two additional calibrators recently available (SN 1974G in NGC 4414 and SN 1998bu in NGC 3369), gives a mean calibration (without second parameter corrections) of $\langle M_B \rangle = -19.49 \pm 0.07$ and $\langle M_V \rangle = -19.48 \pm 0.07$.

(5) The absolute magnitudes $M_{\rm max}$ of blue SNe Ia with $(B_0 - V_0) < 0.20$ correlate with the light curve decay rate Δm_{15}. The correlation is approximated by a cubic equation which has a flat plateau at intermediate values of Δm_{15}. In addition, $M_{\rm max}$ depends on the color $(B_0 - V_0)$. For the derivation of the dependence on these second parameters, a slight decrease of H_0 out to $10,000\,{\rm km\ s^{-1}}$ has been taken into account. Once corrections for these two second parameters are applied, no residual dependence of $M_{\rm max}$ on Hubble type is seen.

(6) The calibrators have somewhat smaller mean values of Δm_{15} and bluer mean colors $(B_0 - V_0)$ than the distant SNe Ia defining the Hubble diagram. The application of second parameter corrections therefore tends to increase H_0, but the effect is less than 10%.

(7) The overall value of the Hubble constant determined here from the current eight calibrators as applied to the distant SNe Ia with $1000\,{\rm km\ s^{-1}} < v < 30,000\,{\rm km\ s^{-1}}$ is $H_0 = 60 \pm 2$ in both B and V (Eqs. 30 and 31).

(8) The Hubble constant derived here rests on Cepheid distances whose zeropoint is set to an LMC modulus of 18.50. If the latter is revised upwards by $\approx 0\overset{\rm m}{.}06$ (Federspiel, Tammann, & Sandage 1998), the consequent value of the Hubble constant is

$$H_0 = 58 \pm 2\,{\rm km\ s^{-1}\ Mpc^{-1}}\,. \tag{32}$$

Acknowledgment

We thank the many individuals at STScI who worked hard behind the scenes to make these observations possible, and wish to particularly mention Doug van Orsow, George Chapman, Bill Workman, Merle Reinhardt and Wayne Kinzel. A.S. and A.S. acknowledge support from NASA through grant GO-5427.02-93A from the Space Telescope Science Institute, which is operated by the Association of Universities for Research in Astronomy. L.L. and G.A.T. thank the Swiss National Science Foundation for continued support.

REFERENCES

Barbon, R., Benetti, S., Cappellaro, E., Rosino, L., & Turatto, M. 1990, A&A, 237, 79

Boughn, S.P., Cheng, E.S., & Wilkinson, D.T. 1981, ApJ, 243, L113

Branch, D., Fisher A., & Nugent, P. 1993, AJ, 106, 2383

Branch, D., & Tammann, G.A. 1992, ARA&A, 30, 359

Burstein, D., & Heiles, C. 1984, ApJS, 54, 33

Cadonau, R., Sandage, A., & Tammann, G.A. 1985, in Supernovae as Distance Indicators, Lecture Notes in Physics 224, ed. N. Bartel (Berlin: Springer), 151

Caldwell, J.A.R., & Coulson, I.M. 1985, MNRAS, 212, 879

Dean, J.F., Warren, P.R., & Cousins, A.W.J. 1978, MNRAS, 183, 569

de Vaucouleurs, G. 1975 in Galaxies and the Universe, eds. A. Sandage, M. Sandage, & J. Kristian, Vol 9 of the Compendium of Astronomy (Chicago: University of Chicago Press), Chapter 14, p 557

de Vaucouleurs, G., & Pence, W.D. 1976, ApJ, 209, 687

Evans, R.O. 1989, IAU Circ.4726

Federspiel, M., Tammann, G.A., & Sandage, A., 1988, ApJ, 286, 1

Ferguson, H.C., & Sandage, A. 1990, AJ, 100, 1

Fernie, J.D. 1990, ApJ, 354, 295

Freedman, W.L 1999, preprint

Graham, J.A., et al. 1997, ApJ, 477, 535

Hamuy, M., Phillips, M.M., Maza, J., Suntzeff, N.B., Schommer, R.A., & Aviles, R. 1995, AJ, 109, 1

Hamuy, M., Phillips, M.M., Schommer, R.A., Suntzeff, N.B., Maza, J., & Aviles, R. 1996a, AJ, 112, 2391

Hamuy, M., Phillips, M.M., Suntzeff, N.B., Schommer, R.A., Maza, J., & Aviles, R. 1996b, AJ, 112, 2398

Höflich, P.A. 1998, in Supernovae and Cosmology, eds. L. Labhardt, B. Binggeli, & R. Buser (Basel: Astron. Inst. Univ. Basel), 25

Holtzman, J.A. et al. 1995a, PASP, 107, 156

Holtzman, J.A. et al. 1995b, PASP, 107, 1065

Humason, M.L., Mayall, N.U., & Sandage, A. 1956, AJ, 61, 97

Jacoby, G.H. & Pierce, M.J. 1996, AJ, 112, 723

Kennicutt, R.C., Mould, J.R., & Freedman, W.L. 1998, preprint

Kraan-Korteweg, R.C. 1986a, A&AS, 66, 255

Kraan-Korteweg, R.C. 1986b, Basel preprint No. 18

Labhardt, L., Sandage, A., & Tammann, G.A. 1997, A&A, 322, 751

Lafler, J. & Kinman, T.D. 1965, ApJS, 11, 216

Lauer, T.R., & Postman, M. 1994, ApJ, 425, 418

Leibundgut, B., Kirshner, R.P., Filippenko, A.V., Shields, J.C., Foltz, C.B., Phillips, M.M., & Sonneborn, G. 1991a, ApJ, 371, L23

Leibundgut, B., Tammann, G.A., Cadonau, R., & Cerrito, D., 1991, A&AS, 89, 537 (The Basel SNe Ia Atlas)

Madore, B.F., & Freedman, W.L. 1991, PASP, 103, 933

Madore, B.F. et al. 1998, Nature, 395, 47

Materne, J. 1978, A&A, 63, 401

Nadyozhin, D.K. 1998, in Supernovae and Cosmology, eds. L. Labhardt, B. Binggeli, & R. Buser (Basel: Astron. Inst. Univ. Basel), 125

Parodi, B.R., Saha, A., Sandage, A., & Tammann, G.A. 1999, ApJ, in press

Phillips, M.M. 1993, ApJ, 413, L105

Phillips, M.M. et al. 1987, PASP, 99, 592

Phillips, M.M., Lira, P., Suntzeff, N.B., Schommer, R.A., Hamuy, M., & Maza, J. 1999 AJ, in press

Pskovskii, Yu. P. 1977, SvA, 21, 675

Pskovskii, Yu. P. 1984, SvA, 28, 658

Riess, A.G., Press, W.H., & Kirshner, R.P. 1996, ApJ, 473, 88

Rust, B.W. 1974, Oak Ridge Nat. Lab. Pub., No. 4953

Saha, A., & Hoessel, J.G. 1990, AJ, 99, 97

Saha, A., Labhardt, L., Schwengeler, H., Macchetto, F.D., Panagia, N, Sandage, A., & Tammann, G.A. 1994, ApJ, 425, 14 (Paper II; IC 4182; SN 1937C)

Saha, A., Sandage, A., Labhardt, L., Schwengeler, H., Tammann, G.A., Panagia, N., & Macchetto, F.D. 1995, ApJ, 438, 8 (Paper IV; NGC 5253; SN 1895B and SN 1972E)

Saha, A., Sandage, A., Labhardt, L., Tammann, G.A., Macchetto, F.D., & Panagia, N. 1996a, ApJ, 466, 55 (Paper V; NGC 4536; SN 1981B)

Saha, A., Sandage, A., Labhardt, L., Tammann, G.A., Macchetto, F.D., & Panagia, N. 1996b, ApJS, 107, 693 (Paper VI; NGC 4496A; SN 1960F)

Saha, A., Sandage, A., Labhardt, L., Tammann, G.A., Macchetto, F.D., & Panagia, N. 1997, ApJ, 486, 1 (Paper VIII; NGC 4639; SN 1990N)

Sandage, A. 1961, The Hubble Atlas (The Carnegie Institution of Washington; Washington D.C.), Pub. No. 618

Sandage, A. 1988, PASP, 100, 935

Sandage, A., Bell, R.A., & Tripicco, M.J. 1999, ApJ, submitted

Sandage, A., & Bedke, J. 1994, The Carnegie Atlas of Galaxies (The Carnegie Institution of Washington with the Flintridge Foundation; Washington D.C.), Carnegie Pub. No. 638

Sandage, A., Saha, A., Tammann, G.A., Labhardt, L., Panagia, N., & Macchetto, F.D. 1996, ApJ, 460, L15 (Paper VII; NGC 4639; SN 1990N)

Sandage, A., Saha, A., Tammann, G.A., Labhardt, L., Schwengeler, H., Panagia, N., & Macchetto, F.D. 1994, ApJ, 423, L13 (Paper III; NGC 5253; SN 1895B and SN 1972E)

Sandage, A., Saha, A., Tammann, G.A., Panagia, N., & Macchetto, F.D. 1992, ApJ, 401, L7 (Paper I; IC 4182; SN 1937C)

Sandage, A., & Tammann, G.A. 1968, ApJ, 151, 531

Sandage, A., & Tammann, G.A. 1993, ApJ, 415, 1

Sandage, A., Tammann, G.A., & Saha, A. 1999, in preparation

Schaefer, B.E. 1995a, ApJ, 447, L13

Schaefer, B.E. 1995b, ApJ, 449, L9

Schaefer, B.E. 1995c, ApJ, 450, L5

Schaefer, B.E. 1996, AJ, 111, 1668

Schaefer, B.E. 1998, ApJ, 509, 80

Schechter, P.L., Mateo, M.L., & Saha, A. 1993, PASP, 105, 1342

Scheffler, H. 1982, in Landolt-Börnstein, Astronomy & Astrophysics, vol. 2c, eds. K. Schaifers & H.H. Voigt (Berlin: Springer), 46

Stetson, P.B. 1995, private communication

Stetson, P.B. et al. 1998, ApJ, 508, 491

Suntzeff, N.B. et al. 1998, preprint, astro-ph/9811205

Tammann, G.A. 1998a, in General Relativity, 8th Marcel Grossmann Symposium, ed. T. Piran, (Singapore: World Scientific), in press

Tammann, G.A. 1998b, in Harmonizing Cosmic Distance Scales in a Post-Hipparcos Era, eds. D. Egret & A. Heck, in press

Tammann, G.A., & Sandage, A. 1985, ApJ, 294, 81

Tammann, G.A., & Sandage, A. 1995, ApJ, 452, 16

Tanvir, N.R., Shanks, T., Ferguson, H.C., & Robinson, D.T.R. 1995, Nature, 377, 27 (NGC 3368, M96)

Tripp, R. 1998, A&A, 331, 815

Turner, A., et al. 1998, ApJ, 505, 207

von Hippel, T., Bothun, G.D., & Schommer, R.A. 1997, AJ, 114, 1154

Wells, L.A. et al. 1994, AJ, 108, 2233

Wilkinson, D.T. 1984, in Large Scale Structure of the Universe, Cosmology, and Fundamental Physics, First ESO-CERN Symposium, ed. G. Setti & L. Van Horne (Geneva: CERN), 153

Yahil, A., Tammann, G.A., & Sandage, A. 1977, ApJ, 217, 903

Zehavi, I., Riess, A.G., Kirshner, R.P., & Dekel, A. 1998, ApJ, 503, 483

This preprint was prepared with the AAS LaTeX macros v4.0.

Fig. 1.— Ground-based image of NGC 3627 made with the Mount Wilson Hooker 100-inch reflector by Hubble on November 29/30, 1946. The image is from the same original negative as used for the short exposure image as an insert in The Carnegie Atlas, Panel 137. The field covered by the WFPC2 of the *HST* is superposed. The position of SN 1989B (Barbon et al. 1990) is marked.

Fig. 2.— Color image of the *HST* field made by stacking several frames in both the V and I passbands and combining.

Fig. 3.— Identifications for all the variable stars found. The numbers are the same as in Tables 3 and 4. Each of the four WFPC2 chips are shown separately.

Fig. 4.— Light curves, plotted in order of period, in the $F555W$ band. The first four variables are plotted with the arbitrary period of 100 days to facilitate the visualization. The actual periods are unknown; the time interval of the observations of 58 days is shorter than the actual periods, if any, of these four stars.

Fig. 5.— Same as Fig. 4 but for the $F814W$ passband, adopting the periods and the phasing used in Fig. 4.

Fig. 6.— The apparent P-L relations in V and I showing all the Cepheid data in Table 4. The solid circles are Cepheids with $\log P > 1.35$ with quality class of 4 or better. Open circles are for the remainder of the variables in Table 4. The drawn lines are the adopted P-L relations in equations (1) and (2) used in the previous papers of this series from Madore & Freedman (1991). The ridge line has been put arbitrarily at a modulus of $(m - M) = 30.2$ simply to guide the eye before analysis of differential extinction.

Fig. 7.— Diagnostic diagram for the detection of differential reddening, described in the text.

Fig. 8.— Correlation of the apparent modulus in V with that in I for the subset of the Cepheids in Table 4 with $(\langle V\rangle - \langle I\rangle) < 1.15$ and $\log P > 1.15$. Open circles are the bluest of the 29 Cepheid subsample. Closed circles are of intermediate color.

Fig. 9.— The P-L relations for the subset of Cepheids in Table 4 with $(\langle V\rangle - \langle I\rangle) < 1.15$ and $\log P > 1.15$. Same coding as in Fig. 8.

Fig. 10.— U_T vs. $\log P$ for the subset of the 29 bluest Cepheids. Same coding as in Figs. 8 and 9.

Fig. 11.— Same as Fig. 7 but for the blue 25 Cepheid subsample. The zero-point of the correlation is assumed to be at $(m - M)_0 = U_T = 30.17$ as in equation (6).

Fig. 12.— Correlation of the kinematic absolute magnitudes M_i ($H_0 = 55$) from columns (9) - (11) of Table 6 with the $\Delta m_{15}(B)$ decay rate from column (12). Open circles are for late type spirals, Roman crosses are for early type spirals, and skipping-jack crosses are for E and S0 galaxies. The lines are from equations (15) - (17) with the adopted zero points at $\Delta m_{15}(B) = 0$ that are listed

in the text.

Fig. 13.— Correlation of $(B_0 - V_0)$ color with the decay-rate corrected magnitudes M_i^{15}. The lines are equations (20) and (21) of the text. The shallow slope coefficients in B and V, and the reverse correlation of color with luminosity for the I band data, show that the correlations are not due to absorption and reddening, but are an intrinsic property of the supernovae.

Fig. 14.— Same as Fig. 13 but for $(V_0 - I_0)$ colors. Note the reverse correlation in V and I, where the absolute magnitude is brighter for redder colors, showing again that the correlation is not due to canonical extinction and reddening.

Table 1. Journal of Observations.

Data Archive Designation	HJD at Midexposure	Filter	Exposure time (s)
U35I0101R + ...02R	2450765.07048	$F555W$	4900
U35I0103R + ...04R	2450765.20105	$F814W$	5000
U35I1201R + ...02R	2450768.96875	$F555W$	4900
U35I0201R + ...02R	2450773.53863	$F555W$	4900
U35I0301R + ...02R	2450780.59626	$F555W$	4900
U35I0401R + ...02R	2450786.37739	$F555W$	4900
U35I0403R + ...04R	2450786.51004	$F555W$	4900
U35I0501R + ...02R	2450791.28343	$F814W$	5000
U35I0601R + ...02R	2450796.66105	$F555W$	4900
U35I0701R + ...02R	2450801.23025	$F555W$	4900
U35I0703R + ...04R	2450801.36499	$F814W$	5000
U35I0801R + ...02R	2450804.39306	$F555W$	4900
U35I0901R + ...02R	2450810.10888	$F555W$	4900
U35I0903R + ...04R	2450810.24084	$F814W$	5000
U35I01001R + ...02R	2450817.03382	$F555W$	4900
U35I01101R + ...02R	2450823.88997	$F555W$	4900
U35I01103R + ...04R	2450824.02262	$F814W$	5000

Table 2. Position of the Variable Stars on *U35I0701R & 02R*

Variable ID	X-position	Y-position	Variable ID	X-position	Y-position
C1-V1	94.3	587.0	C1-V2	163.3	608.5
C1-V3	168.3	472.9	C1-V4	194.6	309.8
C1-V5	266.6	640.5	C1-V6	270.3	389.2
C1-V7	274.8	616.8	C1-V8	315.9	342.7
C1-V9	439.6	378.4	C1-V10	465.4	302.0
C1-V11	517.8	779.0	C1-V12	584.0	272.9
C1-V13	697.6	361.4	C1-V14	718.9	211.4
C2-V1	89.1	381.8	C2-V2	90.9	708.2
C2-V3	108.7	162.3	C2-V4	123.5	193.0
C2-V5	131.8	301.5	C2-V6	142.9	535.1
C2-V7	145.0	164.4	C2-V8	170.3	302.2
C2-V9	171.1	777.3	C2-V10	173.7	203.1
C2-V11	190.9	469.8	C2-V12	194.3	238.3
C2-V13	199.8	169.2	C2-V14	207.2	112.1
C2-V15	224.6	217.9	C2-V16	262.1	492.3
C2-V17	266.2	494.1	C2-V18	280.0	652.0
C2-V19	284.6	516.1	C2-V20	286.8	301.1
C2-V21	307.0	385.9	C2-V22	307.8	220.9
C2-V23	313.8	235.8	C2-V24	351.3	103.8
C2-V25	369.6	652.2	C2-V26	389.0	193.2
C2-V27	416.1	261.2	C2-V28	456.9	265.8
C2-V29	457.5	154.5	C2-V30	468.3	311.4
C2-V31	515.8	337.0	C2-V32	534.6	757.1
C2-V33	548.6	339.4	C2-V34	581.5	254.8
C2-V35	590.1	361.9	C2-V36	676.2	744.1
C2-V37	680.9	749.7	C2-V38	708.9	211.9
C3-V1	156.5	152.1	C3-V2	170.3	736.7
C3-V3	181.0	328.9	C3-V4	235.5	238.9
C3-V5	236.8	393.6	C3-V6	242.9	107.3
C3-V7	245.3	314.0	C3-V8	248.7	209.3
C3-V9	313.8	154.2	C3-V10	343.7	119.8
C3-V11	348.2	394.8	C3-V12	409.5	651.8
C3-V13	429.5	328.0	C3-V14	450.4	267.6
C3-V15	569.6	543.4	C3-V16	607.2	201.2
C3-V17	742.7	275.1			
C4-V1	112.0	73.4	C4-V2	115.3	95.5
C4-V3	143.0	129.2	C4-V4	390.8	106.1
C4-V5	402.0	177.9	C4-V6	467.3	143.3
C4-V7	535.1	476.9	C4-V8	582.2	156.2
C4-V9	585.2	190.8	C4-V10	601.4	168.3
C4-V11	645.7	125.7	C4-V12	655.6	228.8
C4-V13	682.1	120.0	C4-V14	737.7	63.9

Table 3. Photometry of Variable Stars: Magnitudes and Error Estimates

HJD	C1-V1	C1-V2	C1-V3	C1-V4	C1-V5	C1-V6	C1-V7	C1-V8
				F555W				
2450765.0705	24.73 0.11	25.85 0.14	26.09 0.17	27.26 0.38	25.31 0.06	25.59 0.10	25.67 0.12	25.63 0.07
2450768.9688	24.52 0.12	26.35 0.21	25.38 0.09	27.22 0.29	25.05 0.05	25.44 0.10	25.51 0.11	26.01 0.13
2450773.5386	24.74 0.12	26.56 0.21	25.98 0.14	26.58 0.17	25.38 0.07	25.63 0.10	25.30 0.08	27.03 0.24
2450780.5963	24.81 0.10	26.24 0.17	26.72 0.39	26.90 0.23	25.30 0.07	25.88 0.13	24.92 0.08	25.66 0.09
2450786.3774	24.83 0.13	26.47 0.20	26.65 0.36	26.56 0.18	24.90 0.06	26.06 0.16	25.19 0.09	26.67 0.24
2450791.2834	24.88 0.12	26.14 0.18	...	26.89 0.20	25.36 0.07	26.06 0.16	25.35 0.11	26.31 0.16
2450796.6611	24.74 0.10	25.99 0.15	26.50 0.28	26.53 0.18	25.30 0.06	26.03 0.17	25.43 0.10	25.99 0.11
2450801.2303	24.69 0.09	25.69 0.10	25.90 0.12	26.47 0.16	24.88 0.06	25.34 0.09	25.47 0.09	26.49 0.17
2450804.3931	24.50 0.09	26.39 0.22	25.98 0.13	26.68 0.20	25.13 0.07	25.38 0.10	25.55 0.10	26.38 0.14
2450810.1089	24.46 0.08	26.25 0.20	...	26.56 0.15	25.39 0.08	25.42 0.08	25.70 0.10	26.01 0.11
2450817.0338	24.24 0.05	26.96 0.35	26.24 0.21	26.55 0.17	24.96 0.05	25.96 0.16	25.19 0.09	26.69 0.19
2450823.8900	24.32 0.06	26.70 0.38	26.98 0.45	26.13 0.13	25.13 0.06	26.28 0.17	24.98 0.08	25.78 0.10
				F814W				
2450765.2010	23.42 0.08	...	24.94 0.19	...	24.24 0.07	24.25 0.11	24.30 0.08	24.88 0.11
2450786.5100	23.74 0.06	...	24.69 0.13	...	24.13 0.08	24.67 0.14	24.00 0.08	25.21 0.14
2450801.3650	23.58 0.05	...	24.73 0.11	...	23.44 0.08	24.10 0.08	24.24 0.07	25.43 0.16
2450810.2408	23.38 0.06	...	24.73 0.11	...	24.28 0.07	24.26 0.09	24.44 0.10	24.98 0.11
2450824.0226	23.36 0.05	...	24.78 0.12	...	24.35 0.09	24.72 0.10	23.75 0.09	25.05 0.14

HJD	C1-V9	C1-V10	C1-V11	C1-V12	C1-V13	C1-V14	C2-V1	C2-V2
				F555W				
2450765.0705	26.61 0.19	26.28 0.16	26.95 0.26	26.49 0.16	26.65 0.18	26.33 0.13	25.22 0.12	25.06 0.14
2450768.9688	26.15 0.13	27.01 0.31	27.09 0.27	25.59 0.13	...	26.05 0.12	25.41 0.14	25.34 0.17
2450773.5386	26.92 0.20	26.10 0.11	26.86 0.25	25.38 0.12	27.22 0.26	26.85 0.20	24.38 0.09	26.16 0.32
2450780.5963	26.46 0.16	27.14 0.29	26.01 0.12	25.93 0.12	26.44 0.19	26.27 0.14	24.77 0.09	25.13 0.16
2450786.3774	27.06 0.28	26.26 0.15	26.80 0.22	25.96 0.11	27.67 0.40	26.30 0.11	25.02 0.09	25.59 0.21
2450791.2834	26.95 0.25	26.49 0.13	26.95 0.28	26.46 0.18	26.95 0.20	26.17 0.14	24.88 0.10	26.00 0.26
2450796.6611	26.31 0.16	26.73 0.18	26.70 0.18	26.36 0.13	26.97 0.19	26.46 0.15	24.46 0.10	24.81 0.17
2450801.2303	26.75 0.23	26.25 0.11	26.35 0.14	26.15 0.12	26.51 0.14	26.01 0.11	24.55 0.09	25.61 0.19
2450804.3931	...	26.84 0.22	26.63 0.19	26.55 0.21	27.77 0.50	26.78 0.24	24.58 0.08	26.08 0.35
2450810.1089	26.40 0.14	26.65 0.17	26.88 0.23	26.46 0.14	26.63 0.16	25.84 0.08	25.22 0.13	25.66 0.21
2450817.0338	26.96 0.22	26.50 0.20	26.64 0.22	26.44 0.15	26.98 0.25	26.53 0.14	25.13 0.12	25.74 0.23
2450823.8900	26.23 0.13	26.66 0.16	26.15 0.15	26.34 0.12	27.34 0.27	26.43 0.19	24.57 0.09	25.88 0.37
				F814W				
2450765.2010	25.41 0.16	25.06 0.14	25.48 0.18	25.20 0.15	26.26 0.31	25.09 0.12	23.61 0.07	24.14 0.10
2450786.5100	25.36 0.16	25.46 0.18	25.17 0.14	25.13 0.15	26.74 0.49	25.30 0.14	23.63 0.08	24.65 0.19
2450801.3650	24.83 0.11	25.11 0.15	25.36 0.17	25.06 0.14	26.46 0.38	25.13 0.12	23.25 0.07	24.23 0.16
2450810.2408	24.99 0.13	25.70 0.22	25.35 0.18	25.07 0.14	25.95 0.27	24.85 0.10	23.46 0.08	24.50 0.13
2450824.0226	25.26 0.14	25.24 0.14	25.10 0.15	24.95 0.12	26.39 0.35	25.16 0.13	23.43 0.07	24.49 0.19

HJD	C2-V3	C2-V4	C2-V5	C2-V6	C2-V7	C2-V8	C2-V9	C2-V10
				F555W				
2450765.0705	25.88 0.17	24.20 0.06	25.30 0.11	25.63 0.15	25.60 0.17	24.57 0.10	25.16 0.16	25.06 0.10
2450768.9688	25.55 0.13	24.15 0.06	25.74 0.16	25.80 0.18	25.63 0.16	24.63 0.09	25.05 0.12	24.93 0.09
2450773.5386	25.03 0.10	24.47 0.06	25.83 0.17	24.85 0.08	24.76 0.09	24.86 0.12	25.43 0.18	24.24 0.05
2450780.5963	25.46 0.13	24.66 0.09	25.03 0.09	25.65 0.19	25.25 0.16	25.15 0.13	...	24.72 0.08
2450786.3774	25.56 0.13	24.78 0.09	25.55 0.12	25.13 0.11	25.85 0.23	25.20 0.16	...	25.10 0.11
2450791.2834	24.96 0.09	24.90 0.09	25.58 0.13	25.42 0.12	24.68 0.08	25.27 0.15	24.84 0.11	24.95 0.09
2450796.6611	25.21 0.11	25.06 0.11	24.98 0.08	25.47 0.15	24.93 0.09	24.99 0.12	25.66 0.23	24.35 0.06
2450801.2303	25.73 0.14	24.65 0.08	25.38 0.10	25.15 0.11	25.60 0.14	24.47 0.08	26.42 0.34	24.72 0.08
2450804.3931	25.63 0.13	24.20 0.06	25.78 0.16	25.60 0.18	25.72 0.16	24.59 0.10	25.93 0.26	24.83 0.09
2450810.1089	25.18 0.10	24.24 0.05	25.39 0.12	26.14 0.31	24.65 0.08	24.66 0.10	24.81 0.12	25.02 0.09
2450817.0338	25.18 0.11	24.39 0.05	25.35 0.10	25.05 0.10	25.38 0.12	24.97 0.13	25.47 0.17	24.39 0.07
2450823.8900	25.81 0.16	24.84 0.08	25.94 0.19	25.69 0.17	25.51 0.11	25.19 0.15	26.35 0.43	24.78 0.09
				F814W				
2450765.2010	...	23.26 0.05	...	24.65 0.18	24.11 0.10	23.72 0.08	24.24 0.10	24.55 0.12
2450786.5100	...	23.70 0.08	...	24.30 0.10	24.64 0.22	24.19 0.10	23.98 0.08	24.53 0.12
2450801.3650	...	23.59 0.06	...	24.24 0.09	24.24 0.12	23.89 0.11	24.55 0.13	24.08 0.07
2450810.2408	...	23.33 0.05	...	24.73 0.16	23.75 0.08	23.83 0.07	23.78 0.08	24.50 0.09
2450824.0226	...	23.58 0.05	...	24.60 0.14	24.32 0.13	24.38 0.12	24.38 0.11	24.05 0.08

Table 3—Continued

HJD	C2-V11	C2-V12	C2-V13	C2-V14	C2-V15	C2-V16	C2-V17	C2-V18
				F555W				
2450765.0705	25.36 0.13	25.27 0.09	25.74 0.18	25.63 0.16	25.63 0.17	24.00 0.07	24.05 0.06	25.02 0.16
2450768.9688	25.89 0.31	24.73 0.06	25.39 0.14	26.17 0.21	25.97 0.29	24.55 0.11	24.23 0.08	25.17 0.19
2450773.5386	25.89 0.22	24.83 0.06	25.98 0.19	25.99 0.19	26.15 0.29	24.64 0.14	24.26 0.06	25.43 0.29
2450780.5963	24.46 0.13	25.11 0.07	26.34 0.29	···	26.20 0.37	25.10 0.22	24.51 0.14	···
2450786.3774	24.81 0.10	25.21 0.09	25.42 0.12	25.40 0.13	25.27 0.16	24.88 0.19	24.73 0.11	25.16 0.21
2450791.2834	25.48 0.14	25.52 0.13	26.08 0.22	25.72 0.16	25.30 0.14	24.51 0.09	24.38 0.12	24.52 0.12
2450796.6611	25.73 0.22	24.53 0.05	···	26.28 0.26	25.89 0.21	24.61 0.12	24.10 0.14	24.71 0.15
2450801.2303	25.86 0.20	24.98 0.07	···	26.21 0.23	26.16 0.28	24.95 0.12	23.95 0.07	25.13 0.18
2450804.3931	24.65 0.09	25.20 0.09	25.30 0.13	26.13 0.23	26.38 0.38	24.97 0.18	24.03 0.09	25.53 0.30
2450810.1089	25.22 0.10	25.31 0.12	26.22 0.38	25.27 0.12	25.30 0.14	24.21 0.09	24.21 0.08	25.28 0.24
2450817.0338	25.80 0.19	25.35 0.09	26.08 0.23	25.67 0.14	25.45 0.16	24.55 0.13	24.22 0.09	25.55 0.27
2450823.8900	25.76 0.16	24.67 0.06	25.39 0.14	26.21 0.23	26.01 0.27	24.78 0.15	24.60 0.11	24.55 0.13
				F814W				
2450765.2010	23.97 0.10	24.30 0.12	25.45 0.44	24.00 0.09	24.55 0.14	23.14 0.09	22.91 0.12	23.70 0.13
2450786.5100	23.94 0.09	24.10 0.12	24.45 0.12	23.93 0.08	24.33 0.13	23.55 0.13	23.41 0.39	23.90 0.14
2450801.3650	24.23 0.13	23.96 0.09	24.92 0.16	24.33 0.10	···	23.45 0.11	23.13 0.18	23.65 0.10
2450810.2408	23.91 0.10	24.28 0.12	25.25 0.27	24.05 0.09	24.47 0.21	23.10 0.09	23.24 0.18	23.85 0.12
2450824.0226	24.14 0.13	23.89 0.08	24.84 0.16	24.31 0.11	25.25 0.45	23.10 0.07	23.35 0.20	23.50 0.10
HJD	C2-V19	C2-V20	C2-V21	C2-V22	C2-V23	C2-V24	C2-V25	C2-V26
				F555W				
2450765.0705	25.13 0.16	24.45 0.06	25.57 0.15	24.69 0.07	21.46 0.02	25.94 0.16	25.01 0.20	25.05 0.13
2450768.9688	25.03 0.13	24.69 0.07	25.13 0.11	25.06 0.09	21.80 0.02	25.41 0.11	25.01 0.19	25.15 0.12
2450773.5386	24.59 0.10	24.90 0.10	24.69 0.07	25.43 0.13	22.05 0.02	26.01 0.17	25.11 0.18	25.84 0.27
2450780.5963	24.42 0.08	24.67 0.09	25.08 0.11	25.63 0.17	22.45 0.03	25.28 0.11	25.00 0.20	25.77 0.14
2450786.3774	24.64 0.09	25.17 0.14	25.45 0.14	24.65 0.10	22.75 0.03	25.81 0.13	23.80 0.09	25.03 0.08
2450791.2834	24.64 0.08	24.56 0.06	25.33 0.14	25.25 0.12	22.89 0.03	25.74 0.17	22.53 0.06	24.92 0.09
2450796.6611	25.25 0.47	24.74 0.07	24.73 0.07	25.55 0.14	22.90 0.04	25.58 0.13	22.35 0.05	25.66 0.16
2450801.2303	24.92 0.13	24.92 0.10	25.01 0.11	24.88 0.08	23.13 0.03	26.25 0.20	23.63 0.07	25.48 0.16
2450804.3931	24.90 0.11	25.32 0.14	25.15 0.11	25.13 0.10	23.18 0.03	26.20 0.22	24.08 0.11	25.88 0.17
2450810.1089	24.86 0.12	25.33 0.13	25.21 0.12	25.49 0.12	23.26 0.03	25.60 0.13	24.34 0.12	25.71 0.16
2450817.0338	25.01 0.12	24.38 0.08	25.05 0.09	25.55 0.13	23.35 0.04	26.22 0.22	24.59 0.13	24.67 0.09
2450823.8900	25.36 0.32	24.96 0.09	24.93 0.08	25.26 0.10	23.49 0.03	25.55 0.12	24.64 0.15	25.22 0.11
				F814W				
2450765.2010	23.93 0.13	23.76 0.08	···	23.98 0.08	···	24.46 0.11	22.66 0.10	23.81 0.08
2450786.5100	23.58 0.10	24.35 0.14	···	24.41 0.12	···	24.45 0.12	21.21 0.05	23.97 0.08
2450801.3650	23.76 0.12	24.05 0.10	···	24.45 0.12	···	24.39 0.13	21.16 0.05	24.21 0.08
2450810.2408	24.01 0.17	24.36 0.19	···	24.84 0.19	20.09 0.05	24.19 0.10	21.91 0.06	24.38 0.11
2450824.0226	24.36 0.24	23.97 0.08	···	24.41 0.13	20.39 0.05	24.34 0.10	22.30 0.08	23.91 0.08
HJD	C2-V27	C2-V28	C2-V29	C2-V30	C2-V31	C2-V32	C2-V33	C2-V34
				F555W				
2450765.0705	25.34 0.13	25.42 0.16	24.95 0.09	25.60 0.12	25.36 0.10	24.93 0.10	25.11 0.12	24.73 0.09
2450768.9688	25.88 0.19	25.47 0.16	25.45 0.11	25.76 0.25	25.80 0.16	25.14 0.10	24.15 0.07	24.49 0.07
2450773.5386	25.30 0.13	25.02 0.11	26.25 0.21	25.05 0.07	25.16 0.10	25.74 0.16	24.21 0.06	23.96 0.06
2450780.5963	24.89 0.09	25.26 0.14	25.48 0.11	25.72 0.13	24.67 0.08	25.59 0.14	24.65 0.09	24.00 0.06
2450786.3774	25.10 0.10	25.53 0.19	25.41 0.10	25.31 0.10	25.21 0.09	24.91 0.12	25.07 0.12	24.22 0.06
2450791.2834	25.35 0.12	24.89 0.12	25.63 0.12	25.25 0.09	25.27 0.09	25.22 0.16	25.17 0.11	24.40 0.07
2450796.6611	25.35 0.11	25.35 0.14	26.23 0.19	25.58 0.14	25.63 0.15	25.65 0.18	24.98 0.10	24.55 0.07
2450801.2303	25.45 0.11	25.47 0.17	25.27 0.09	25.33 0.18	25.55 0.10	···	24.10 0.05	24.57 0.09
2450804.3931	24.67 0.08	25.23 0.14	25.27 0.09	25.16 0.09	25.51 0.16	25.97 0.27	24.38 0.06	24.66 0.09
2450810.1089	24.81 0.08	25.05 0.11	25.98 0.17	25.72 0.13	24.80 0.08	24.98 0.14	24.52 0.09	24.83 0.11
2450817.0338	25.27 0.11	25.43 0.16	25.96 0.15	25.27 0.08	25.01 0.08	25.14 0.07	24.94 0.12	24.35 0.07
2450823.8900	25.46 0.13	24.82 0.07	25.40 0.10	25.21 0.10	25.23 0.10	25.57 0.22	25.15 0.13	24.11 0.07
				F814W				
2450765.2010	23.98 0.11	24.24 0.14	24.32 0.11	···	24.22 0.12	24.31 0.12	24.11 0.16	23.57 0.06
2450786.5100	23.86 0.09	24.43 0.13	24.60 0.11	24.19 0.15	23.60 0.08	23.91 0.10	23.88 0.10	23.15 0.05
2450801.3650	23.92 0.11	24.57 0.12	24.56 0.13	···	24.13 0.11	24.73 0.28	23.38 0.07	23.40 0.05
2450810.2408	23.69 0.06	24.14 0.09	24.67 0.13	···	23.67 0.08	24.31 0.16	23.51 0.09	23.43 0.05
2450824.0226	24.15 0.10	23.98 0.08	24.48 0.13	24.47 0.19	23.88 0.07	24.17 0.09	24.07 0.16	23.10 0.05

Table 3—Continued

HJD	C2-V35	C2-V36	C2-V37	C2-V38	C3-V1	C3-V2	C3-V3	C3-V4
				F555W				
2450765.0705	26.16 0.32	22.81 0.03	23.45 0.05	24.38 0.09	25.66 0.14	25.57 0.11	24.89 0.09	24.65 0.07
2450768.9688	24.56 0.09	22.83 0.03	23.52 0.04	24.41 0.08	26.21 0.26	25.97 0.16	25.46 0.10	25.23 0.08
2450773.5386	24.89 0.12	22.84 0.03	23.45 0.04	24.40 0.06	26.15 0.20	26.22 0.20	25.24 0.09	25.63 0.12
2450780.5963	25.51 0.17	22.71 0.04	23.36 0.04	24.64 0.10	25.49 0.12	26.06 0.13	24.43 0.05	25.72 0.12
2450786.3774	25.94 0.24	...	23.38 0.04	24.48 0.08	25.74 0.16	26.34 0.19	24.80 0.06	24.95 0.07
2450791.2834	26.32 0.35	22.77 0.03	23.25 0.04	24.74 0.08	26.02 0.20	25.63 0.12	25.22 0.09	24.94 0.06
2450796.6611	24.65 0.10	22.60 0.02	23.24 0.04	24.73 0.08	25.82 0.12	25.99 0.21	25.41 0.09	25.30 0.11
2450801.2303	24.56 0.10	22.40 0.04	23.17 0.04	24.63 0.09	25.46 0.11	25.75 0.10	25.40 0.09	25.65 0.10
2450804.3931	24.95 0.10	22.35 0.03	23.18 0.04	24.86 0.10	25.53 0.09	25.33 0.10	25.55 0.11	25.67 0.12
2450810.1089	25.46 0.17	22.33 0.02	23.09 0.04	24.96 0.10	26.41 0.23	26.27 0.20	24.55 0.05	25.59 0.11
2450817.0338	25.91 0.26	22.40 0.03	23.02 0.05	25.05 0.13	25.41 0.09	25.80 0.12	25.01 0.07	24.84 0.06
2450823.8900	25.30 0.14	22.46 0.03	23.00 0.04	25.13 0.12	25.64 0.12	26.23 0.23	25.22 0.10	25.24 0.10
				F814W				
2450765.2010	24.95 0.22	22.44 0.05	22.22 0.05	23.01 0.05	24.74 0.13	...	23.63 0.06	24.19 0.10
2450786.5100	...	22.45 0.06	...	23.14 0.05	24.83 0.13	...	...	24.15 0.09
2450801.3650	24.05 0.12	22.06 0.05	22.05 0.05	23.18 0.05	24.81 0.17	...	24.32 0.11	24.63 0.11
2450810.2408	24.60 0.19	21.98 0.05	21.96 0.05	23.40 0.05	25.09 0.19	...	...	24.90 0.28
2450824.0226	24.43 0.16	22.08 0.05	21.58 0.09	23.56 0.06	24.74 0.10	...	24.34 0.10	24.30 0.08

HJD	C3-V5	C3-V6	C3-V7	C3-V8	C3-V9	C3-V10	C3-V11	C3-V12
				F555W				
2450765.0705	24.72 0.06	25.48 0.12	26.56 0.20	24.55 0.17	24.89 0.08	23.97 0.06	25.63 0.10	25.55 0.19
2450768.9688	25.09 0.09	25.33 0.11	26.10 0.14	25.40 0.11	24.96 0.10	23.92 0.05	25.25 0.08	25.39 0.07
2450773.5386	25.38 0.11	24.81 0.06	26.63 0.20	25.92 0.17	25.18 0.13	24.16 0.06	25.52 0.09	25.73 0.12
2450780.5963	25.18 0.10	25.36 0.12	27.34 0.39	25.50 0.12	25.68 0.16	24.28 0.07	25.61 0.09	26.31 0.15
2450786.3774	24.91 0.08	25.39 0.12	26.14 0.22	25.38 0.10	25.40 0.17	24.09 0.06	25.51 0.08	26.36 0.14
2450791.2834	25.15 0.09	25.53 0.12	26.26 0.16	25.65 0.10	25.03 0.11	24.66 0.07	25.63 0.10	25.07 0.06
2450796.6611	25.13 0.08	24.83 0.10	26.63 0.25	25.91 0.13	25.33 0.12	24.76 0.08	25.13 0.06	25.58 0.08
2450801.2303	24.53 0.06	24.90 0.15	27.26 0.40	25.05 0.08	25.41 0.14	24.26 0.07	25.59 0.08	25.91 0.12
2450804.3931	24.88 0.09	25.31 0.09	26.03 0.12	25.14 0.08	25.55 0.15	23.98 0.05	25.50 0.09	26.28 0.15
2450810.1089	25.16 0.11	25.64 0.16	26.34 0.20	25.43 0.11	25.06 0.15	23.91 0.04	25.17 0.09	26.22 0.16
2450817.0338	25.41 0.11	24.78 0.05	26.95 0.31	25.96 0.15	25.10 0.10	24.11 0.05	25.49 0.09	25.25 0.09
2450823.8900	24.76 0.06	25.28 0.09	25.96 0.14	24.99 0.07	25.71 0.15	24.27 0.06	25.13 0.09	25.82 0.12
				F814W				
2450765.2010	...	24.40 0.11	...	24.13 0.09	...	23.20 0.05	24.24 0.08	24.43 0.08
2450786.5100	...	24.30 0.09	...	24.38 0.12	...	23.34 0.06	24.24 0.10	24.80 0.12
2450801.3650	24.01 0.12	24.17 0.08	...	24.11 0.09	...	23.33 0.06	24.30 0.09	24.67 0.10
2450810.2408	24.27 0.10	24.39 0.11	...	24.33 0.10	...	23.17 0.05	24.21 0.09	24.93 0.13
2450824.0226	...	24.13 0.08	...	24.13 0.09	...	23.38 0.06	24.28 0.08	24.67 0.11

HJD	C3-V13	C3-V14	C3-V15	C3-V16	C3-V17	C4-V1	C4-V2	C4-V3
				F555W				
2450765.0705	26.49 0.23	26.46 0.17	26.09 0.18	25.73 0.15	25.56 0.11	25.73 0.18	26.14 0.19	24.77 0.14
2450768.9688	26.23 0.21	...	25.81 0.09	26.34 0.25	25.78 0.14	26.19 0.25	25.34 0.11	24.65 0.09
2450773.5386	25.36 0.10	27.31 0.44	25.82 0.09	26.83 0.35	25.49 0.10	26.38 0.29	25.53 0.10	25.07 0.10
2450780.5963	26.45 0.22	26.22 0.14	25.92 0.09	26.05 0.15	24.96 0.05	25.89 0.19	25.98 0.12	25.14 0.13
2450786.3774	26.59 0.28	26.50 0.21	25.70 0.24	26.26 0.21	25.38 0.10	25.16 0.11	25.84 0.14	25.10 0.12
2450791.2834	25.70 0.12	26.93 0.30	25.13 0.06	26.68 0.24	25.90 0.15	25.21 0.11	25.56 0.10	25.27 0.15
2450796.6611	26.00 0.21	26.05 0.14	25.55 0.07	25.61 0.13	25.86 0.13	25.64 0.19	25.82 0.12	25.18 0.13
2450801.2303	26.68 0.25	26.91 0.27	25.55 0.08	26.65 0.25	25.26 0.09	25.67 0.18	26.31 0.35	25.36 0.14
2450804.3931	26.15 0.20	26.75 0.23	25.61 0.10	26.76 0.28	24.90 0.06	25.76 0.23	26.24 0.16	25.47 0.29
2450810.1089	26.03 0.19	25.83 0.12	25.46 0.09	25.76 0.14	25.34 0.09	26.05 0.23	25.36 0.08	25.46 0.16
2450817.0338	26.26 0.17	27.33 0.42	25.26 0.06	26.63 0.28	25.67 0.12	25.95 0.20	25.90 0.12	25.33 0.14
2450823.8900	25.56 0.13	26.30 0.17	25.28 0.06	26.50 0.23	25.93 0.13	25.23 0.13	25.59 0.14	24.90 0.16
				F814W				
2450765.2010	...	...	23.03 0.05	24.88 0.15	...	24.44 0.15	25.43 0.25	...
2450786.5100	...	...	23.26 0.05	25.05 0.15	...	23.84 0.11	25.41 0.26	24.06 0.30
2450801.3650	...	...	23.21 0.05	25.05 0.18	...	24.40 0.12	25.61 0.23	...
2450810.2408	...	...	23.27 0.05	25.34 0.18	...	24.50 0.15	24.76 0.14	...
2450824.0226	...	25.55 0.23	23.19 0.05	25.15 0.19	...	23.76 0.08	25.44 0.27	...

Table 3—Continued

HJD	C4-V4	C4-V5	C4-V6	C4-V7	C4-V8	C4-V9	C4-V10	C4-V11
				F555W				
2450765.0705	26.08 0.22	25.70 0.10	25.20 0.08	···	24.83 0.09	24.67 0.06	25.05 0.06	25.18 0.09
2450768.9688	24.83 0.13	26.08 0.15	25.49 0.10	26.07 0.14	25.35 0.19	25.03 0.09	25.35 0.09	25.10 0.10
2450773.5386	25.15 0.09	26.01 0.13	25.96 0.13	26.05 0.13	24.90 0.09	25.51 0.12	25.90 0.12	24.63 0.06
2450780.5963	25.45 0.11	26.18 0.12	25.13 0.10	26.24 0.14	24.99 0.11	25.80 0.14	26.21 0.14	25.02 0.07
2450786.3774	25.81 0.21	26.80 0.46	25.36 0.09	26.17 0.12	24.23 0.07	25.48 0.11	25.22 0.08	25.15 0.08
2450791.2834	25.64 0.16	26.46 0.21	25.76 0.10	26.81 0.33	25.26 0.16	24.89 0.06	25.19 0.07	25.11 0.09
2450796.6611	25.25 0.16	26.00 0.11	25.78 0.10	25.66 0.08	25.46 0.16	25.23 0.09	25.52 0.07	24.46 0.05
2450801.2303	25.30 0.10	25.69 0.08	24.81 0.07	26.44 0.14	25.32 0.14	25.70 0.11	25.91 0.11	24.81 0.06
2450804.3931	25.40 0.13	25.95 0.12	25.41 0.09	27.05 0.27	25.28 0.09	25.70 0.12	26.60 0.38	24.97 0.07
2450810.1089	25.91 0.16	25.93 0.11	25.59 0.12	26.00 0.10	24.84 0.16	25.56 0.10	25.53 0.09	25.24 0.13
2450817.0338	25.52 0.12	26.28 0.18	25.85 0.26	26.65 0.18	25.32 0.11	25.03 0.08	25.33 0.08	25.26 0.15
2450823.8900	25.41 0.12	26.59 0.16	25.63 0.26	26.00 0.11	25.69 0.26	25.40 0.14	26.03 0.14	24.72 0.07
				F814W				
2450765.2010	25.22 0.19	24.08 0.06	24.21 0.15	25.16 0.17	23.70 0.06	23.84 0.05	24.31 0.09	23.80 0.07
2450786.5100	25.33 0.24	24.60 0.10	24.58 0.19	25.24 0.14	23.38 0.08	24.47 0.09	23.81 0.09	23.65 0.07
2450801.3650	24.64 0.12	24.27 0.10	24.30 0.14	25.24 0.14	23.76 0.08	24.34 0.07	24.60 0.11	23.53 0.05
2450810.2408	24.82 0.16	24.46 0.10	···	24.78 0.10	24.05 0.07	24.39 0.08	24.58 0.09	23.99 0.10
2450824.0226	24.32 0.13	24.67 0.10	24.45 0.19	25.00 0.11	24.06 0.07	24.16 0.06	24.85 0.11	23.82 0.07

HJD	C4-V12	C4-V13	C4-V14
			F555W
2450765.0705	25.85 0.13	24.92 0.10	25.27 0.12
2450768.9688	26.42 0.19	24.96 0.11	25.33 0.14
2450773.5386	26.38 0.14	25.45 0.15	25.14 0.10
2450780.5963	26.02 0.26	25.71 0.20	25.20 0.10
2450786.3774	26.19 0.13	25.98 0.23	25.05 0.10
2450791.2834	25.88 0.12	25.01 0.25	25.30 0.11
2450796.6611	26.45 0.20	25.24 0.10	25.50 0.12
2450801.2303	26.16 0.11	25.06 0.14	25.34 0.11
2450804.3931	25.80 0.10	25.66 0.16	25.61 0.12
2450810.1089	26.18 0.14	26.05 0.21	25.70 0.14
2450817.0338	26.03 0.13	24.76 0.08	25.97 0.16
2450823.8900	25.74 0.16	25.53 0.13	25.71 0.16
			F814W
2450765.2010	···	23.80 0.09	23.18 0.06
2450786.5100	···	24.65 0.19	···
2450801.3650	···	24.31 0.12	23.34 0.07
2450810.2408	···	24.53 0.16	23.40 0.06
2450824.0226	···	24.06 0.08	23.59 0.07

Table 4. Characteristics of the Cepheids

Object (1)	Period (days) (2)	$\langle V \rangle$ (3)	$\sigma_{\langle V \rangle}$ (4)	$\langle I \rangle$ (5)	$\sigma_{\langle I \rangle}$ (6)	U_V (7)	U_I (8)	U_T (9)	σ_{U_T} (10)	Quality Index (11)
C1-V1	75.0	24.56	0.09	23.47	0.10	31.134	31.020	30.857	0.484	4
C1-V3	39.0	26.17	0.27	24.84	0.42	31.959	31.515	30.880	1.167	2
C1-V5	17.0	25.16	0.07	24.07	0.31	29.959	29.644	29.194	0.848	2
C1-V6	33.9	25.74	0.14	24.37	0.17	31.365	30.865	30.152	0.605	6
C1-V7	42.0	25.30	0.10	24.08	0.13	31.179	30.858	30.399	0.529	6
C1-V8	14.5	26.14	0.16	25.11	0.15	30.745	30.468	30.073	0.587	5
C1-V9	13.7	26.63	0.21	25.22	0.34	31.171	30.511	29.568	0.966	1
C1-V10	12.9	26.54	0.20	25.28	0.25	31.002	30.486	29.749	0.785	2
C1-V11	38.0	26.60	0.22	25.20	0.14	32.360	31.840	31.096	0.605	3
C1-V12	58.0	26.08	0.14	24.75	0.38	32.345	31.959	31.408	1.024	3
C1-V13	17.0	26.90	0.27	26.33	0.28	31.698	31.904	32.198	0.871	3
C1-V14	10.6	26.26	0.16	25.16	0.12	30.494	30.106	29.552	0.542	3
C2-V1	24.0	24.78	0.11	23.46	0.12	29.991	29.493	28.782	0.519	2
C2-V2	16.0	25.52	0.25	24.36	0.20	30.247	29.859	29.304	0.720	3
C2-V4	42.0	24.55	0.08	23.50	0.09	30.430	30.281	30.068	0.478	6
C2-V6	14.2	25.39	0.16	24.50	0.13	29.972	29.833	29.634	0.558	4
C2-V7	18.5	25.13	0.13	23.97	0.17	30.029	29.659	29.130	0.599	6
C2-V8	40.0	24.87	0.13	24.02	0.12	30.693	30.727	30.776	0.527	5
C2-V9	22.0	25.42	0.24	24.00	0.21	30.523	29.918	29.054	0.726	4
C2-V10	22.0	24.71	0.09	24.20	0.18	29.810	30.118	30.557	0.601	5
C2-V11	24.0	25.23	0.16	23.94	0.33	30.436	29.969	29.302	0.933	4
C2-V12	26.0	25.03	0.09	24.02	0.12	30.333	30.160	29.912	0.508	5
C2-V13	18.2	25.83	0.25	24.96	0.30	30.711	30.630	30.514	0.899	4
C2-V14	27.0	25.73	0.18	24.13	0.13	31.081	30.324	29.243	0.578	4
C2-V15	27.0	25.71	0.26	24.67	0.30	31.064	30.862	30.573	0.920	5
C2-V16	23.0	24.61	0.15	23.25	0.20	29.773	29.230	28.453	0.667	1
C2-V17	41.0	24.24	0.10	23.17	0.15	30.091	29.911	29.653	0.561	3
C2-V18	34.0	25.04	0.22	23.66	0.12	30.665	30.160	29.439	0.592	4
C2-V19	58.0	24.80	0.18	23.83	0.21	31.063	31.038	31.002	0.705	5
C2-V20	26.0	24.84	0.11	24.00	0.08	30.144	30.138	30.129	0.469	6
C2-V22	18.0	25.19	0.12	24.45	0.28	30.051	30.104	30.179	0.807	6
C2-V24	13.4	25.72	0.16	24.35	0.19	30.235	29.613	28.723	0.648	3
C2-V26	27.5	25.32	0.15	23.97	0.10	30.690	30.185	29.464	0.520	5
C2-V27	27.5	25.08	0.10	23.80	0.25	30.456	30.017	29.390	0.751	4
C2-V28	16.5	25.20	0.14	24.22	0.14	29.956	29.757	29.472	0.572	4
C2-V29	18.7	25.58	0.14	24.58	0.14	30.493	30.279	29.972	0.566	4
C2-V30	14.9	25.35	0.14	24.39	0.42	29.985	29.791	29.515	1.114	2
C2-V31	33.0	25.16	0.11	23.73	0.19	30.750	30.190	29.389	0.636	6
C2-V32	25.5	25.29	0.16	24.23	0.23	30.570	30.345	30.025	0.729	4
C2-V33	32.0	24.64	0.10	23.65	0.09	30.196	30.061	29.868	0.476	6
C2-V34	48.0	24.35	0.08	23.25	0.08	30.388	30.202	29.937	0.459	4
C2-V35	28.3	25.24	0.20	24.32	0.44	30.646	30.573	30.469	1.185	6
C2-V38	75.0	24.69	0.10	23.15	0.11	31.260	30.701	29.903	0.502	5
C3-V1	19.4	25.77	0.17	24.91	0.14	30.722	30.665	30.583	0.574	4
C3-V3	30.0	24.99	0.08	23.91	0.47	30.462	30.236	29.912	1.217	3
C3-V4	27.0	25.22	0.10	24.28	0.21	30.569	30.469	30.326	0.665	6
C3-V5	19.4	25.01	0.08	24.25	0.10	29.965	30.004	30.060	0.480	3
C3-V6	22.0	25.14	0.11	24.17	0.09	30.243	30.083	29.854	0.483	4
C3-V8	19.4	25.38	0.13	24.31	0.17	30.332	30.055	29.660	0.602	3
C3-V10	41.0	24.21	0.06	23.28	0.11	30.060	30.024	29.973	0.489	3
C3-V11	13.5	25.43	0.09	24.26	0.13	29.954	29.529	28.923	0.528	0
C3-V12	24.1	25.74	0.13	24.52	0.19	30.954	30.562	30.002	0.649	5

Table 4—Continued

Object (1)	Period (days) (2)	$\langle V \rangle$ (3)	$\sigma_{\langle V \rangle}$ (4)	$\langle I \rangle$ (5)	$\sigma_{\langle I \rangle}$ (6)	U_V (7)	U_I (8)	U_T (9)	σ_{U_T} (10)	Quality Index (11)
C3-V14	14.4	26.47	0.25	25.31	1.44	31.067	30.663	30.085	3.545	2
C3-V15	8.3	25.60	0.12	23.20	0.24	29.538	27.818	25.362	0.729	1
C3-V16	16.0	26.18	0.23	25.08	0.24	30.901	30.571	30.099	0.781	4
C4-V1	39.0	25.63	0.19	24.09	0.29	31.423	30.772	29.843	0.848	6
C4-V2	18.7	25.73	0.16	25.10	0.20	30.637	30.799	31.030	0.662	5
C4-V3	60.0	25.13	0.15	24.10	1.45	31.436	31.347	31.219	3.556	1
C4-V4	26.0	25.39	0.14	24.69	0.26	30.697	30.831	31.021	0.767	6
C4-V5	38.0	26.13	0.19	24.38	0.15	31.887	31.028	29.801	0.605	5
C4-V6	19.2	25.44	0.13	24.51	0.18	30.380	30.244	30.051	0.625	4
C4-V7	13.2	26.23	0.17	25.06	0.21	30.721	30.298	29.692	0.690	3
C4-V8	25.0	25.00	0.14	23.74	0.27	30.254	29.830	29.223	0.795	2
C4-V9	24.0	25.28	0.11	24.08	0.14	30.485	30.111	29.578	0.556	4
C4-V10	24.5	25.56	0.14	24.34	0.42	30.798	30.399	29.829	1.125	3
C4-V11	24.5	24.93	0.09	23.72	0.19	30.166	29.779	29.225	0.621	2
C4-V13	25.0	25.31	0.16	24.03	0.19	30.573	30.118	29.468	0.663	6
C4-V14	70.0	25.44	0.13	23.27	0.09	31.933	30.728	29.007	0.499	1

Table 5. Data for Nine Cepheid-Calibrated SNe Ia

SN Ia	Galaxy (Cepheids)	$(m-M)_{AB}$	$(m-M)_{AV}$	M_B^0(max)	M_V^0(max)	Δm_{15}	Sources
1937C	IC 4182 (39)	28.36 ± 0.09	28.36 ± 0.12	-19.53 ± 0.15	-19.48 ± 0.17	0.87 ± 0.10	1,2
1895B	NGC 5253 (15)	28.13 ± 0.08	28.10 ± 0.07	-19.87 ± 0.22	···		3,4
1972E	NGC 5253 (15)	28.13 ± 0.08	28.10 ± 0.07	-19.52 ± 0.22	-19.49 ± 0.14	0.87 ± 0.10	3,5
1981B	NGC 4536 (74)	31.10 ± 0.05[a]	31.10 ± 0.05[a]	-19.46 ± 0.21	-19.44 ± 0.18	1.10 ± 0.07	6,7
1960F	NGC 4496A (95)	31.16 ± 0.10	31.13 ± 0.10	-19.56 ± 0.14	-19.62 ± 0.18	1.06 ± 0.12	8,9
1990N	NGC 4639 (20)	32.03 ± 0.22[a]	32.03 ± 0.22[a]	-19.33 ± 0.23	-19.42 ± 0.23	1.07 ± 0.05	10,11
1989B	NGC 3627 (58)	30.22 ± 0.12[a]	30.22 ± 0.12[a]	-19.36 ± 0.18	-19.34 ± 0.16	1.31 ± 0.07	12,13
1974G	NGC 4414 (9)	31.41 ± 0.17[a]	31.41 ± 0.17[a]	-19.59 ± 0.35	-19.61 ± 0.30	1.11 ± 0.06	14
1998bu	NGC 3368 (7)	30.37 ± 0.16[a]	30.37 ± 0.16[a]	-19.53 ± 0.30	-19.51 ± 0.25	1.01 ± 0.05	15,16
Straight mean (neglects 1895B)				-19.49 ± 0.03	-19.49 ± 0.03		
Weighted mean (neglects 1895B)				-19.49 ± 0.07	-19.48 ± 0.07		

[a]The true modulus is listed.

References. — (1) Sandage et al. 1992; Saha et al. 1994; (2) Schaefer 1996; Jacoby & Pierce 1996; (3) Sandage et al. 1994; Saha et al. 1995; (4) Schaefer 1995a; (5) Hamuy et al. 1995; (6) Saha et al. 1996a; (7) Schaefer 1995a, b; Phillips 1993; (8) Saha et al. 1996b; (9) Leibundgut et al. 1991b; Schaefer 1995c; (10) Sandage et al. 1996; (11) Leibundgut et al. 1991a; (12) Wells et al. 1994; (13) this paper; (14) Schaefer 1998; (15) Tanvir et al. 1995; (16) Suntzeff et al.1998.

Table 6. Fiducial Sample Reduced with Variable H_0

SN Ia (1)	T (2)	$\log v$ (3)	B_0 (4)	V_0 (5)	I_0 (6)	H_0 (7)	$m-M$ (8)	$M_B^0(v)$ (9)	$M_V^0(v)$ (10)	$M_I^0(v)$ (11)	Δm_{15}^B (12)
1937C	5		8.83	8.86							0.87 ± 0.10
1956A	3	3.160	12.69	12.49		59.5	31.93	−19.24	−19.44		
1959C	5	3.526	13.65	13.76		57.5	33.83	−20.18	−20.07		
1960F	5		11.60	11.51							
1967C	5	3.198	13.25	13.26		59.3	32.12	−18.87	−18.86		
1969C	5	3.537	13.78	13.71		57.4	33.89	−20.11	−20.18		
1971L	3	3.279	12.59	12.42		58.8	32.55	−19.96	−20.13		
1972E	5		8.49	8.52							0.87 ± 0.10
1972H	3	3.504	14.35	14.19		57.6	33.72	−19.37	−19.53		
1973N	5	3.656	14.76	14.82		56.8	34.51	−19.75	−19.69		
1974G	5		12.48	12.27							1.11 ± 0.06
1975O	3	3.701	15.17	15.04		56.6	34.74	−19.57	−19.70		
1976J	5	3.637	14.28	14.26		56.9	34.41	−20.13	−20.15		0.90 ± 0.10
1981B	4		11.64	11.66							1.10 ± 0.07
1990N	3		12.67	12.63							1.07 ± 0.05
1991S	3	4.223	17.81	17.77	18.07	55.0	37.41	−19.60	−19.64	−19.34	1.04 ± 0.10
1991T	3	3.072	11.69	11.51	11.62	59.9	31.47	−19.78	−19.96	−19.85	0.94 ± 0.10
1991U	4	3.992	16.40	16.34	16.52	55.0	36.26	−19.86	−19.92	−19.74	1.06 ± 0.10
1991ag	3	3.616	14.62	14.54	14.86	57.0	34.30	−19.68	−19.76	−19.44	0.87 ± 0.10
1992ag	5	3.891	16.41	16.28	16.41	55.5	35.73	−19.32	−19.45	−19.32	1.19 ± 0.10
1992al	3	3.627	14.60	14.65	14.94	57.0	34.36	−19.76	−19.71	−19.42	1.11 ± 0.05
1992bh	4	4.131	17.70	17.62	17.80	55.0	36.95	−19.25	−19.33	−19.15	1.05 ± 0.10
1992bs	3	4.279	18.37	18.30		55.0	37.69	−19.32	−19.39		1.13 ± 0.10
1993B	3	4.326	18.53	18.41	18.70	55.0	37.93	−19.40	−19.52	−19.23	1.04 ± 0.10
1994S	4	3.684	14.81	14.82		56.6	34.66	−19.85	−19.84		
1994ae	5	3.198	13.12	13.02		59.3	32.12	−19.00	−19.10		
							Mean	−19.60	−19.67	−19.44	1.03
							rms	0.347	0.353	0.242	0.10
1991G	1	3.343	13.85	13.94		58.5	32.88	−19.03	−18.94		
1980N	1	3.158	12.49	12.44	12.70	59.5	32.88	−19.43	−19.48	−19.22	1.07 ± 0.04
1981D	1	3.158	12.59	12.40		59.5	31.92	−19.33	−19.52		1.28 ± 0.10
1984A	1	3.072	12.45	12.26		59.9	31.47	−19.02	−19.21		1.20 ± 0.12
1990O	1	3.958	16.32	16.31	16.70	55.2	36.08	−19.76	−19.77	−19.38	0.96 ± 0.10
1990T	1	4.080	17.16	17.12	17.35	55.0	36.70	−19.54	−19.58	−19.35	1.15 ± 0.10
1992P	1	3.897	16.08	16.11	16.39	55.5	35.76	−19.68	−19.65	−19.37	0.87 ± 0.10
1992aq	1	4.481	19.45	19.35	19.77	55.0	38.70	−19.25	−19.35	−18.93	1.46 ± 0.10
1992bg	1	4.030	16.72	16.76	17.04	55.0	36.45	−19.73	−19.69	−19.41	1.15 ± 0.10
1992bc	2	3.774	15.16	15.24	15.58	56.2	35.12	−19.96	−19.88	−19.54	0.87 ± 0.05
							Mean	−19.47	−19.51	−19.54	1.11
							rms	0.317	0.279	0.194	0.19
1961D	−2	3.913	16.46	16.67		55.4	35.85	−19.39	−19.18		
1962A	−2	3.804	15.56	15.67		56.0	35.28	−19.72	−19.61		
1965I	−1	3.214	12.40	12.57		59.2	32.21	−19.81	−19.64		
1966K	−1	4.005	17.00	17.00		55.0	36.32	−19.32	−19.32		
1970J	−3	3.536	14.84	14.74		57.4	33.89	−19.05	−19.15		1.30 ± 0.12
1972J	−1	3.457	14.64	14.54		57.9	33.47	−18.83	−18.93		
1990af	−1	4.178	17.87	17.82		55.0	37.19	−19.32	−19.37		1.56 ± 0.05
1992A	0	3.158	12.57	12.55	12.80	59.5	31.92	−19.35	−19.37	−19.12	1.47 ± 0.05
1992J	−2	4.137	17.70	17.58	17.84	55.0	36.98	−19.28	−19.40	−19.14	1.56 ± 0.10
1992ae	−3	4.351	18.62	18.51		55.0	38.05	−19.43	−19.54		1.28 ± 0.10
1992au	−3	4.260.	18.21	18.16	18.41	55.0	37.60	−19.39	−19.44	−19.19	1.49 ± 0.10
1992bk	−3	4.240	18.11	18.11	18.31	55.0	37.50	−19.39	−19.39	−19.19	1.57 ± 0.10

Table 6—Continued

SN Ia (1)	T (2)	$\log v$ (3)	B_0 (4)	V_0 (5)	I_0 (6)	H_0 (7)	$m-M$ (8)	$M_B^0(v)$ (9)	$M_V^0(v)$ (10)	$M_I^0(v)$ (11)	Δm_{15}^B (12)
1992bl	0	4.110	17.36	17.36	17.64	55.0	36.85	−19.49	−19.49	−19.21	1.51 ± 0.10
1992bo	−2	3.736	15.86	15.85	15.97	56.4	34.92	−19.06	−19.07	−18.95	1.69 ± 0.10
1992bp	−2	4.374	18.41	18.46	18.78	55.0	38.17	−19.76	−19.71	−19.39	1.32 ± 0.10
1992br	−3	4.420	19.38	19.34		55.0	38.40	−19.02	−19.06		1.69 ± 0.10
1993O	−2	4.193	17.67	17.76	17.99	55.0	37.26	−19.59	−19.50	−19.27	1.22 ± 0.05
1993ag	−2	4.177	17.72	17.69	18.01	55.0	37.18	−19.46	−19.49	−19.17	1.32 ± 0.10
1993ah	−1	3.935	16.33	16.37	16.68	55.3	35.96	−19.63	−19.59	−19.28	1.30 ± 0.10
1994D	−1	3.072	11.86	11.90	12.11	59.9	31.47	−19.61	−19.57	−19.36	1.32 ± 0.05
1994M	−3	3.862	16.42	16.29		55.7	35.58	−19.16	−19.29		
1994Q	−1	3.938	16.83	16.83		55.3	35.98	−19.15	−19.15		
1995D	0	3.328	13.33	13.35		58.6	32.80	−19.47	−19.45		
							Mean	−19.38	−19.38	−19.21	1.44
							rms	0.258	0.207	0.121	0.155

Table 7. Mean Absolute Magnitudes Corrected for Decay Rate as Function of Morphological Type based on H_0 (global) = 55[a]

T (1)	$\langle M_B^{15} \rangle$ (2)	$\langle M_V^{15} \rangle$ (3)	$\langle M_I^{15} \rangle$ (4)	$n(B,V)$ (5)	$n(I)$ (6)
3, 4, 5	−19.54 ± 0.078	−19.58 ± 0.071	−19.38 ± 0.088	10	8
1, 2	−19.51 ± 0.071	−19.48 ± 0.054	−19.24 ± 0.054	9	7
−3 to 0	−19.64 ± 0.043	−19.54 ± 0.032	−19.32 ± 0.024	15	11
All	−19.57 ± 0.034	−19.54 ± 0.028	−19.32 ± 0.032	34	26
		Calibrators from Table 5			
3, 4, 5	−19.43 ± 0.047	−19.39 ± 0.071	···	8	···

[a]Listed are the magnitudes corrected for decay rate via equations (15), (16), and (17).

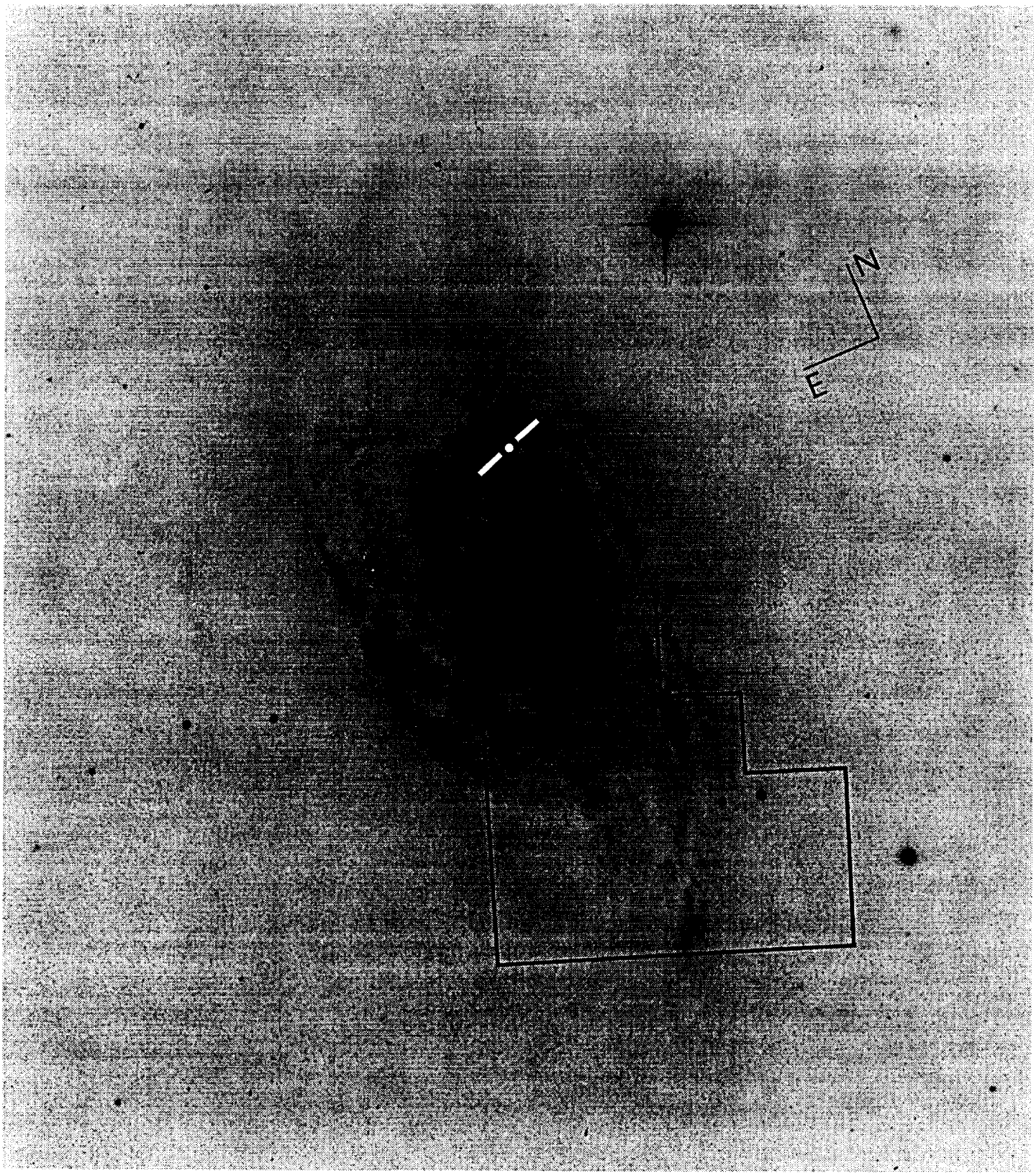
N
E

Fig 3a

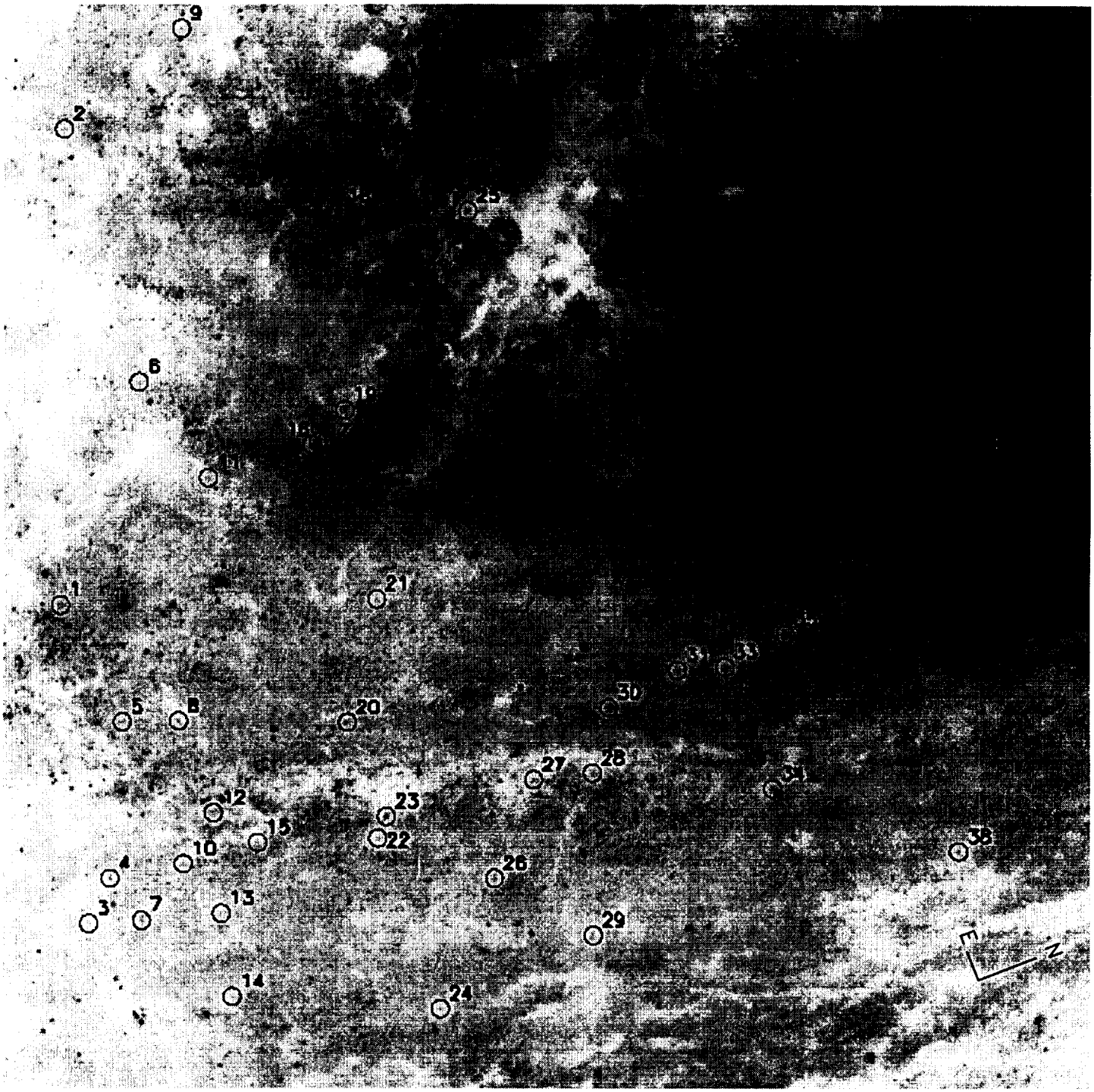

Fig 3b

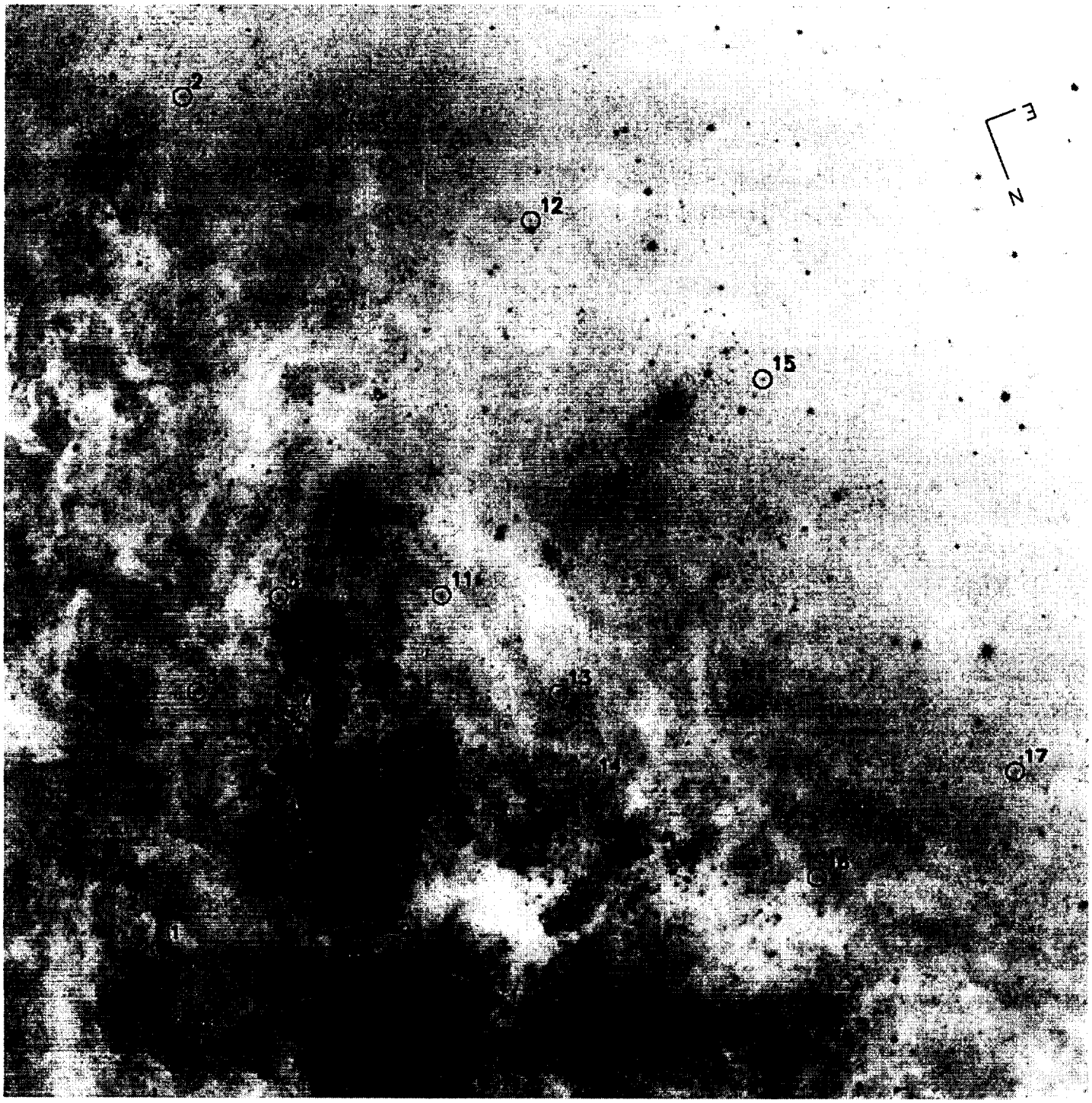

Fig 3c.

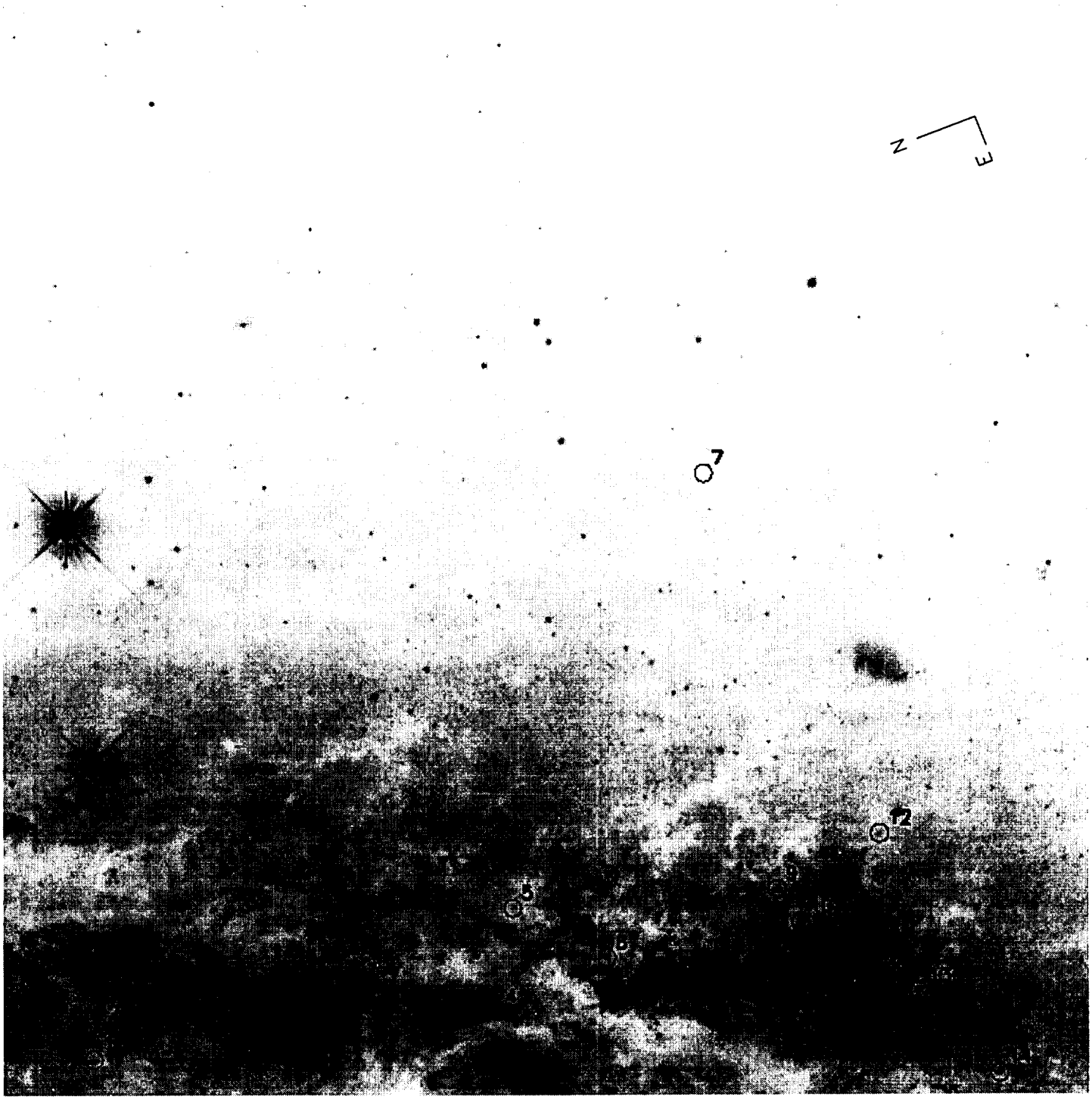

Fig 3d

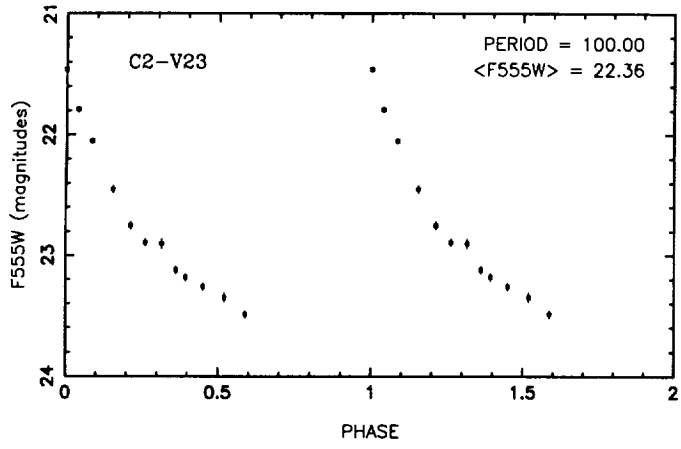
C2-V23
PERIOD = 100.00
<F555W> = 22.36
F555W (magnitudes)
PHASE

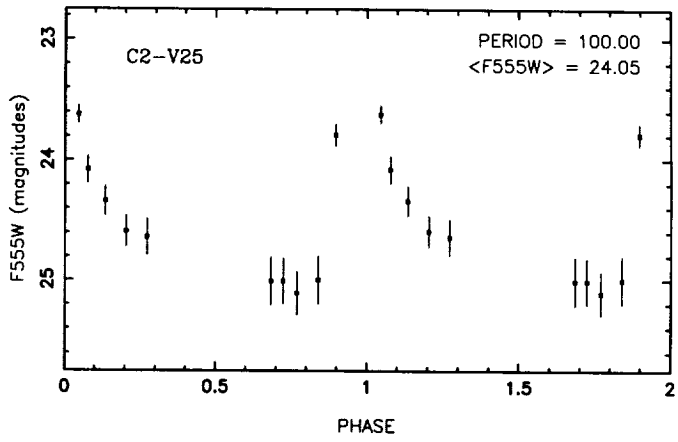
C2-V25
PERIOD = 100.00
<F555W> = 24.05
F555W (magnitudes)
PHASE

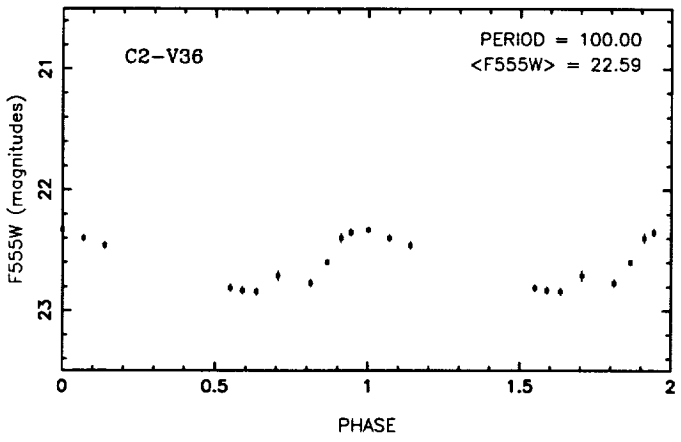
C2-V36
PERIOD = 100.00
<F555W> = 22.59
F555W (magnitudes)
PHASE

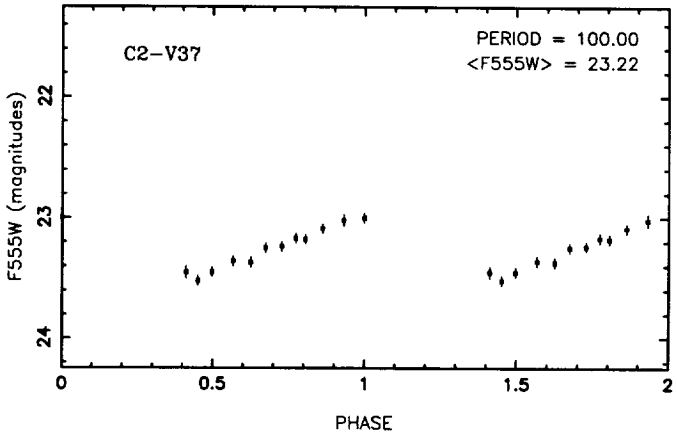
C2-V37
PERIOD = 100.00
<F555W> = 23.22
F555W (magnitudes)
PHASE

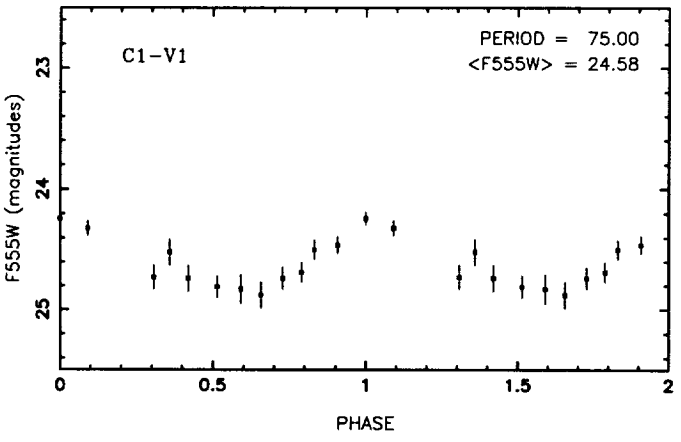
C1-V1
PERIOD = 75.00
<F555W> = 24.58
F555W (magnitudes)
PHASE

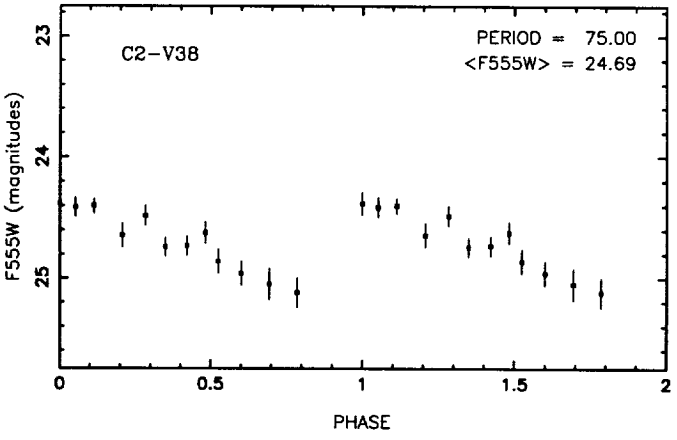
C2-V38
PERIOD = 75.00
<F555W> = 24.69
F555W (magnitudes)
PHASE

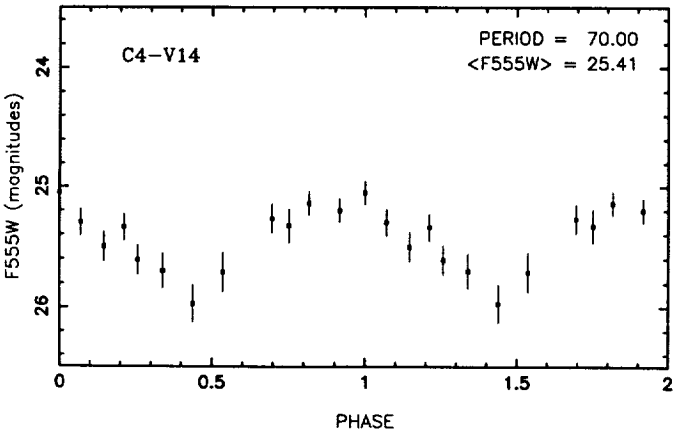
C4-V14
PERIOD = 70.00
<F555W> = 25.41
F555W (magnitudes)
PHASE

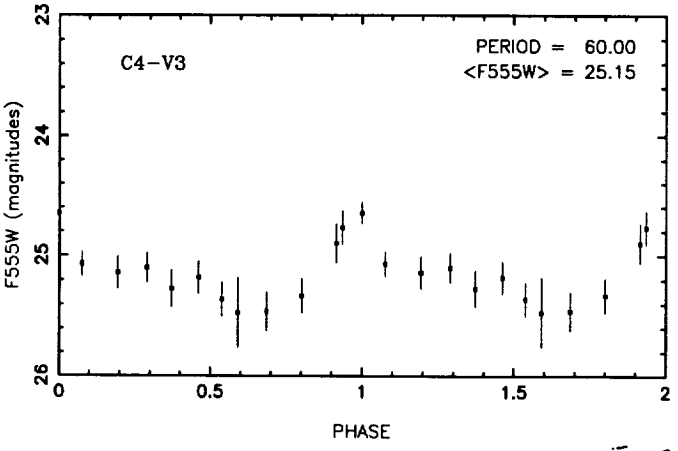
C4-V3
PERIOD = 60.00
<F555W> = 25.15
F555W (magnitudes)
PHASE

Fig. 1

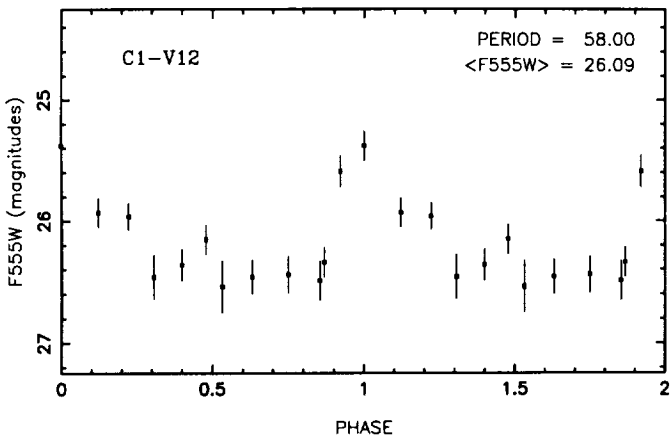
C1-V12
PERIOD = 58.00
<F555W> = 26.09
F555W (magnitudes)
PHASE

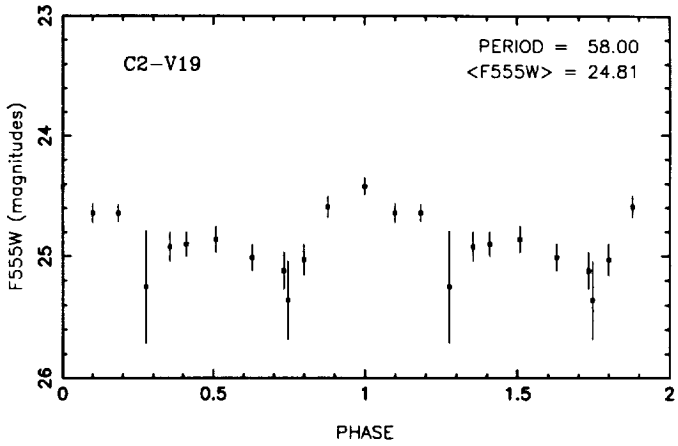
C2-V19
PERIOD = 58.00
<F555W> = 24.81
F555W (magnitudes)
PHASE

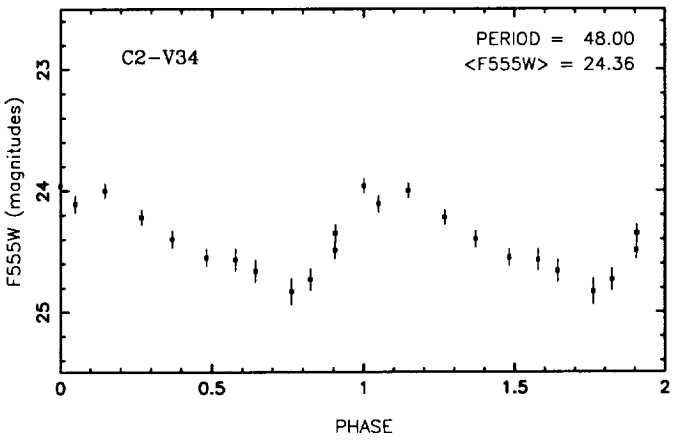
C2-V34
PERIOD = 48.00
<F555W> = 24.36
F555W (magnitudes)
PHASE

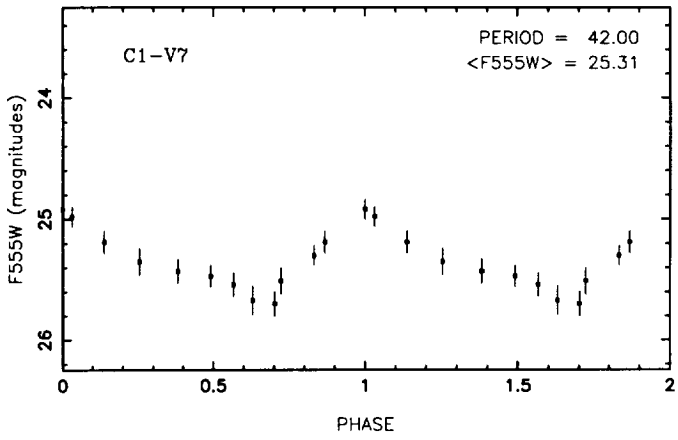
C1-V7
PERIOD = 42.00
<F555W> = 25.31
F555W (magnitudes)
PHASE

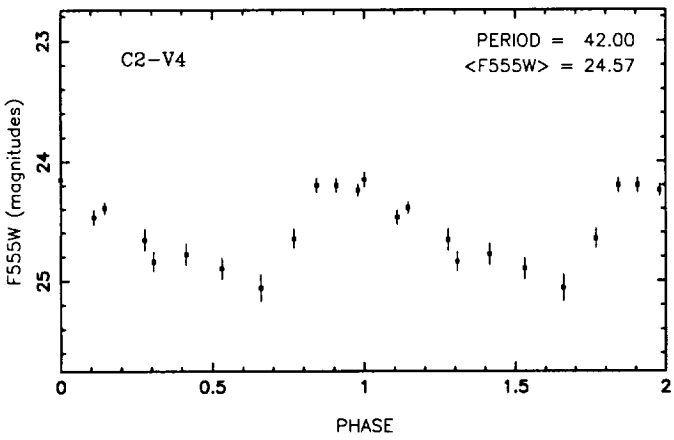
C2-V4
PERIOD = 42.00
<F555W> = 24.57
F555W (magnitudes)
PHASE

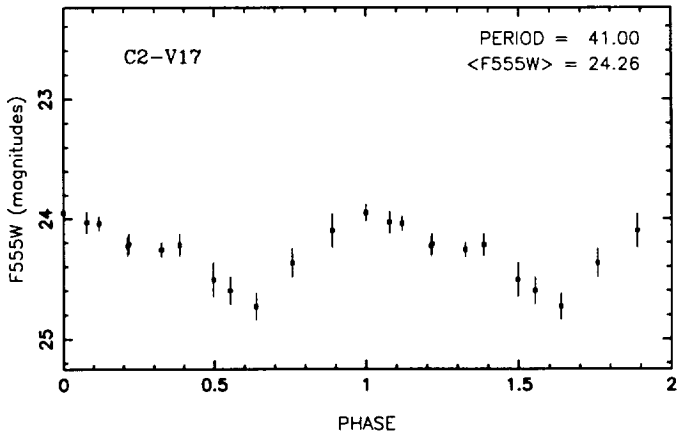
C2-V17
PERIOD = 41.00
<F555W> = 24.26
F555W (magnitudes)
PHASE

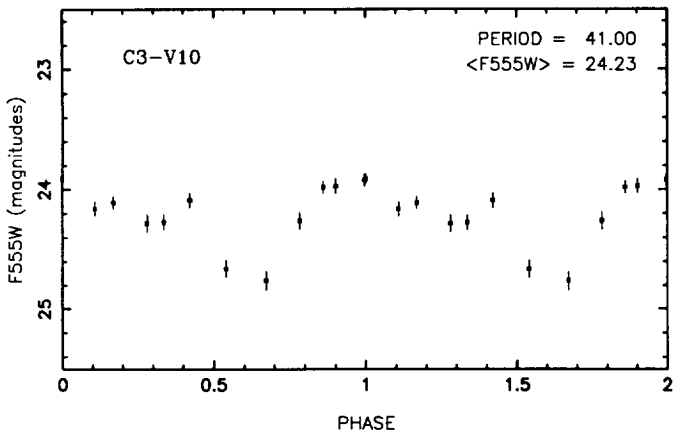
C3-V10
PERIOD = 41.00
<F555W> = 24.23
F555W (magnitudes)
PHASE

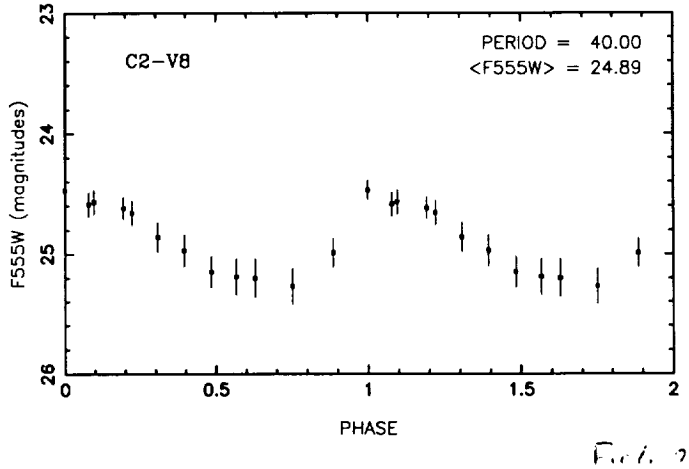
C2-V8
PERIOD = 40.00
<F555W> = 24.89
F555W (magnitudes)
PHASE

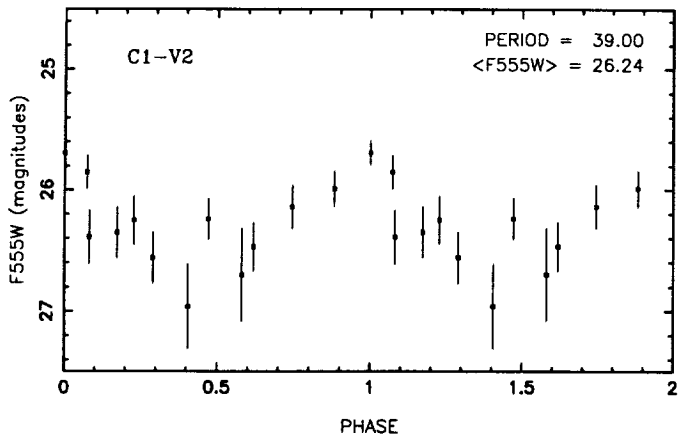
C1–V2
PERIOD = 39.00
<F555W> = 26.24
F555W (magnitudes)
PHASE

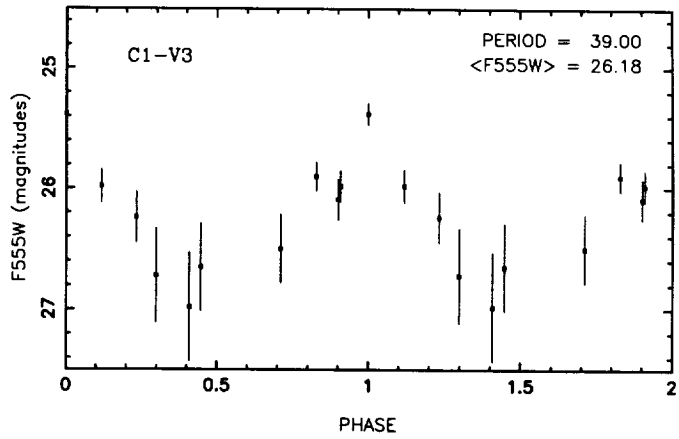
C1–V3
PERIOD = 39.00
<F555W> = 26.18
F555W (magnitudes)
PHASE

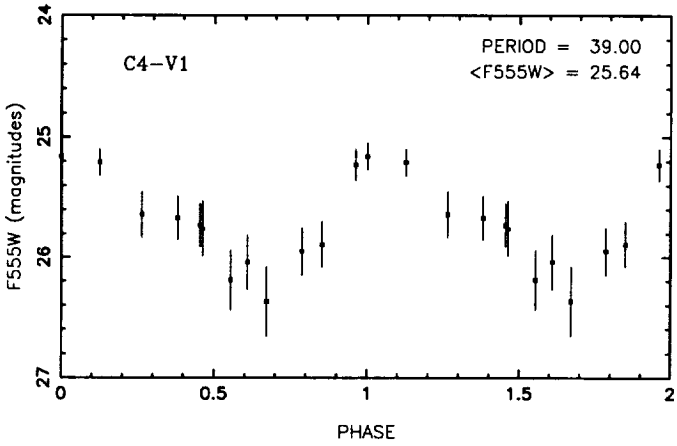
C4–V1
PERIOD = 39.00
<F555W> = 25.64
F555W (magnitudes)
PHASE

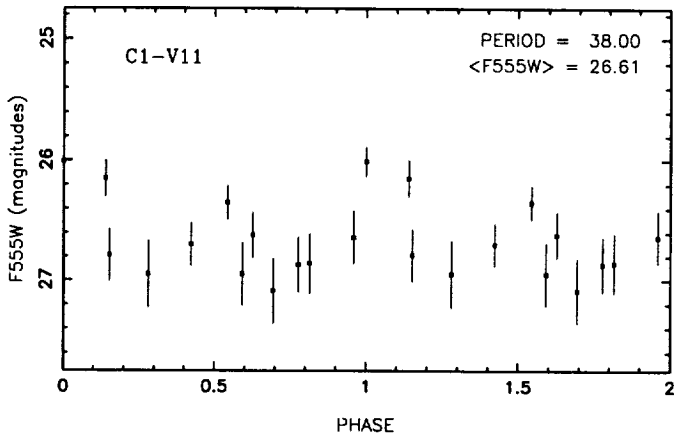
C1–V11
PERIOD = 38.00
<F555W> = 26.61
F555W (magnitudes)
PHASE

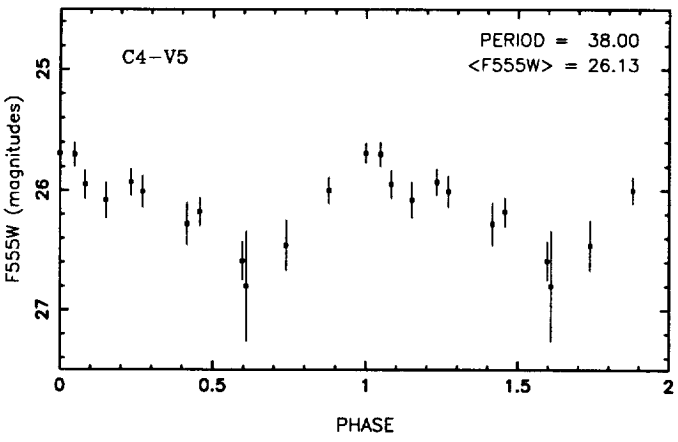
C4–V5
PERIOD = 38.00
<F555W> = 26.13
F555W (magnitudes)
PHASE

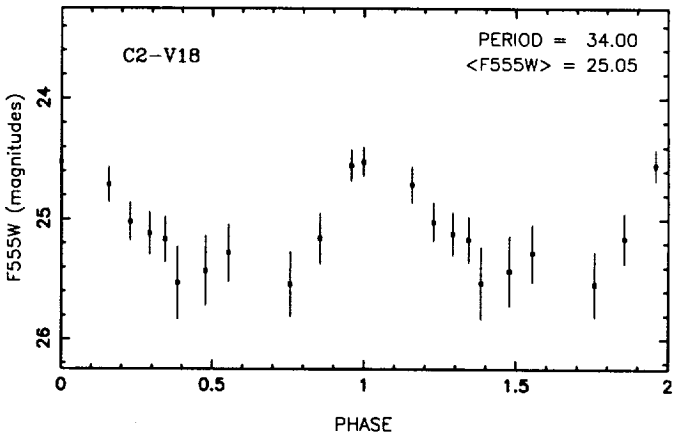
C2–V18
PERIOD = 34.00
<F555W> = 25.05
F555W (magnitudes)
PHASE

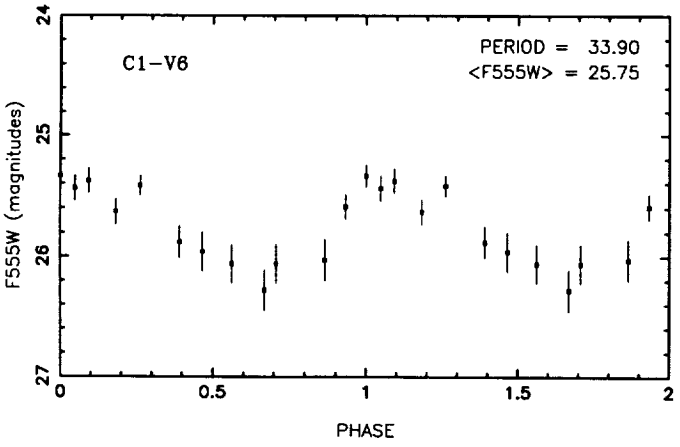
C1–V6
PERIOD = 33.90
<F555W> = 25.75
F555W (magnitudes)
PHASE

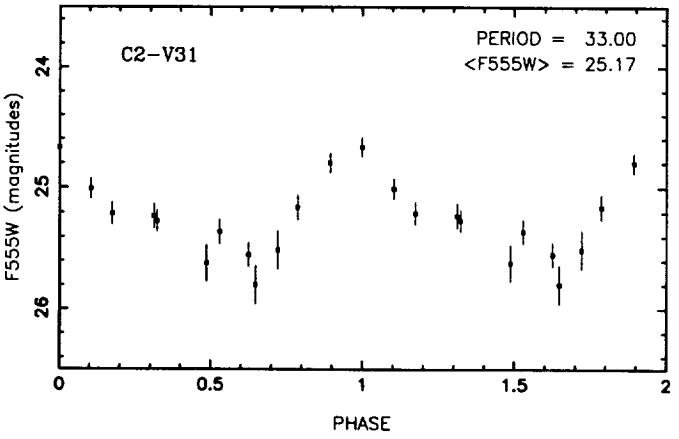
C2–V31
PERIOD = 33.00
<F555W> = 25.17
F555W (magnitudes)
PHASE

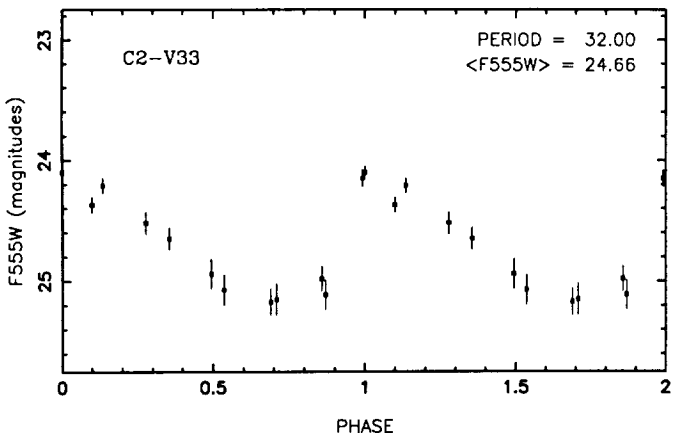
C2-V33
PERIOD = 32.00
<F555W> = 24.66
F555W (magnitudes)
PHASE

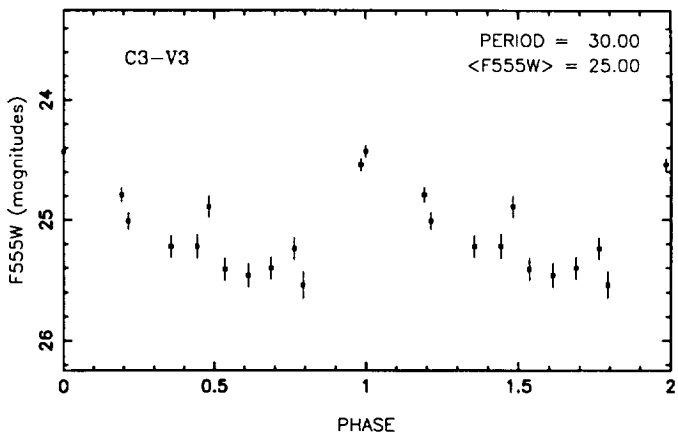
C3-V3
PERIOD = 30.00
<F555W> = 25.00
F555W (magnitudes)
PHASE

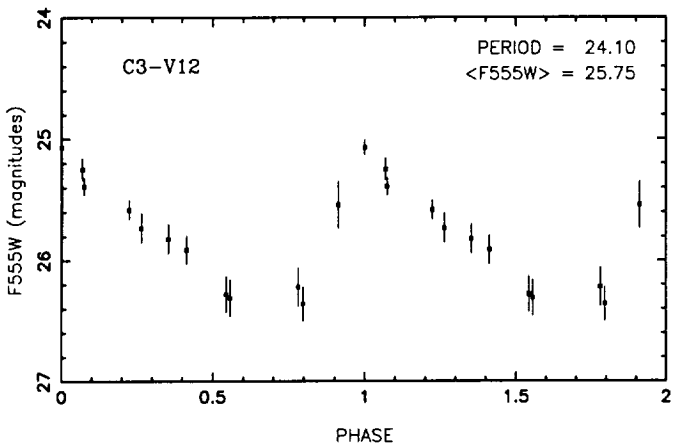
C3-V12
PERIOD = 24.10
<F555W> = 25.75
F555W (magnitudes)
PHASE

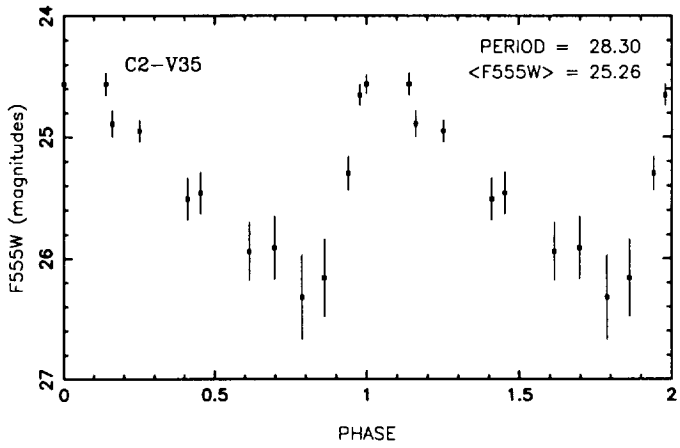
C2-V35
PERIOD = 28.30
<F555W> = 25.26
F555W (magnitudes)
PHASE

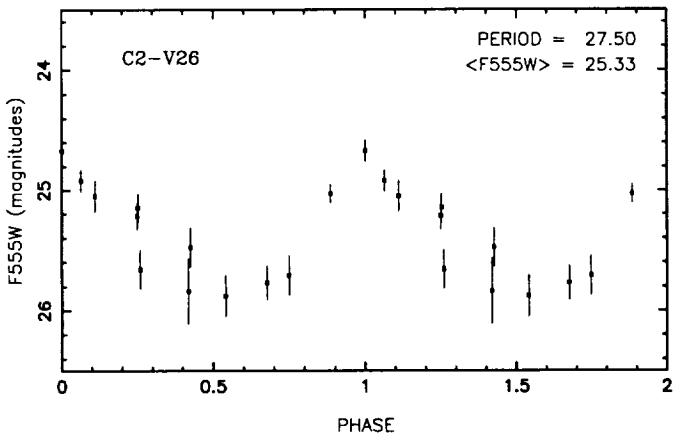
C2-V26
PERIOD = 27.50
<F555W> = 25.33
F555W (magnitudes)
PHASE

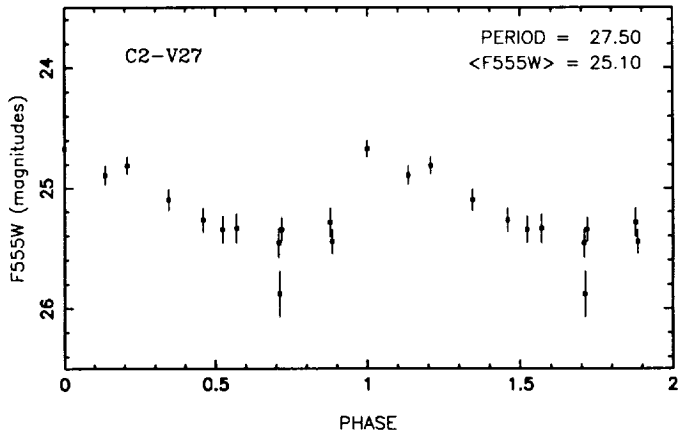
C2-V27
PERIOD = 27.50
<F555W> = 25.10
F555W (magnitudes)
PHASE

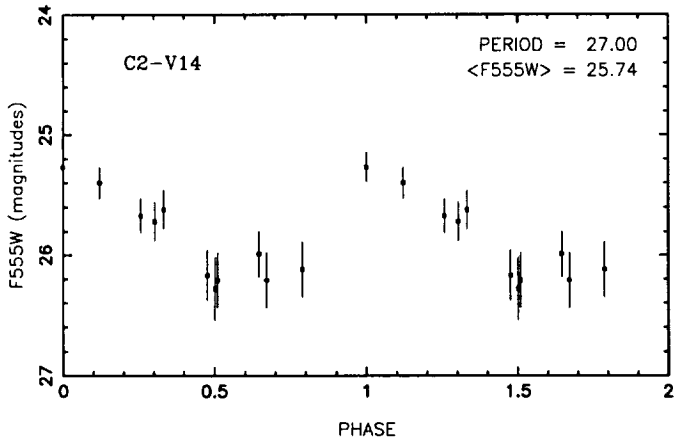
C2-V14
PERIOD = 27.00
<F555W> = 25.74
F555W (magnitudes)
PHASE

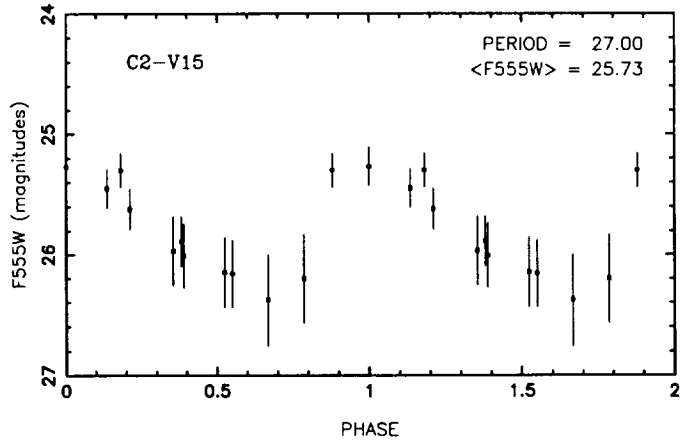
C2-V15
PERIOD = 27.00
<F555W> = 25.73
F555W (magnitudes)
PHASE

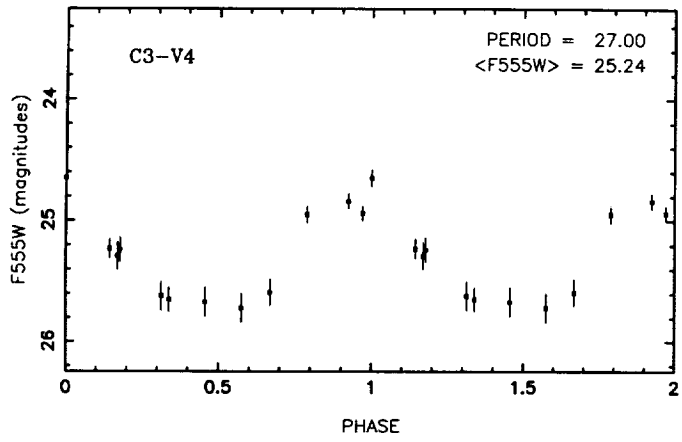
C3-V4
PERIOD = 27.00
<F555W> = 25.24
F555W (magnitudes)
PHASE

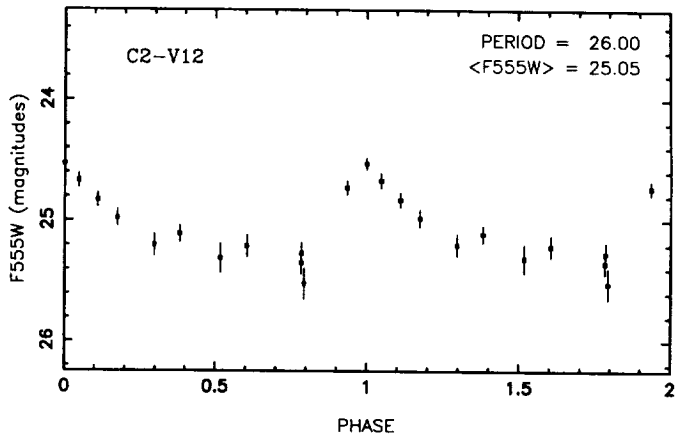
C2-V12
PERIOD = 26.00
<F555W> = 25.05
F555W (magnitudes)
PHASE

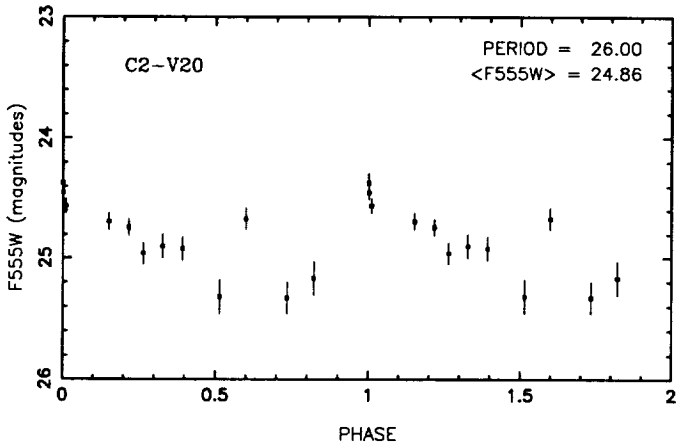
C2-V20
PERIOD = 26.00
<F555W> = 24.86
F555W (magnitudes)
PHASE

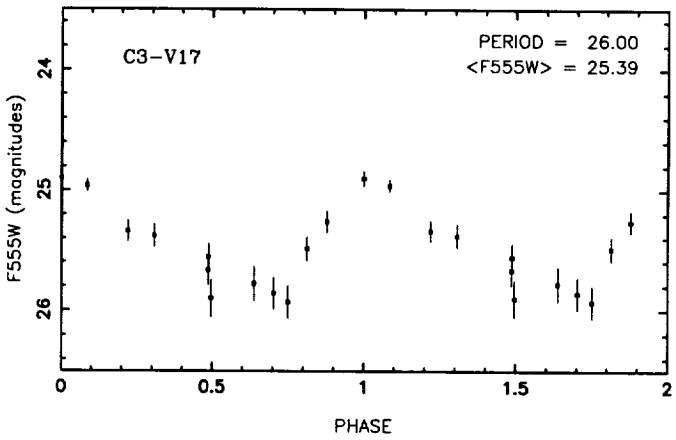
C3-V17
PERIOD = 26.00
<F555W> = 25.39
F555W (magnitudes)
PHASE

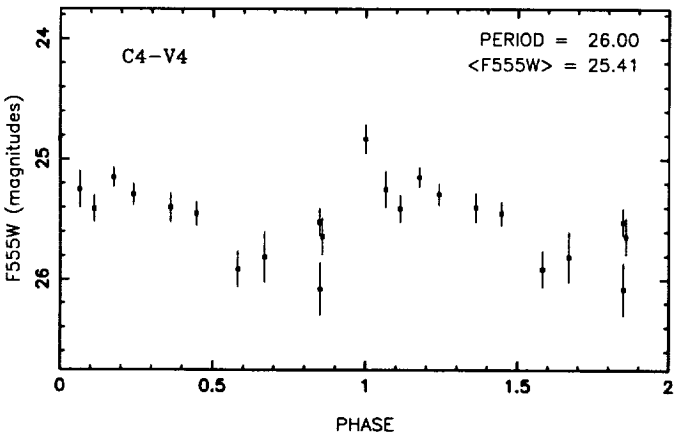
C4-V4
PERIOD = 26.00
<F555W> = 25.41
F555W (magnitudes)
PHASE

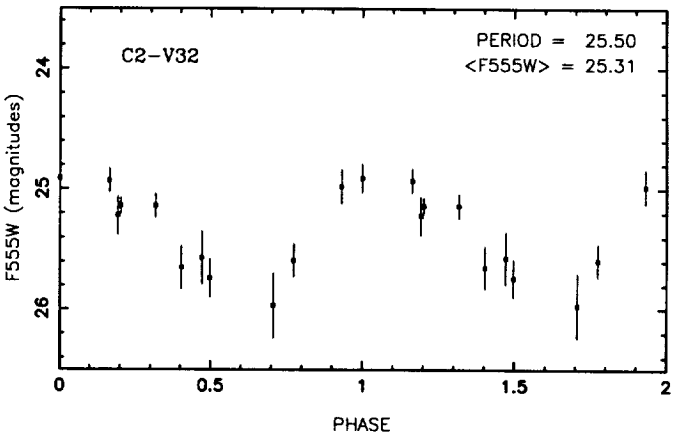
C2-V32
PERIOD = 25.50
<F555W> = 25.31
F555W (magnitudes)
PHASE

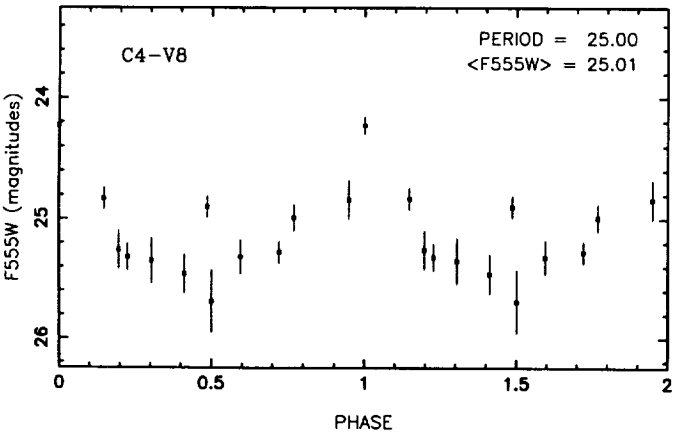
C4-V8
PERIOD = 25.00
<F555W> = 25.01
F555W (magnitudes)
PHASE

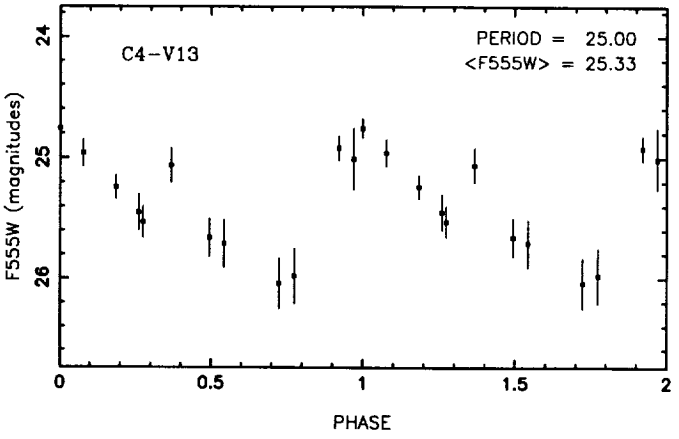
C4-V13
PERIOD = 25.00
<F555W> = 25.33
F555W (magnitudes)
PHASE

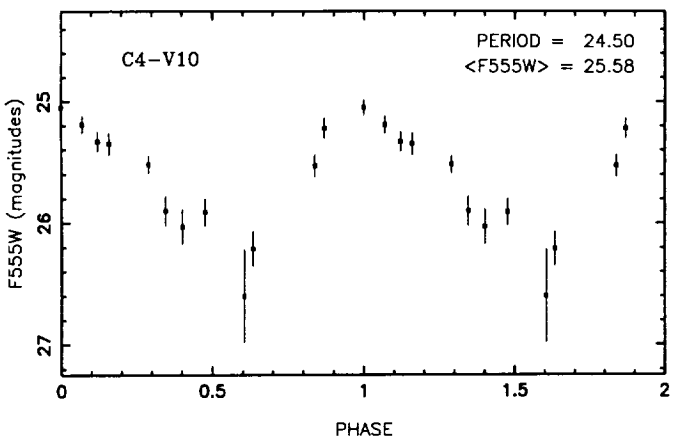
C4-V10
PERIOD = 24.50
<F555W> = 25.58
F555W (magnitudes)
PHASE

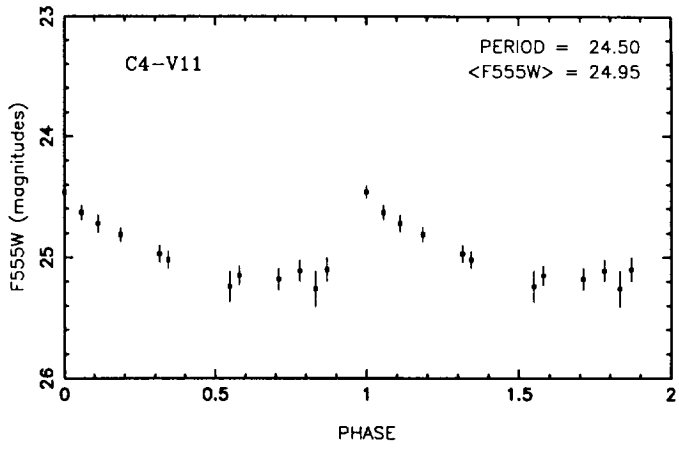
C4-V11
PERIOD = 24.50
<F555W> = 24.95
F555W (magnitudes)
PHASE

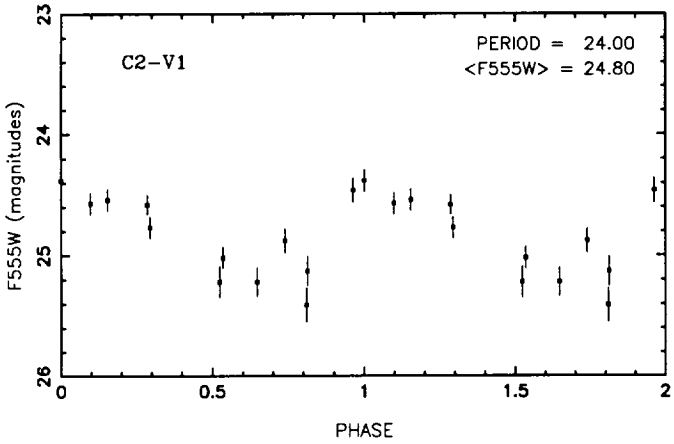
C2-V1
PERIOD = 24.00
<F555W> = 24.80
F555W (magnitudes)
PHASE

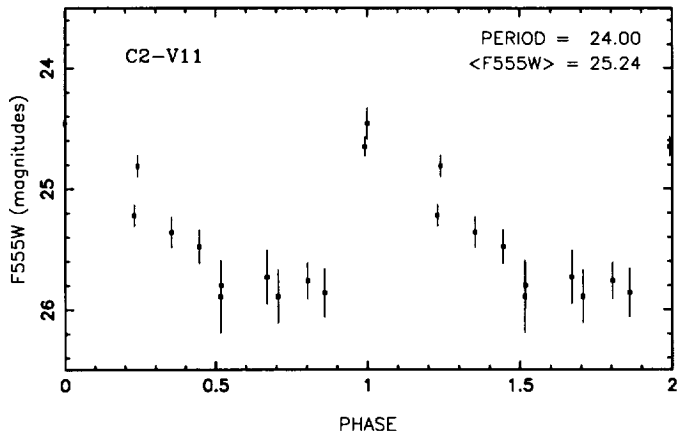
C2-V11
PERIOD = 24.00
<F555W> = 25.24
F555W (magnitudes)
PHASE

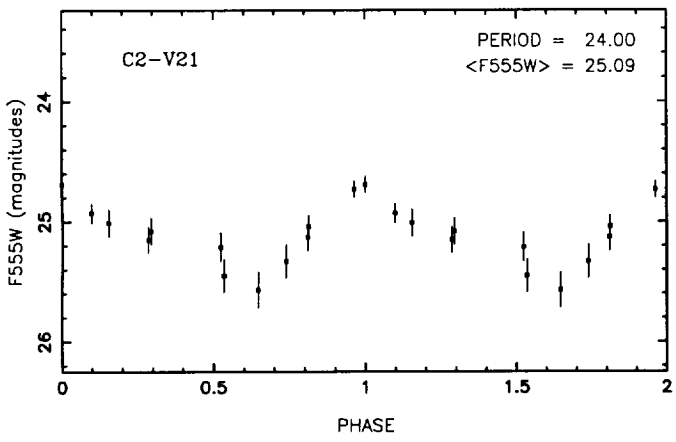
C2-V21
PERIOD = 24.00
<F555W> = 25.09
F555W (magnitudes)
PHASE

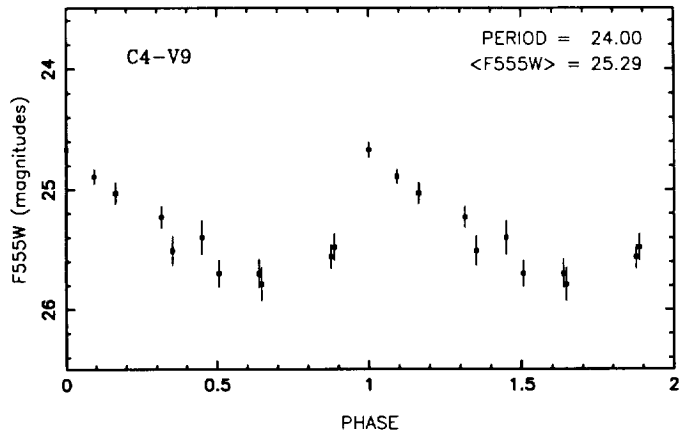
C4-V9
PERIOD = 24.00
<F555W> = 25.29
F555W (magnitudes)
PHASE

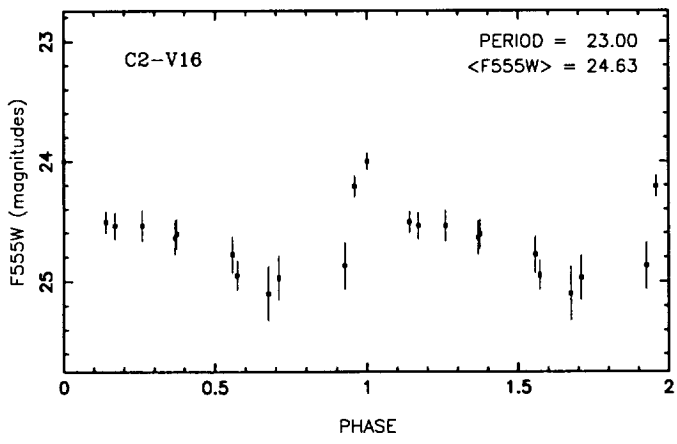
C2-V16
PERIOD = 23.00
<F555W> = 24.63
F555W (magnitudes)
PHASE

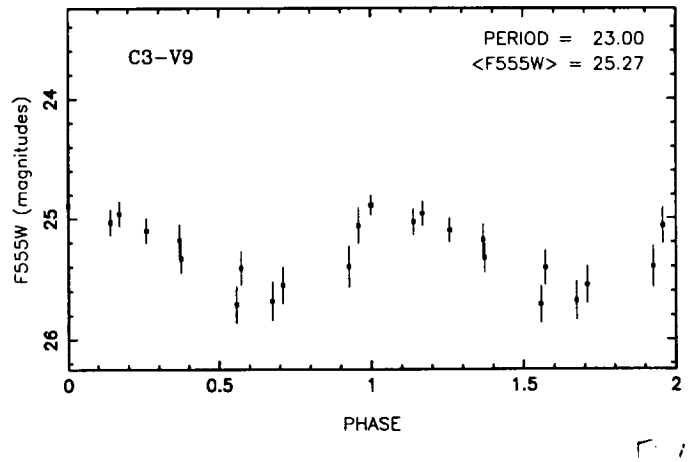
C3-V9
PERIOD = 23.00
<F555W> = 25.27
F555W (magnitudes)
PHASE

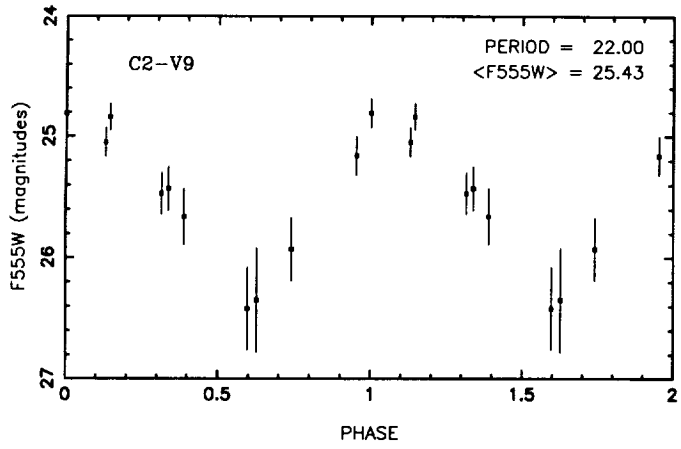
C2-V9
PERIOD = 22.00
<F555W> = 25.43
F555W (magnitudes)
PHASE

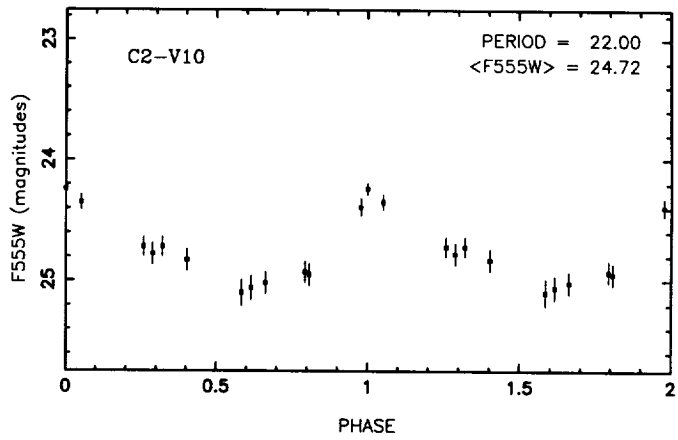
C2-V10
PERIOD = 22.00
<F555W> = 24.72
F555W (magnitudes)
PHASE

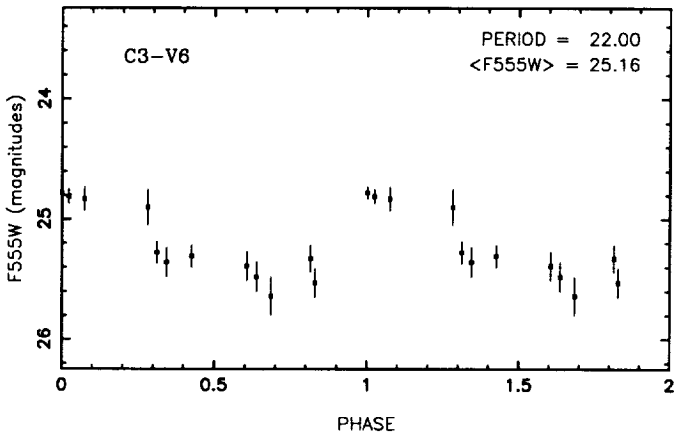
C3-V6
PERIOD = 22.00
<F555W> = 25.16
F555W (magnitudes)
PHASE

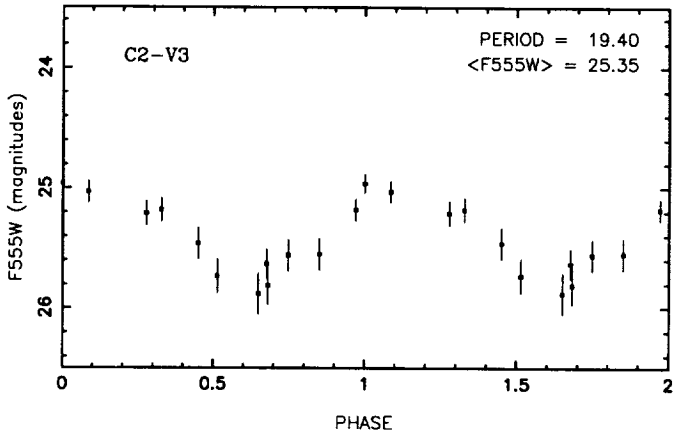
C2-V3
PERIOD = 19.40
<F555W> = 25.35
F555W (magnitudes)
PHASE

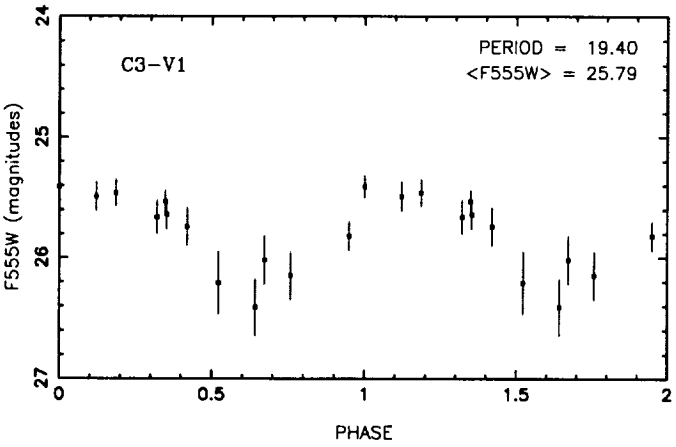
C3-V1
PERIOD = 19.40
<F555W> = 25.79
F555W (magnitudes)
PHASE

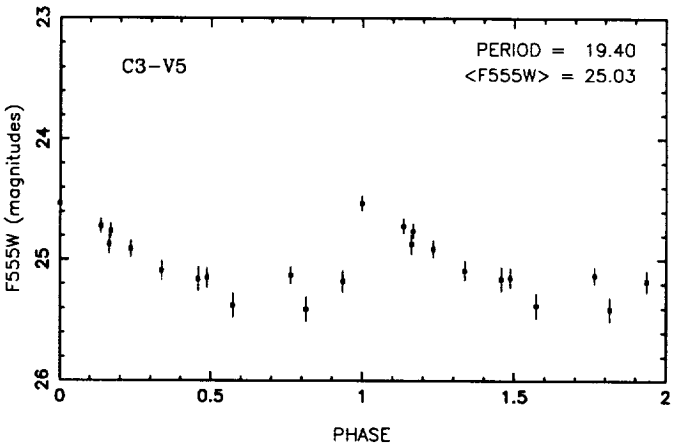
C3-V5
PERIOD = 19.40
<F555W> = 25.03
F555W (magnitudes)
PHASE

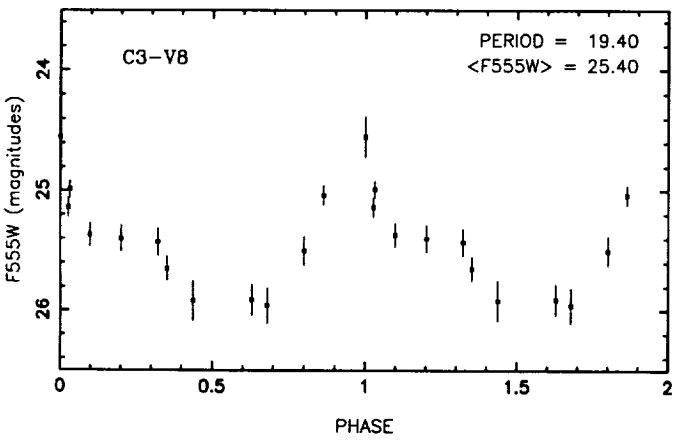
C3-V8
PERIOD = 19.40
<F555W> = 25.40
F555W (magnitudes)
PHASE

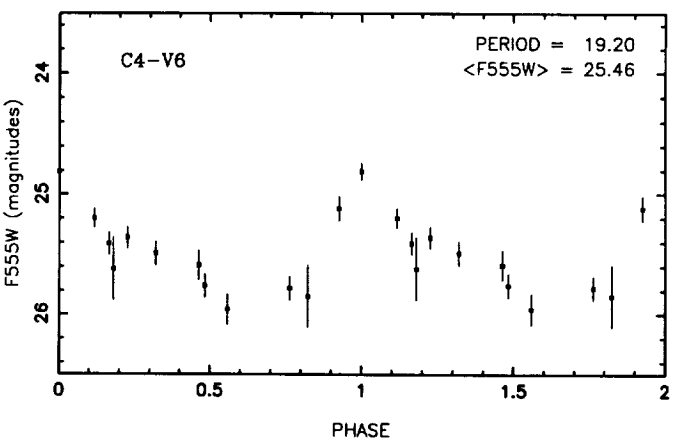
C4-V6
PERIOD = 19.20
<F555W> = 25.46
F555W (magnitudes)
PHASE

Fig 4.7

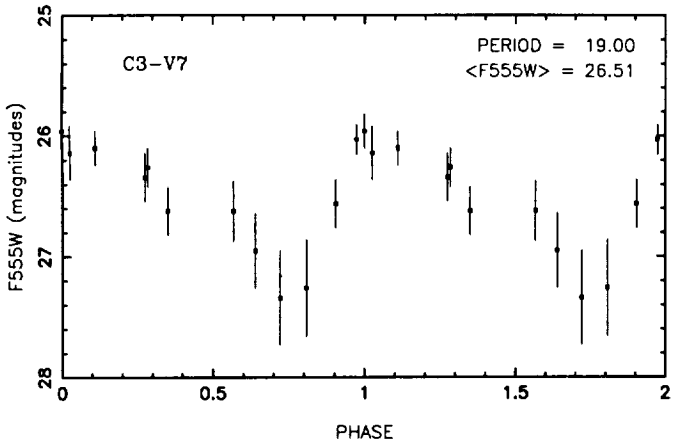
C3-V7
PERIOD = 19.00
<F555W> = 26.51
F555W (magnitudes)
PHASE

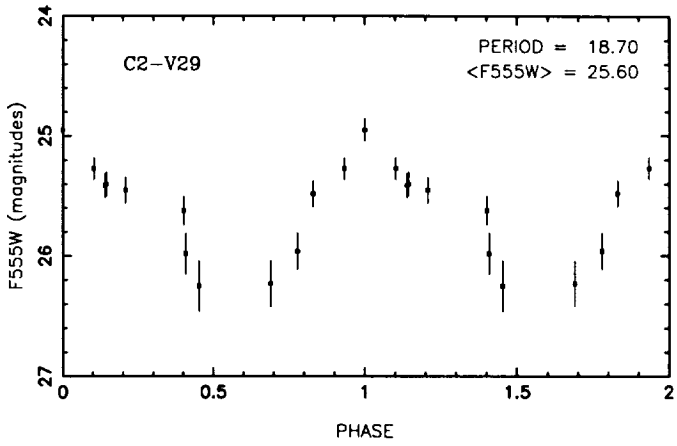
C2-V29
PERIOD = 18.70
<F555W> = 25.60
F555W (magnitudes)
PHASE

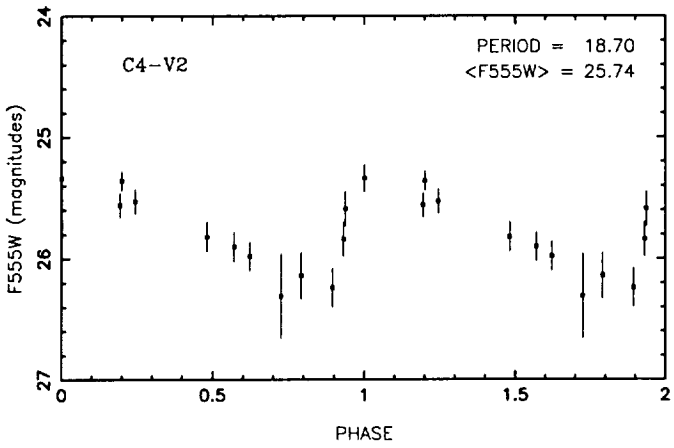
C4-V2
PERIOD = 18.70
<F555W> = 25.74
F555W (magnitudes)
PHASE

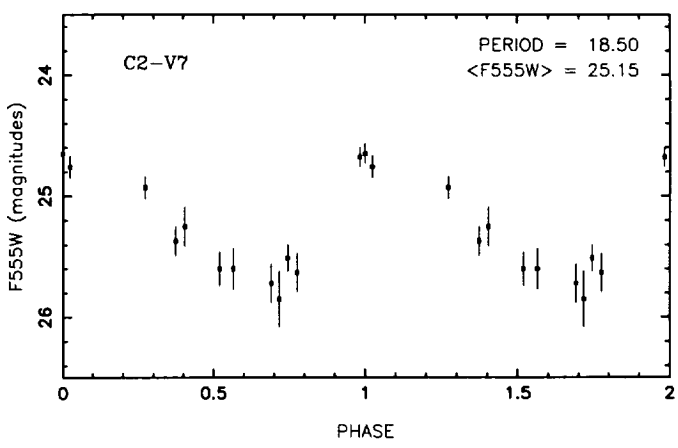
C2-V7
PERIOD = 18.50
<F555W> = 25.15
F555W (magnitudes)
PHASE

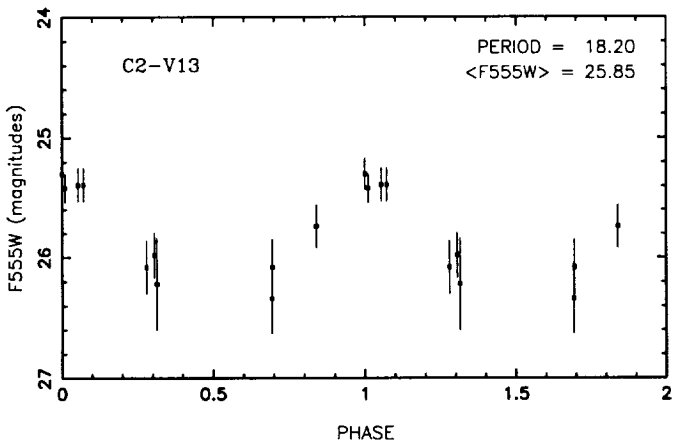
C2-V13
PERIOD = 18.20
<F555W> = 25.85
F555W (magnitudes)
PHASE

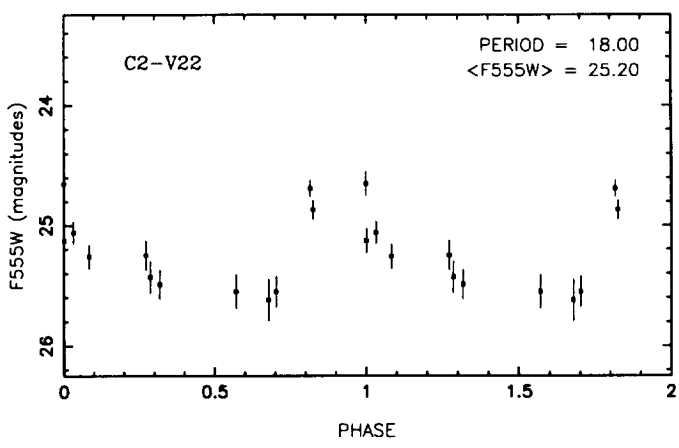
C2-V22
PERIOD = 18.00
<F555W> = 25.20
F555W (magnitudes)
PHASE

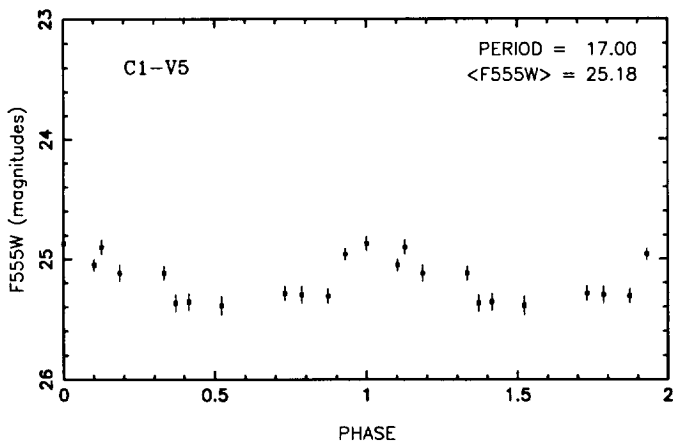
C1-V5
PERIOD = 17.00
<F555W> = 25.18
F555W (magnitudes)
PHASE

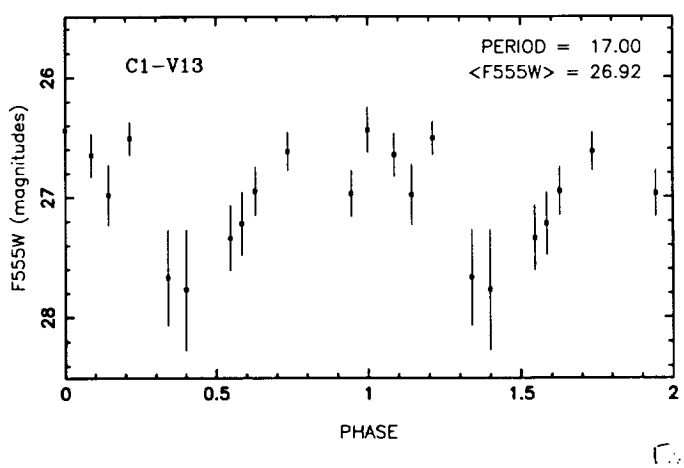
C1-V13
PERIOD = 17.00
<F555W> = 26.92
F555W (magnitudes)
PHASE

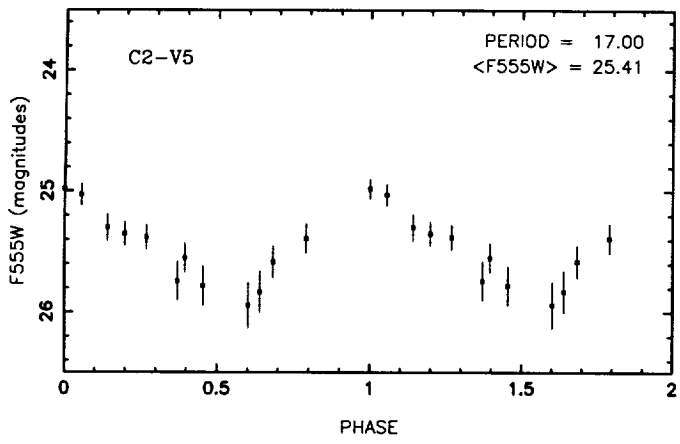
C2-V5
PERIOD = 17.00
<F555W> = 25.41
F555W (magnitudes)
PHASE

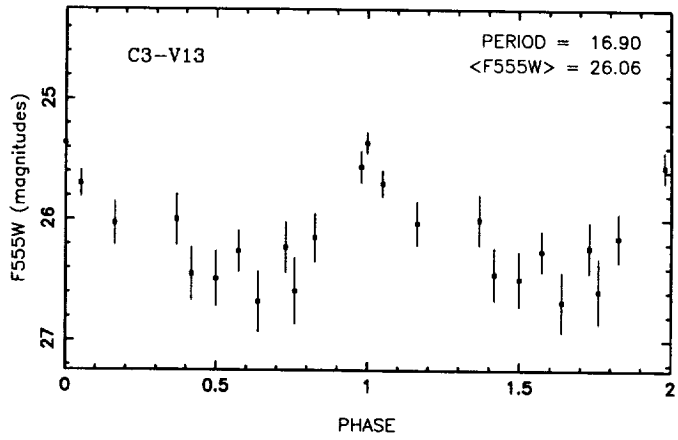
C3-V13
PERIOD = 16.90
<F555W> = 26.06
F555W (magnitudes)
PHASE

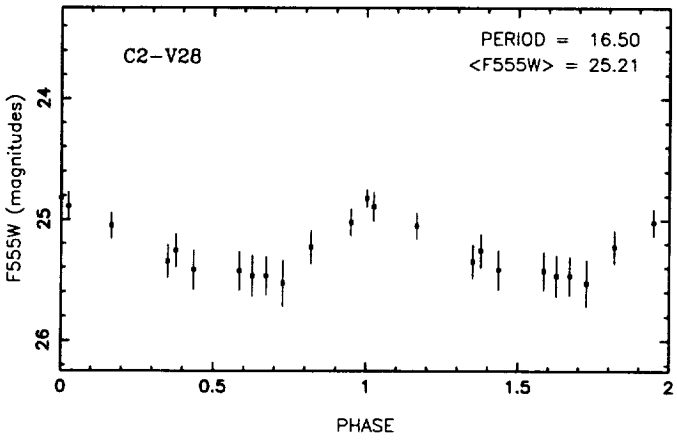
C2-V28
PERIOD = 16.50
<F555W> = 25.21
F555W (magnitudes)
PHASE

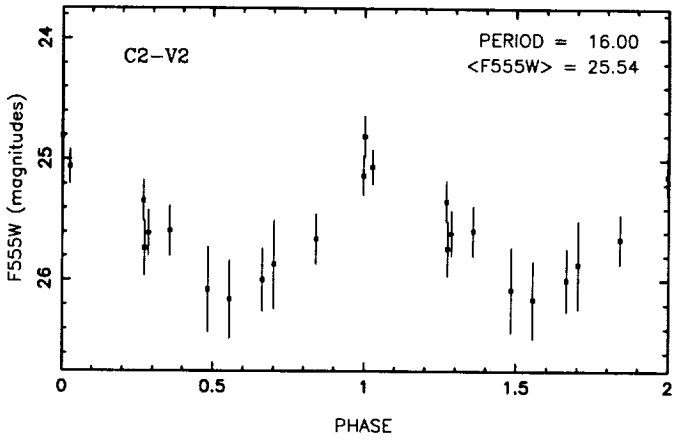
C2-V2
PERIOD = 16.00
<F555W> = 25.54
F555W (magnitudes)
PHASE

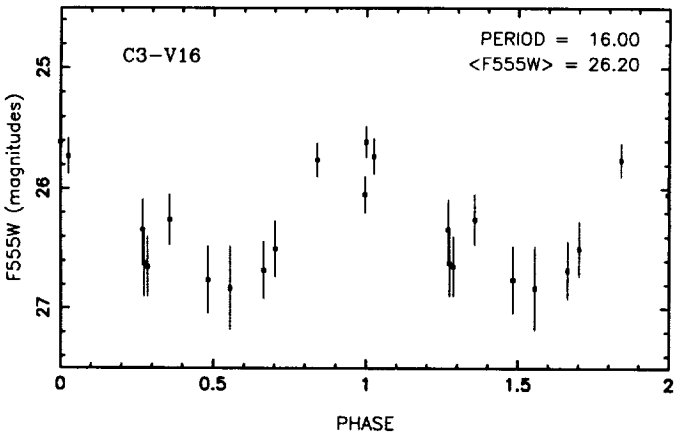
C3-V16
PERIOD = 16.00
<F555W> = 26.20
F555W (magnitudes)
PHASE

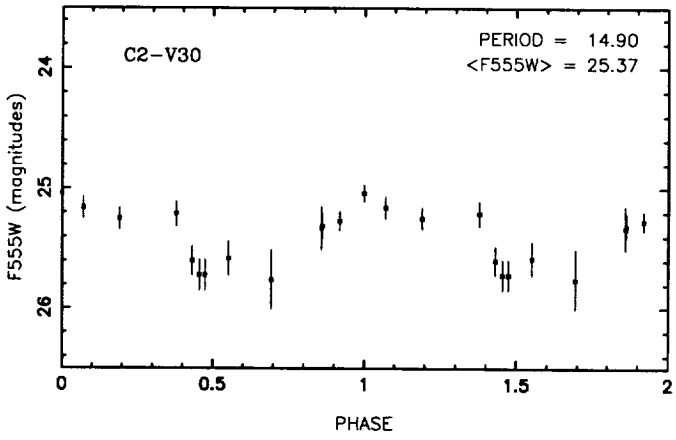
C2-V30
PERIOD = 14.90
<F555W> = 25.37
F555W (magnitudes)
PHASE

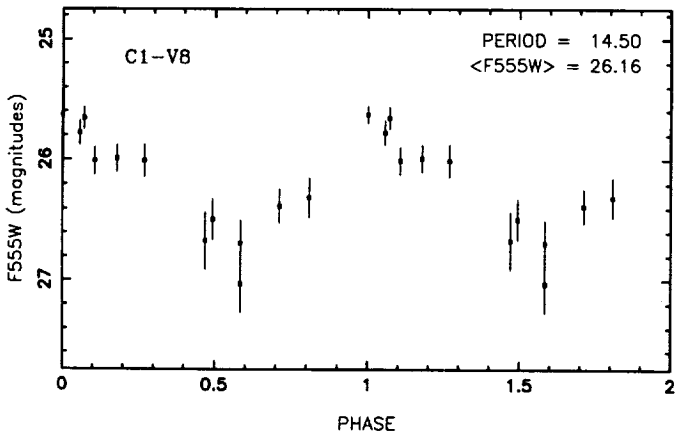
C1-V8
PERIOD = 14.50
<F555W> = 26.16
F555W (magnitudes)
PHASE

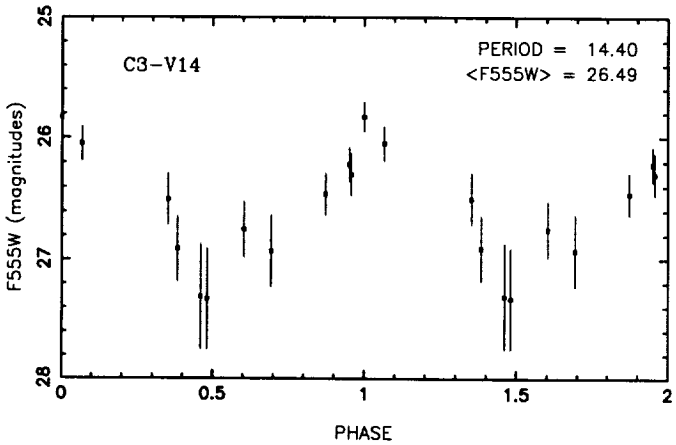
C3-V14
PERIOD = 14.40
<F555W> = 26.49
F555W (magnitudes)
PHASE

Fig 9

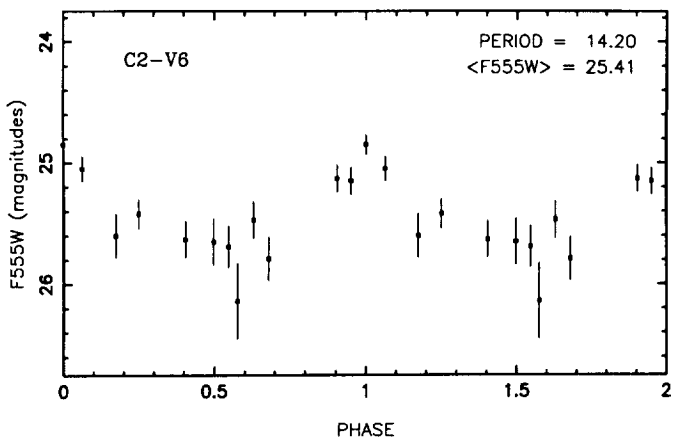
C2–V6
PERIOD = 14.20
<F555W> = 25.41
F555W (magnitudes)
PHASE

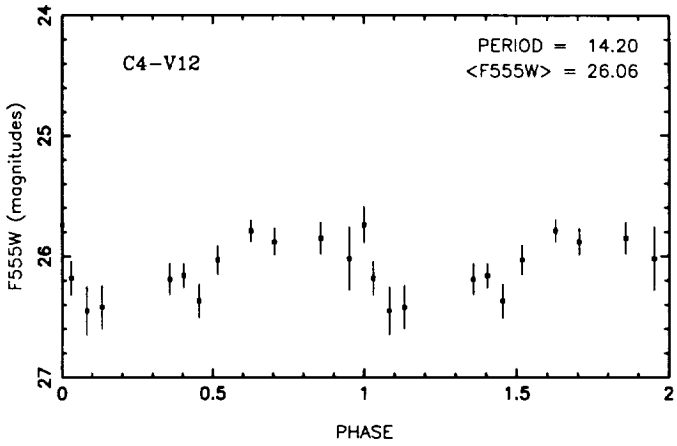
C4–V12
PERIOD = 14.20
<F555W> = 26.06
F555W (magnitudes)
PHASE

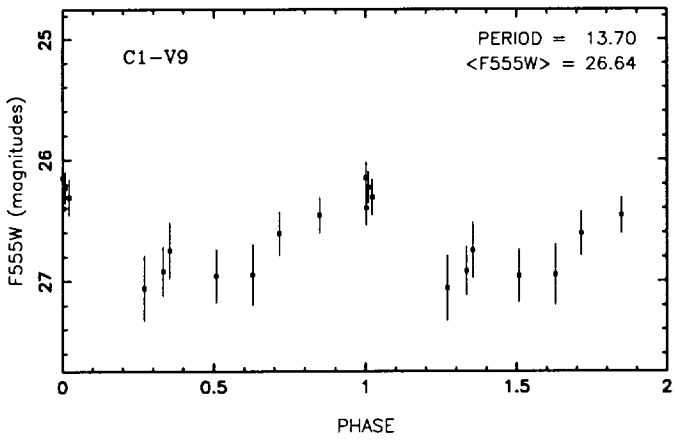
C1–V9
PERIOD = 13.70
<F555W> = 26.64
F555W (magnitudes)
PHASE

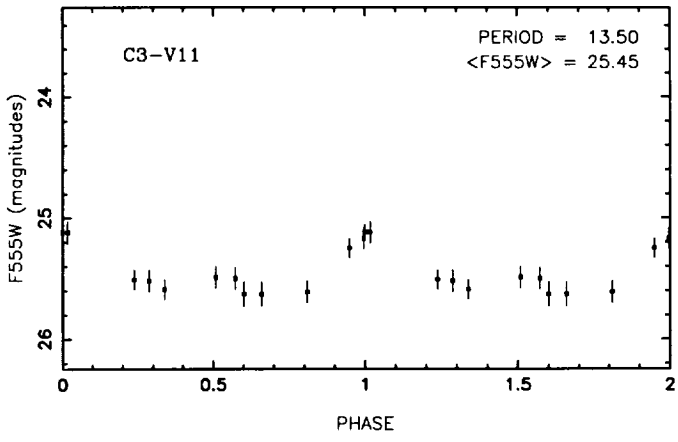
C3–V11
PERIOD = 13.50
<F555W> = 25.45
F555W (magnitudes)
PHASE

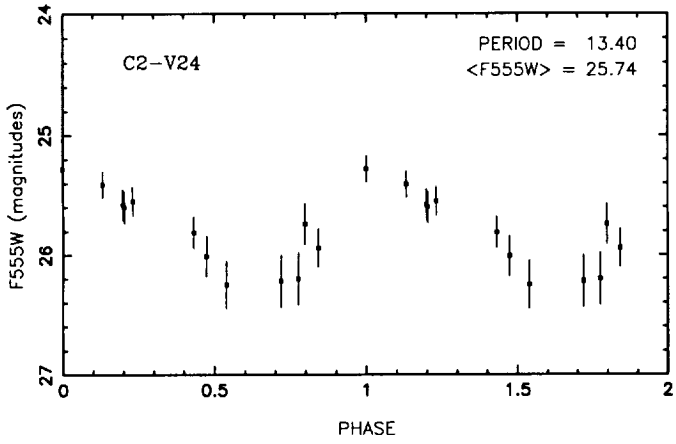
C2–V24
PERIOD = 13.40
<F555W> = 25.74
F555W (magnitudes)
PHASE

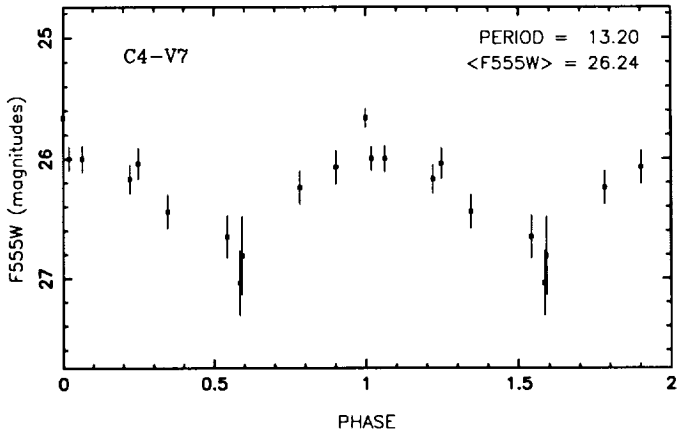
C4–V7
PERIOD = 13.20
<F555W> = 26.24
F555W (magnitudes)
PHASE

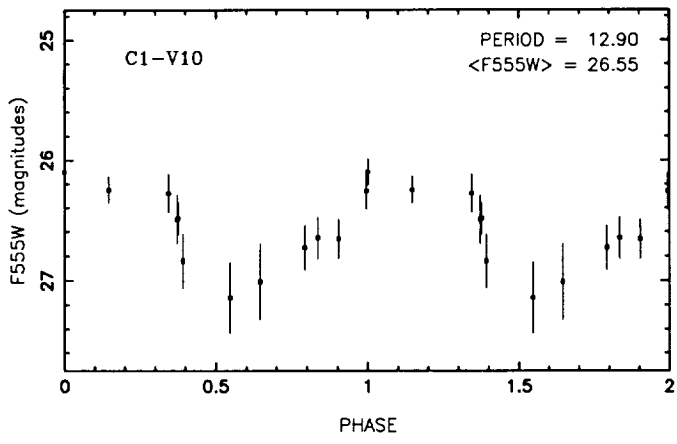
C1–V10
PERIOD = 12.90
<F555W> = 26.55
F555W (magnitudes)
PHASE

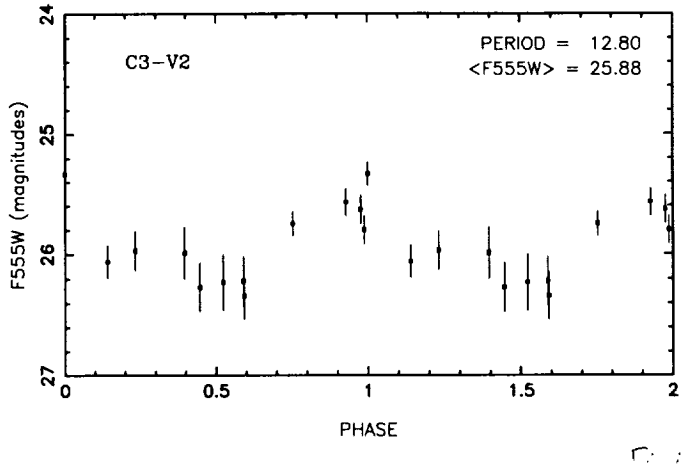
C3–V2
PERIOD = 12.80
<F555W> = 25.88
F555W (magnitudes)
PHASE

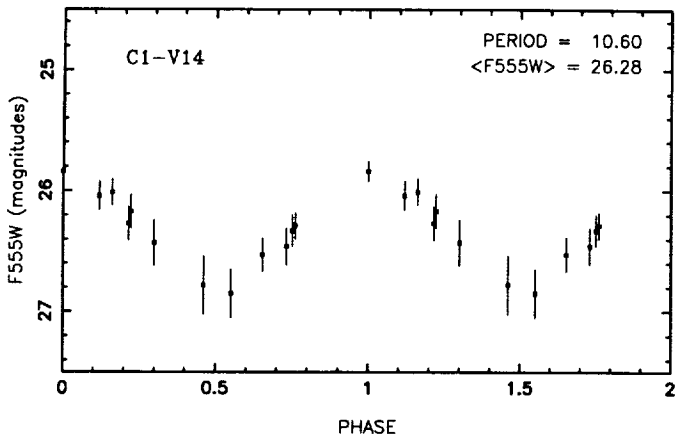
C1−V14
PERIOD = 10.60
<F555W> = 26.28
F555W (magnitudes)
PHASE

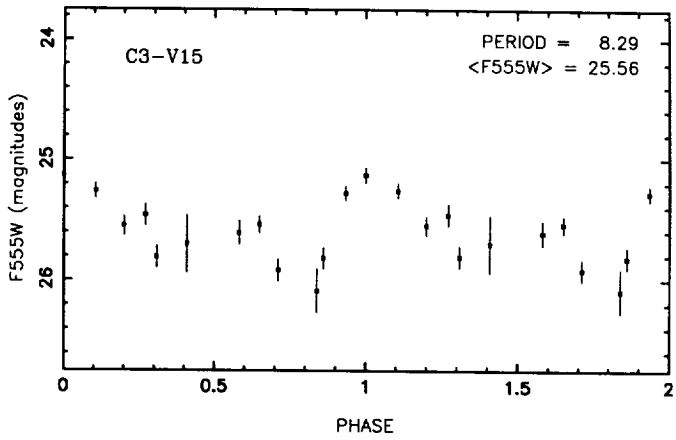
C3−V15
PERIOD = 8.29
<F555W> = 25.56
F555W (magnitudes)
PHASE

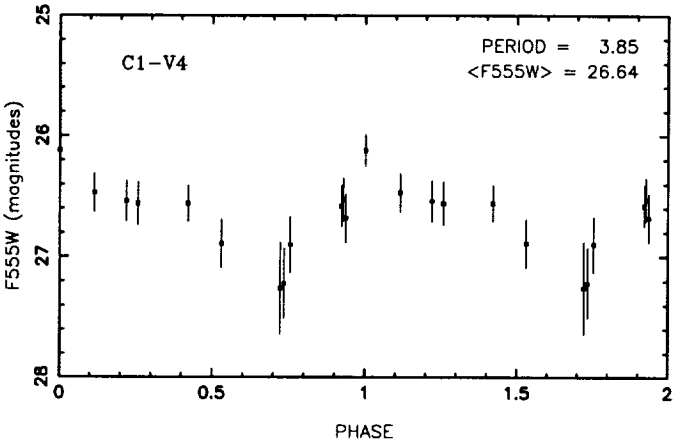
C1−V4
PERIOD = 3.85
<F555W> = 26.64
F555W (magnitudes)
PHASE

Fig 4.11

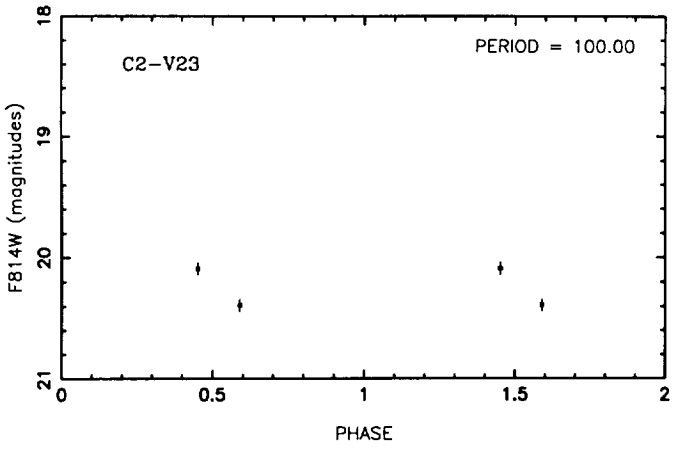
C2-V23
PERIOD = 100.00
F814W (magnitudes)
PHASE

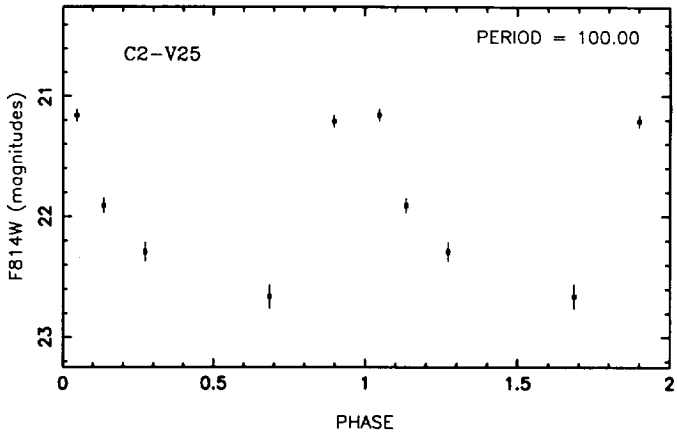
C2-V25
PERIOD = 100.00
F814W (magnitudes)
PHASE

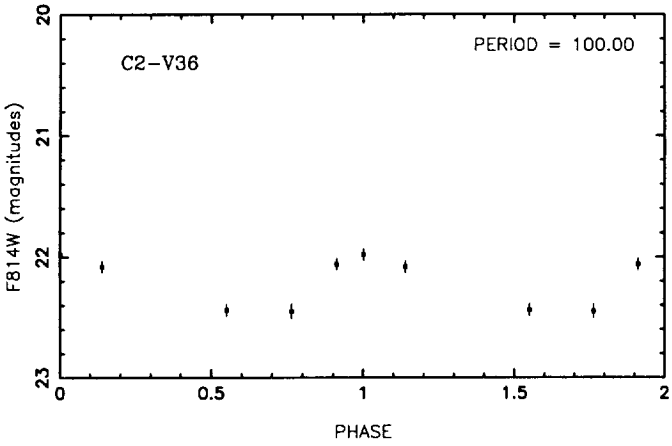
C2-V36
PERIOD = 100.00
F814W (magnitudes)
PHASE

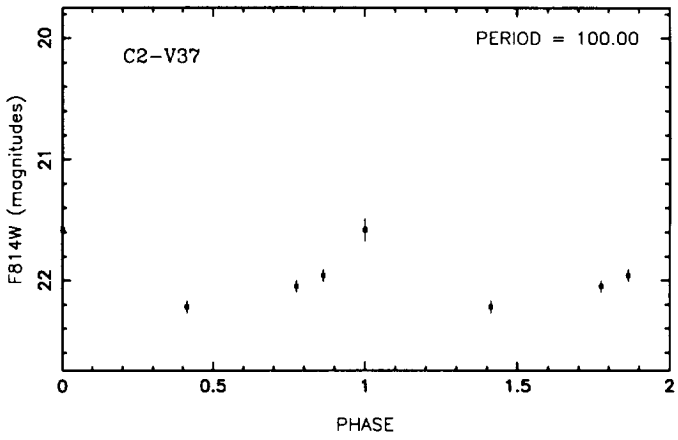
C2-V37
PERIOD = 100.00
F814W (magnitudes)
PHASE

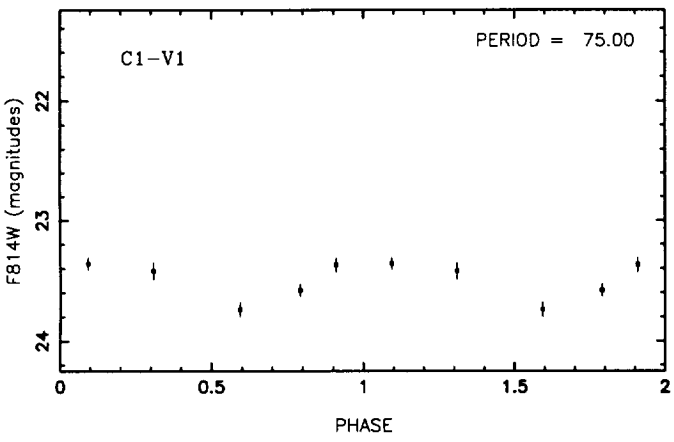
C1-V1
PERIOD = 75.00
F814W (magnitudes)
PHASE

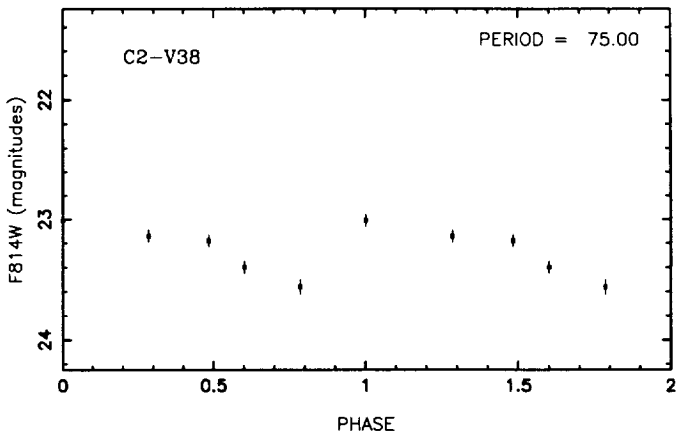
C2-V38
PERIOD = 75.00
F814W (magnitudes)
PHASE

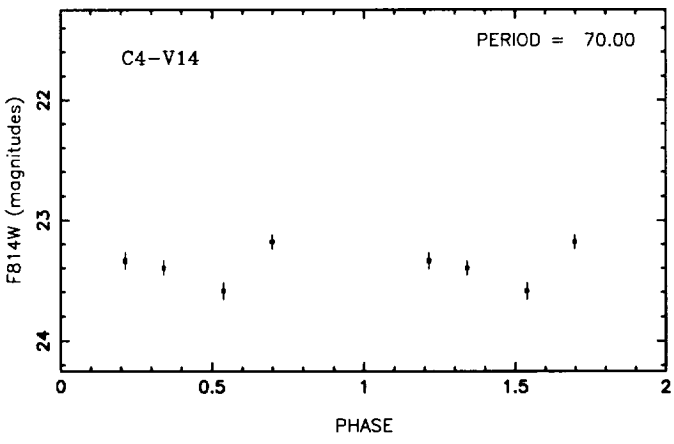
C4-V14
PERIOD = 70.00
F814W (magnitudes)
PHASE

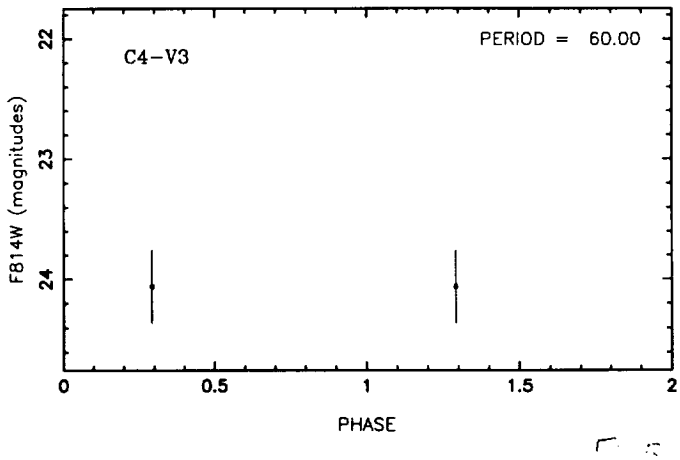
C4-V3
PERIOD = 60.00
F814W (magnitudes)
PHASE

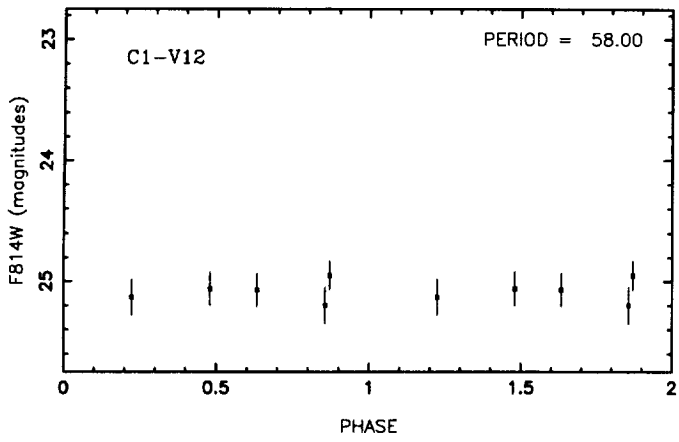
C1-V12
PERIOD = 58.00
F814W (magnitudes)
PHASE

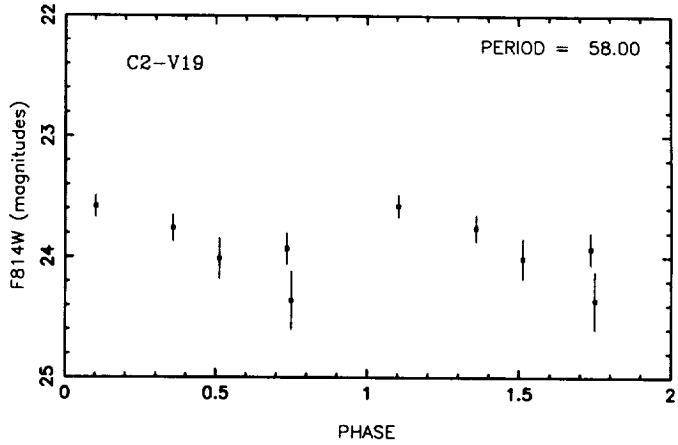
C2-V19
PERIOD = 58.00
F814W (magnitudes)
PHASE

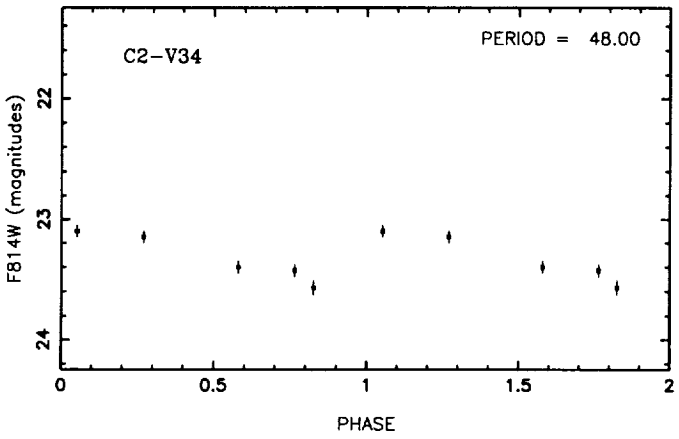
C2-V34
PERIOD = 48.00
F814W (magnitudes)
PHASE

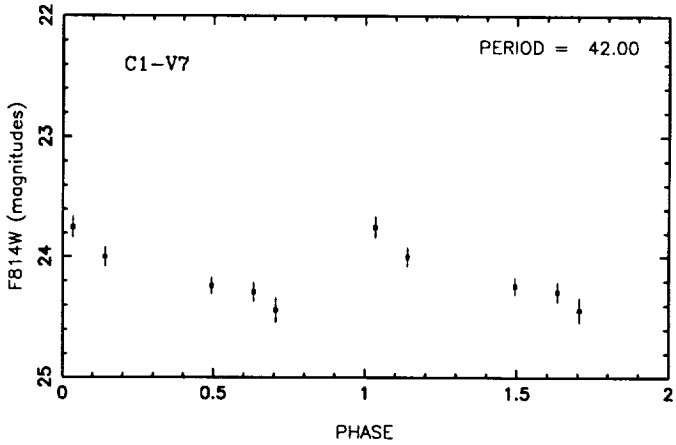
C1-V7
PERIOD = 42.00
F814W (magnitudes)
PHASE

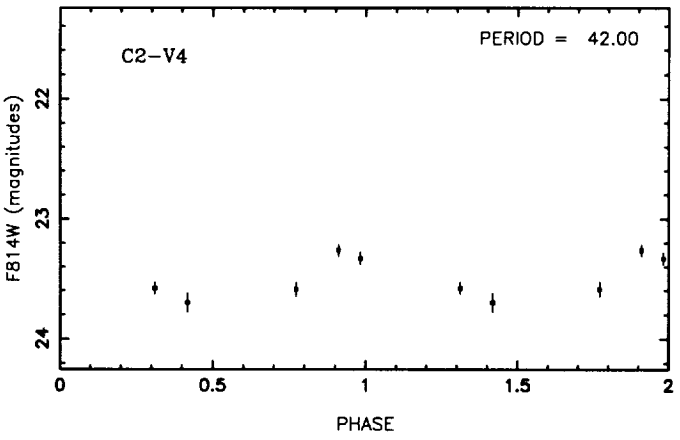
C2-V4
PERIOD = 42.00
F814W (magnitudes)
PHASE

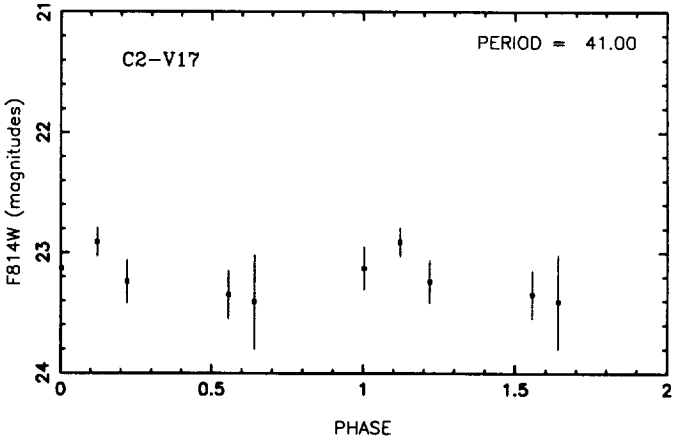
C2-V17
PERIOD = 41.00
F814W (magnitudes)
PHASE

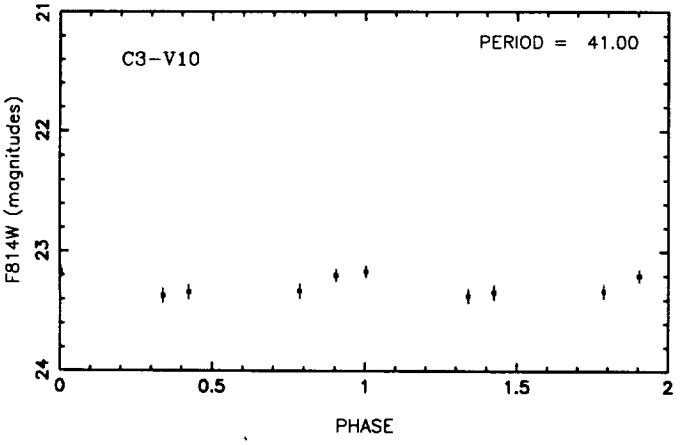
C3-V10
PERIOD = 41.00
F814W (magnitudes)
PHASE

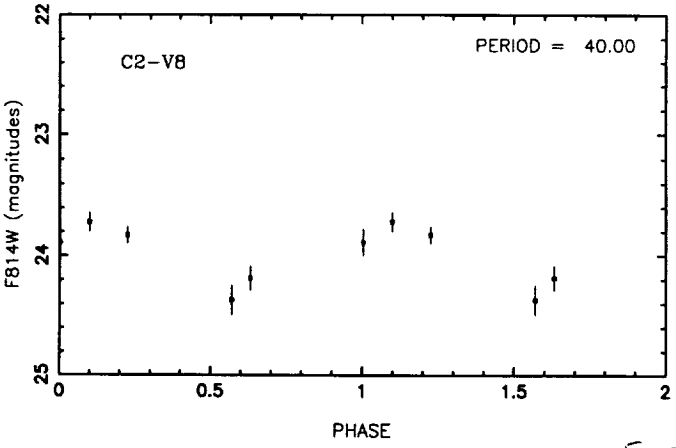
C2-V8
PERIOD = 40.00
F814W (magnitudes)
PHASE

Fig. 2

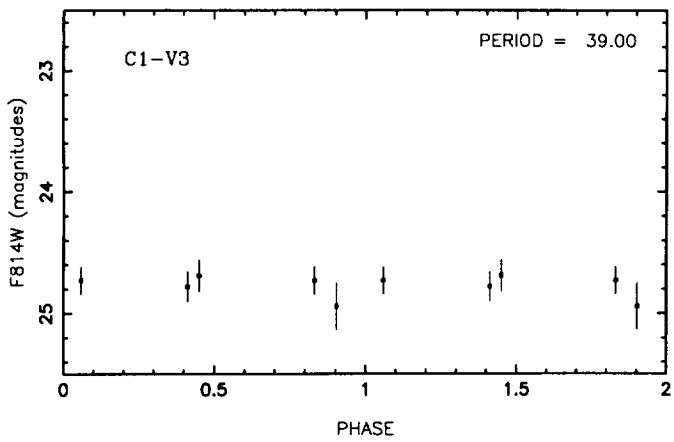
C1-V3
PERIOD = 39.00
F814W (magnitudes)
PHASE

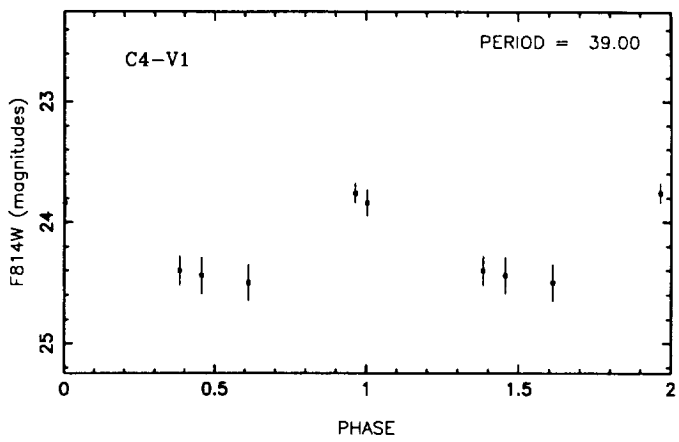
C4-V1
PERIOD = 39.00
F814W (magnitudes)
PHASE

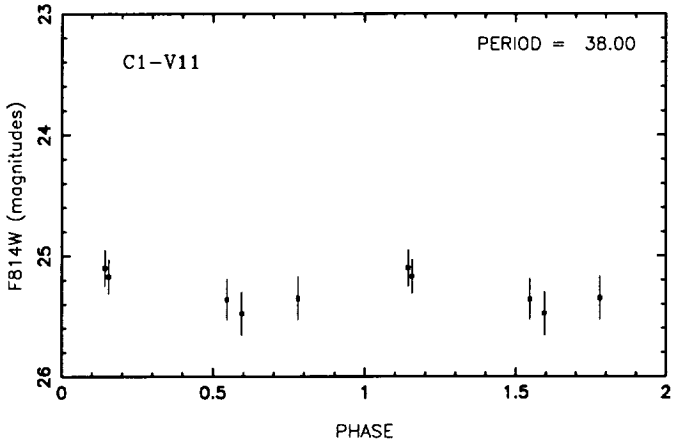
C1-V11
PERIOD = 38.00
F814W (magnitudes)
PHASE

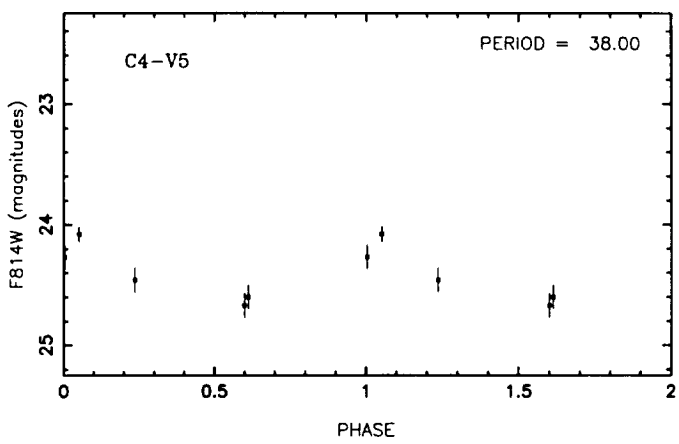
C4-V5
PERIOD = 38.00
F814W (magnitudes)
PHASE

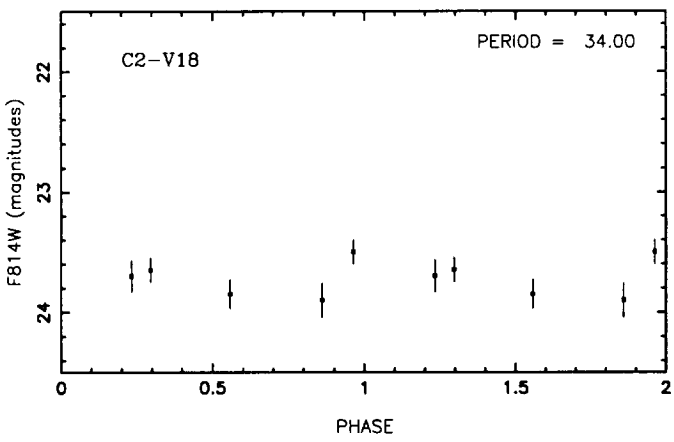
C2-V18
PERIOD = 34.00
F814W (magnitudes)
PHASE

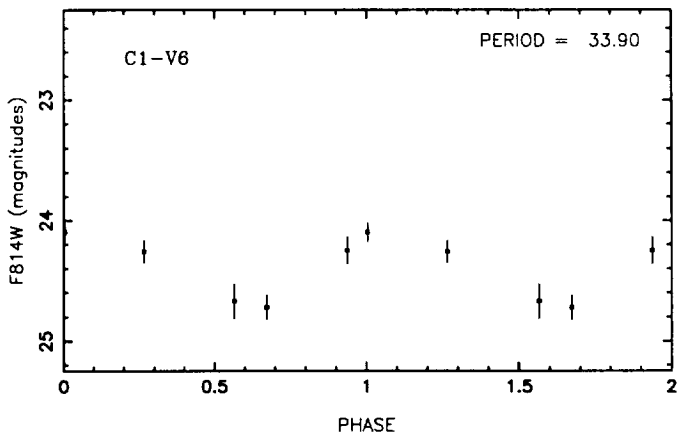
C1-V6
PERIOD = 33.90
F814W (magnitudes)
PHASE

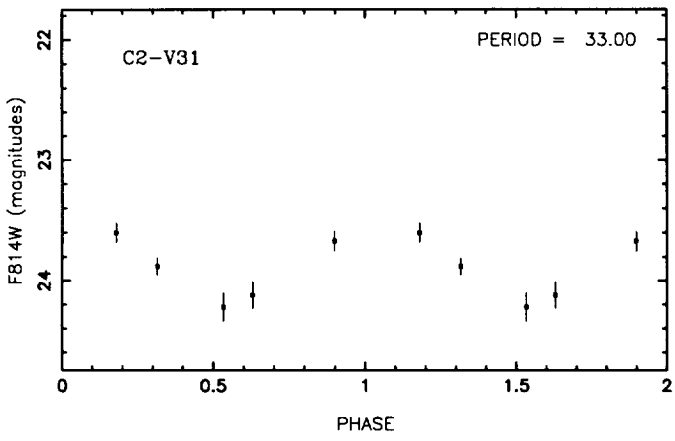
C2-V31
PERIOD = 33.00
F814W (magnitudes)
PHASE

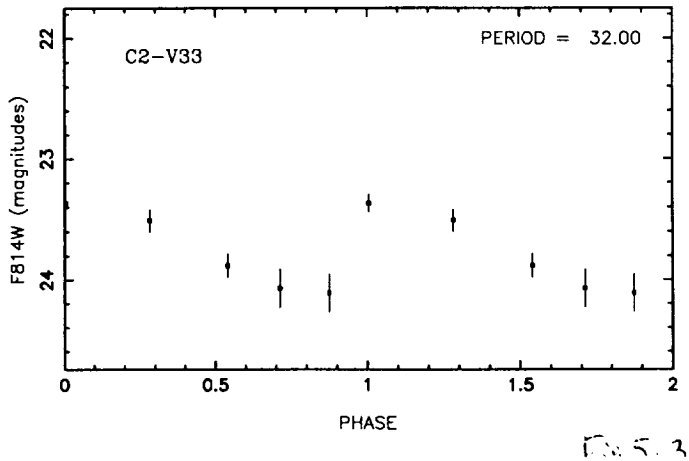
C2-V33
PERIOD = 32.00
F814W (magnitudes)
PHASE

Fig. 5.3

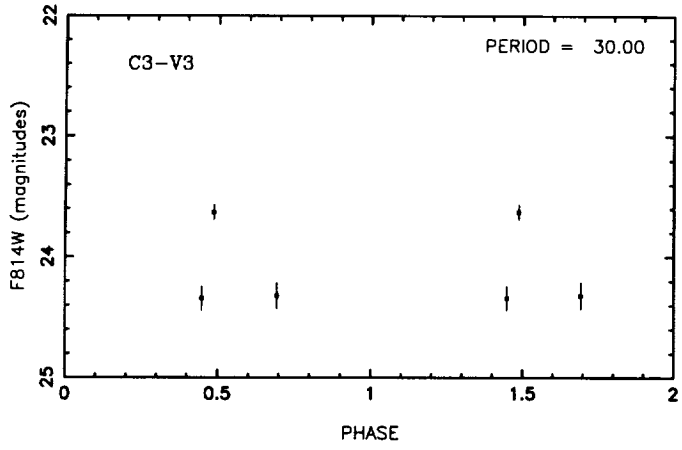
C3-V3
PERIOD = 30.00
F814W (magnitudes)
PHASE

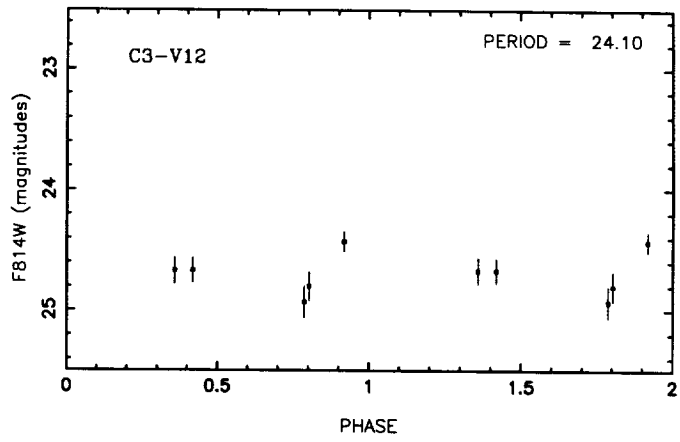
C3-V12
PERIOD = 24.10
F814W (magnitudes)
PHASE

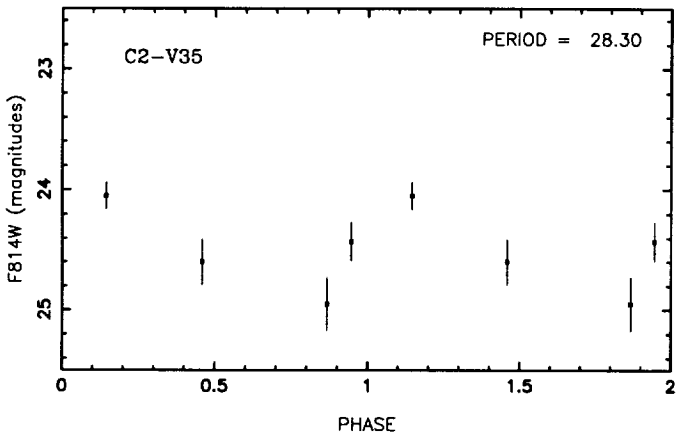
C2-V35
PERIOD = 28.30
F814W (magnitudes)
PHASE

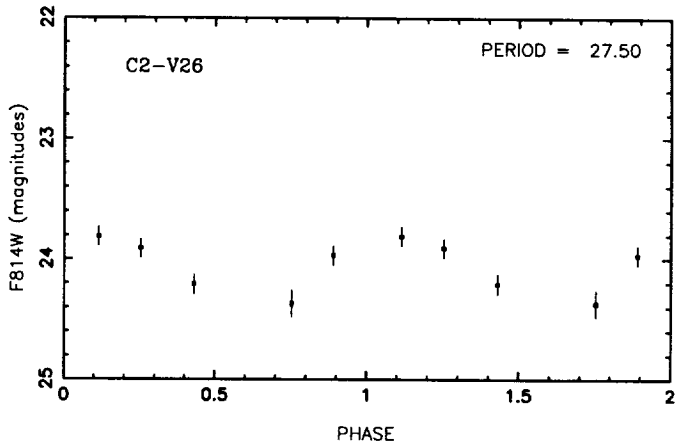
C2-V26
PERIOD = 27.50
F814W (magnitudes)
PHASE

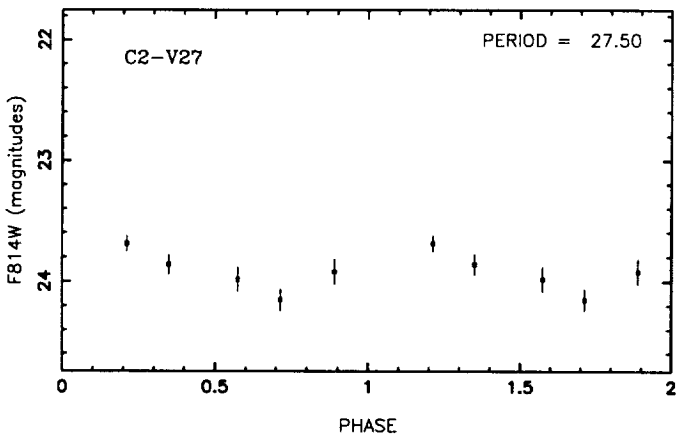
C2-V27
PERIOD = 27.50
F814W (magnitudes)
PHASE

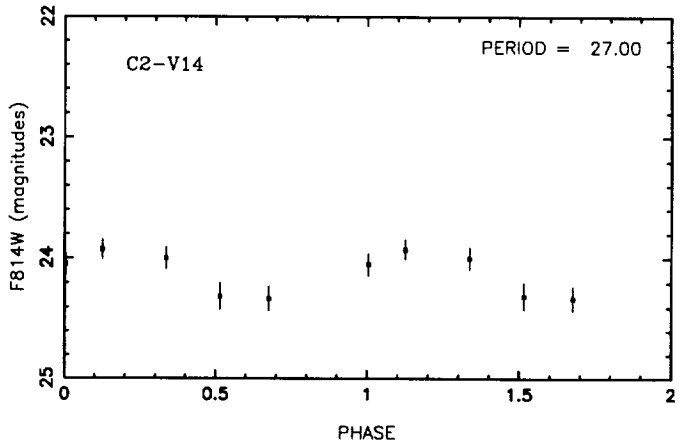
C2-V14
PERIOD = 27.00
F814W (magnitudes)
PHASE

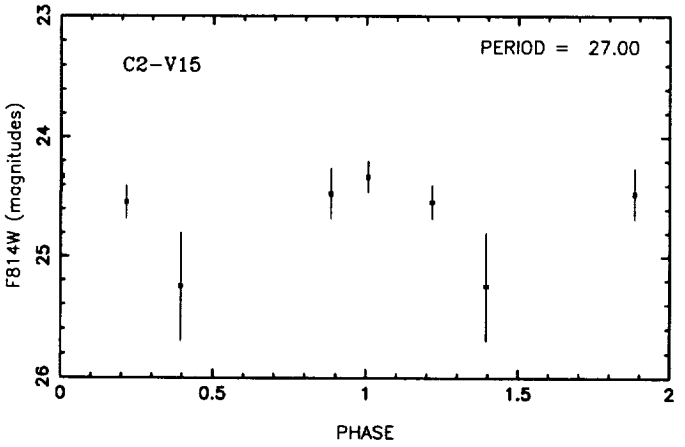
C2-V15
PERIOD = 27.00
F814W (magnitudes)
PHASE

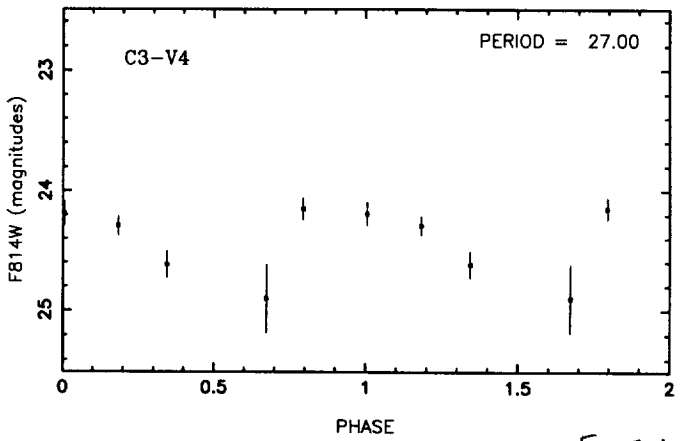
C3-V4
PERIOD = 27.00
F814W (magnitudes)
PHASE

Fig 5.4

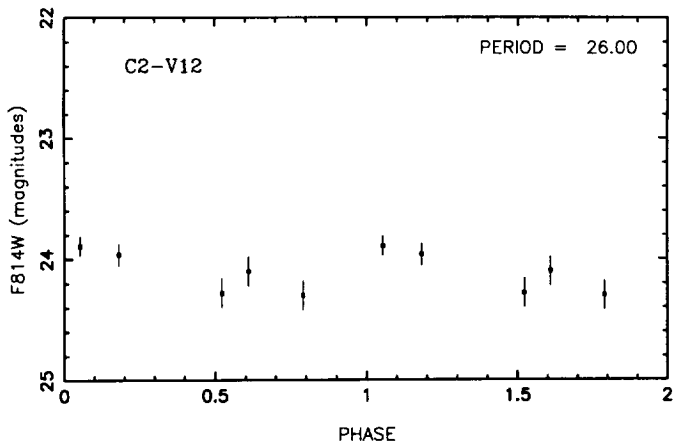
C2-V12
PERIOD = 26.00
F814W (magnitudes)
PHASE

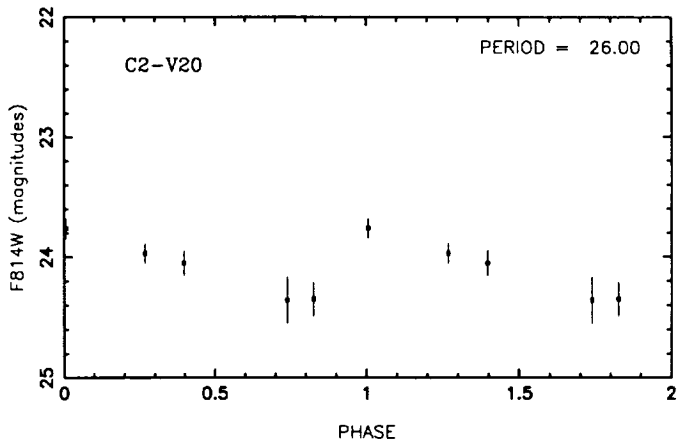
C2-V20
PERIOD = 26.00
F814W (magnitudes)
PHASE

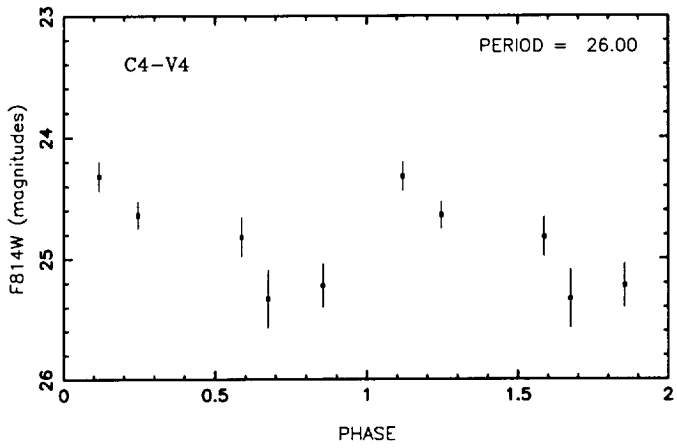
C4-V4
PERIOD = 26.00
F814W (magnitudes)
PHASE

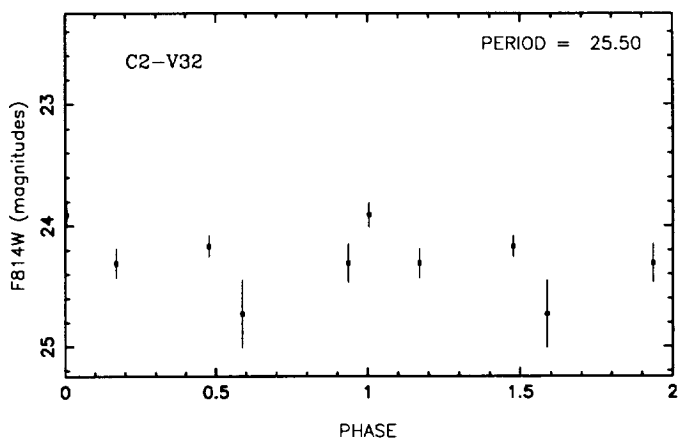
C2-V32
PERIOD = 25.50
F814W (magnitudes)
PHASE

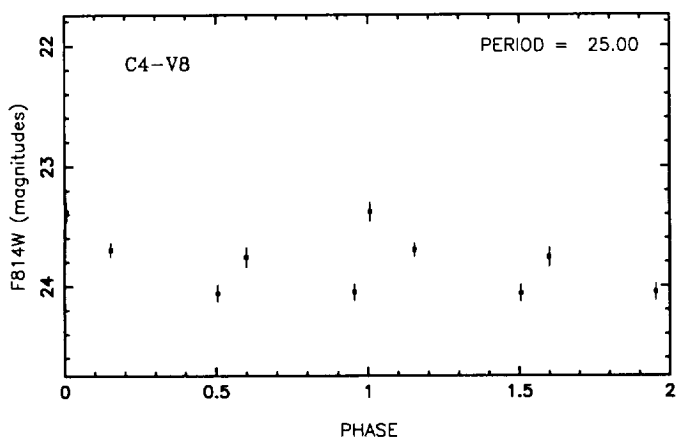
C4-V8
PERIOD = 25.00
F814W (magnitudes)
PHASE

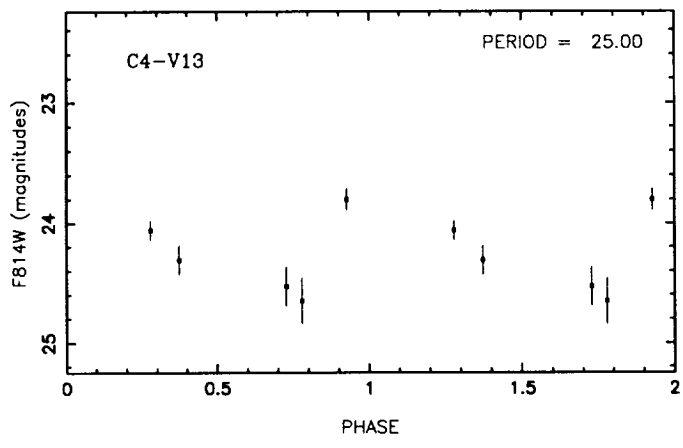
C4-V13
PERIOD = 25.00
F814W (magnitudes)
PHASE

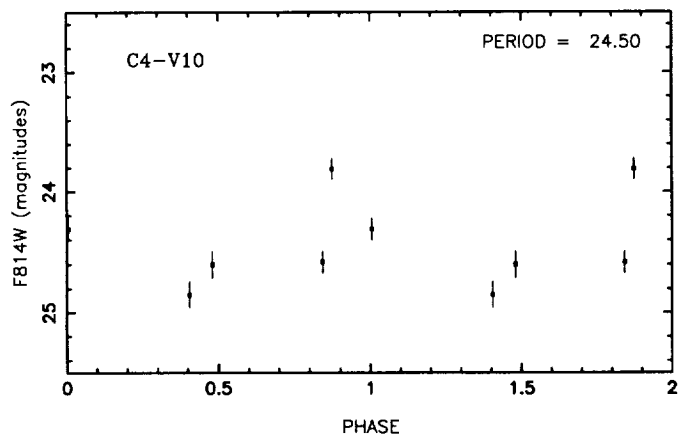
C4-V10
PERIOD = 24.50
F814W (magnitudes)
PHASE

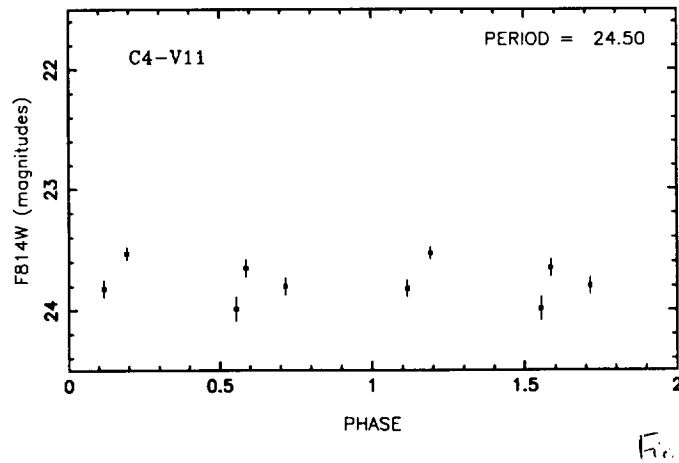
C4-V11
PERIOD = 24.50
F814W (magnitudes)
PHASE

Fig 5

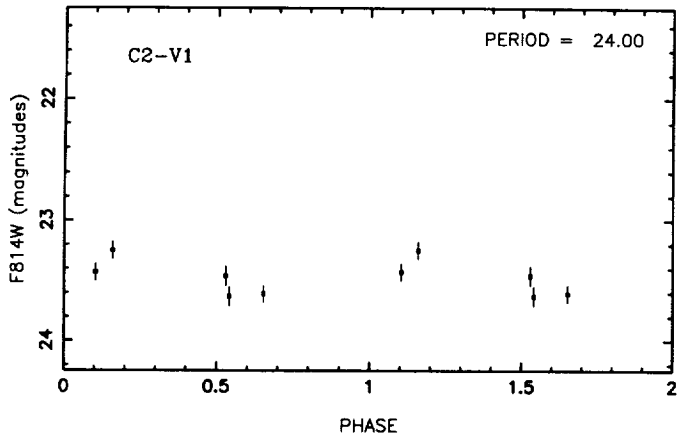
C2-V1
PERIOD = 24.00
F814W (magnitudes)
PHASE

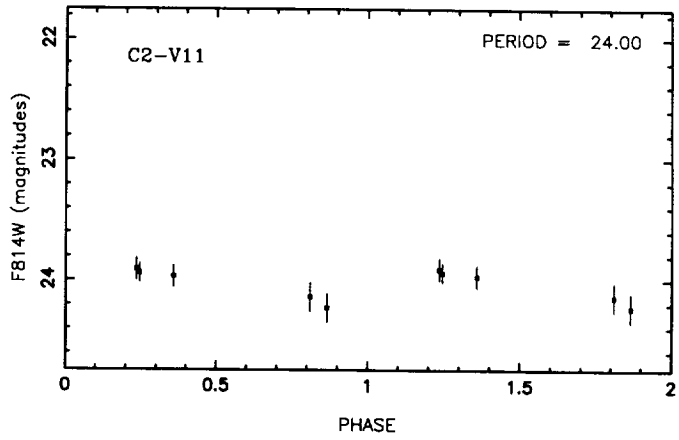
C2-V11
PERIOD = 24.00
F814W (magnitudes)
PHASE

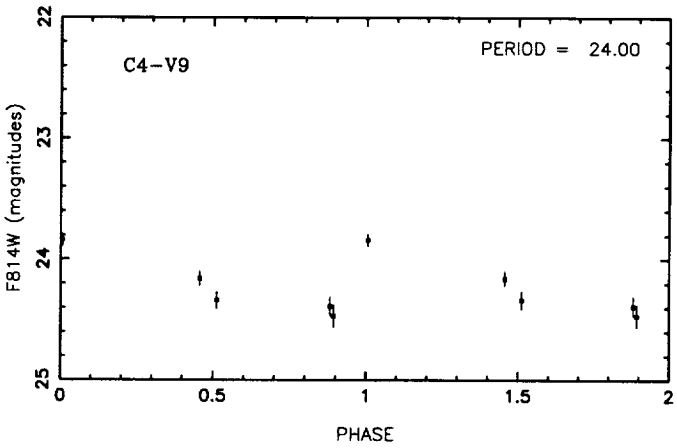
C4-V9
PERIOD = 24.00
F814W (magnitudes)
PHASE

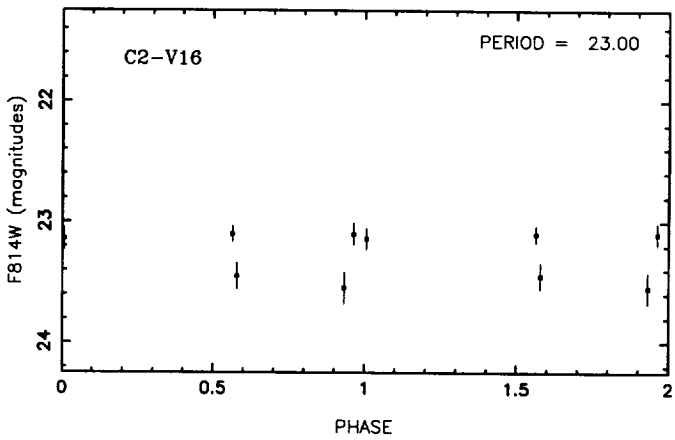
C2-V16
PERIOD = 23.00
F814W (magnitudes)
PHASE

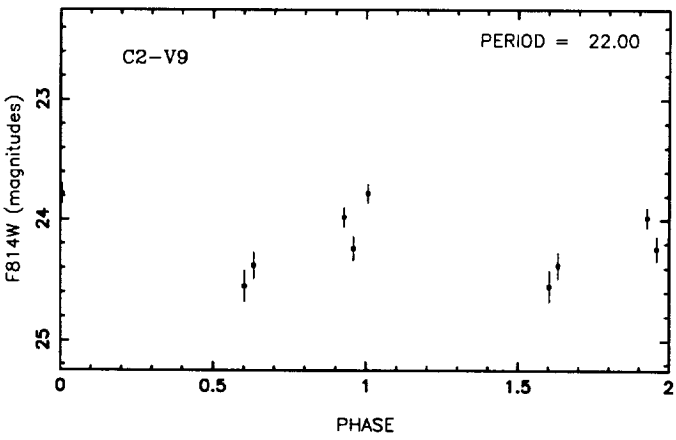
C2-V9
PERIOD = 22.00
F814W (magnitudes)
PHASE

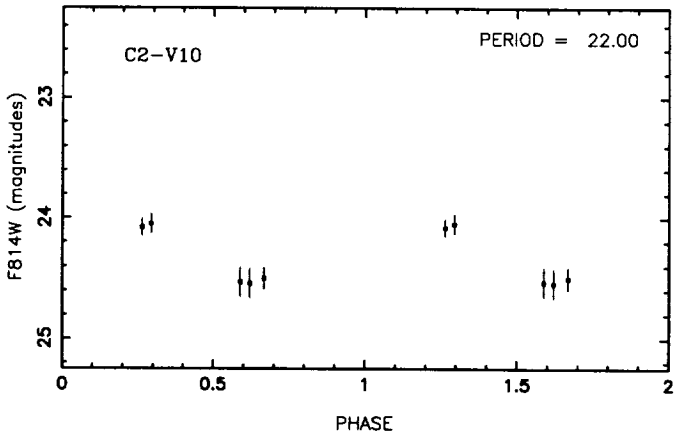
C2-V10
PERIOD = 22.00
F814W (magnitudes)
PHASE

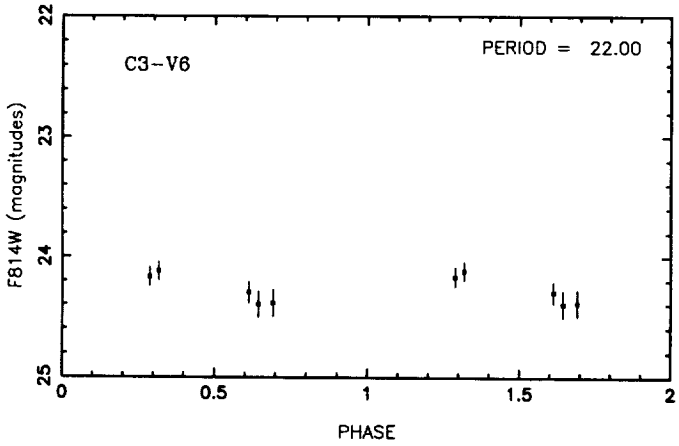
C3-V6
PERIOD = 22.00
F814W (magnitudes)
PHASE

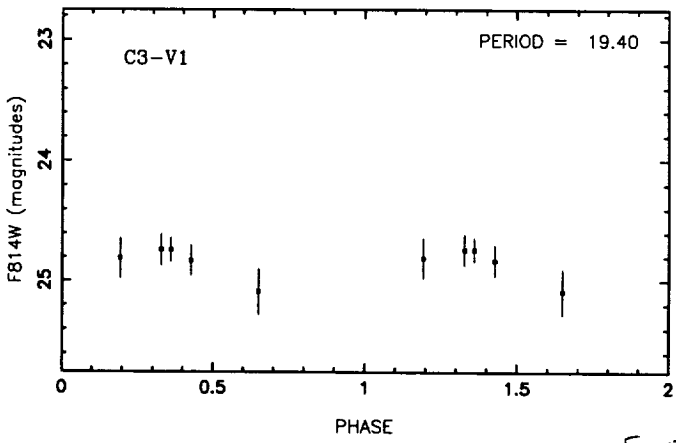
C3-V1
PERIOD = 19.40
F814W (magnitudes)
PHASE

Fig 5.6

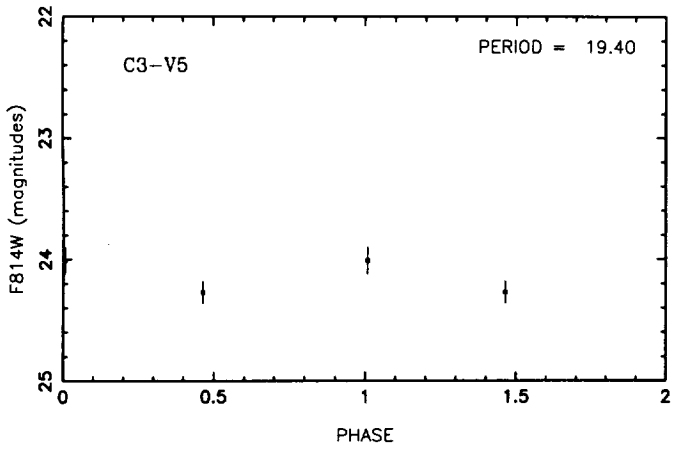
C3-V5
PERIOD = 19.40
F814W (magnitudes)
PHASE

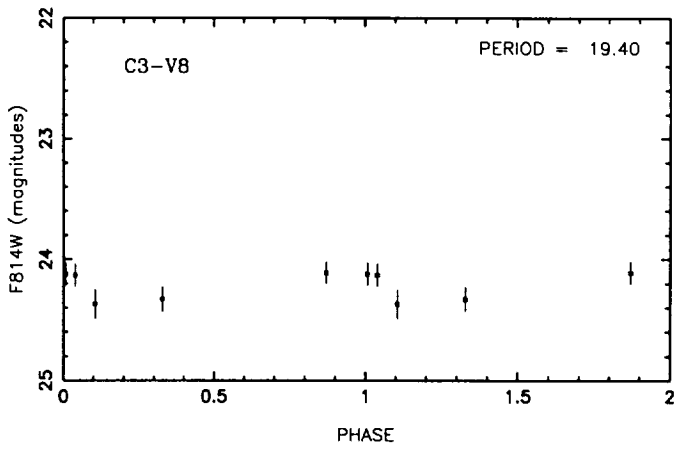
C3-V8
PERIOD = 19.40
F814W (magnitudes)
PHASE

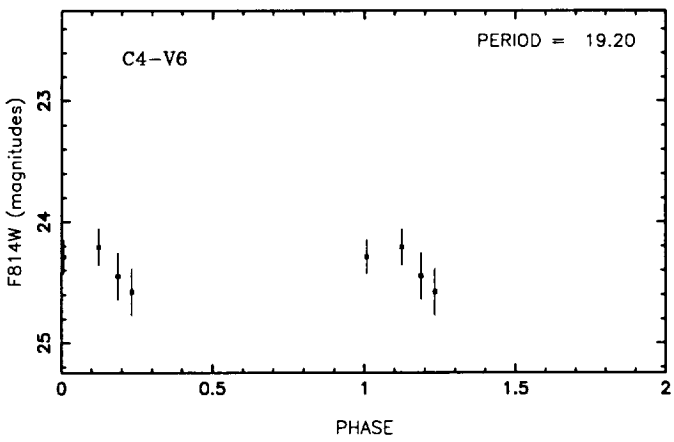
C4-V6
PERIOD = 19.20
F814W (magnitudes)
PHASE

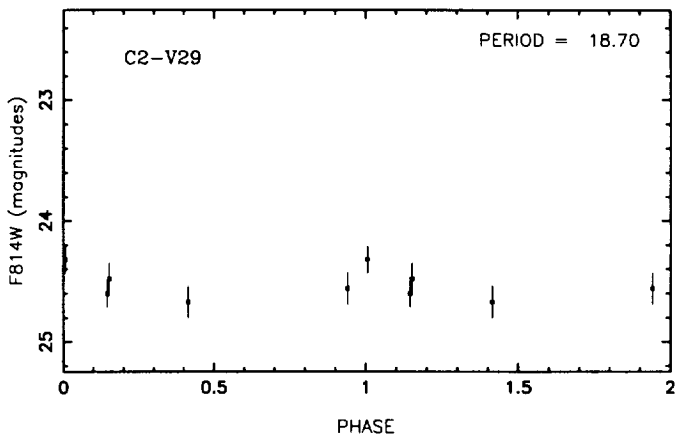
C2-V29
PERIOD = 18.70
F814W (magnitudes)
PHASE

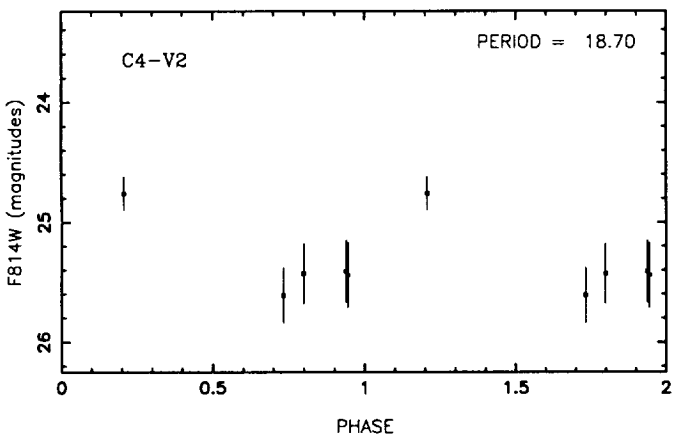
C4-V2
PERIOD = 18.70
F814W (magnitudes)
PHASE

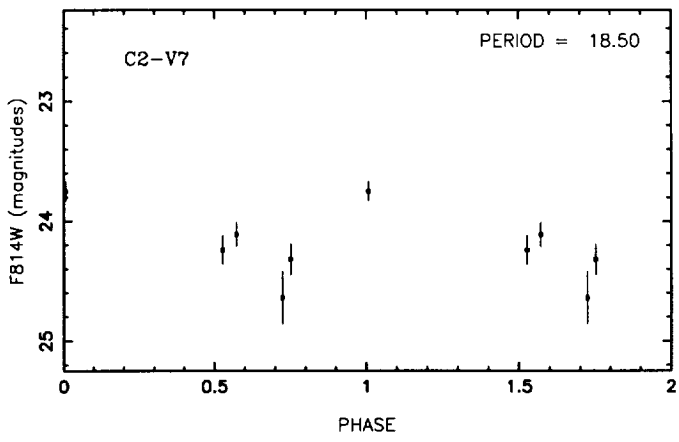
C2-V7
PERIOD = 18.50
F814W (magnitudes)
PHASE

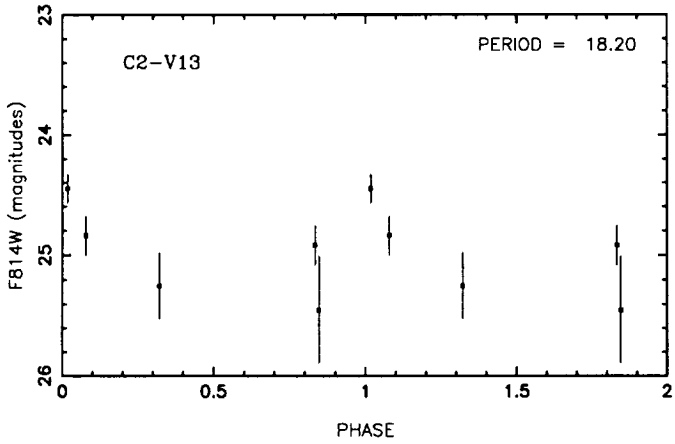
C2-V13
PERIOD = 18.20
F814W (magnitudes)
PHASE

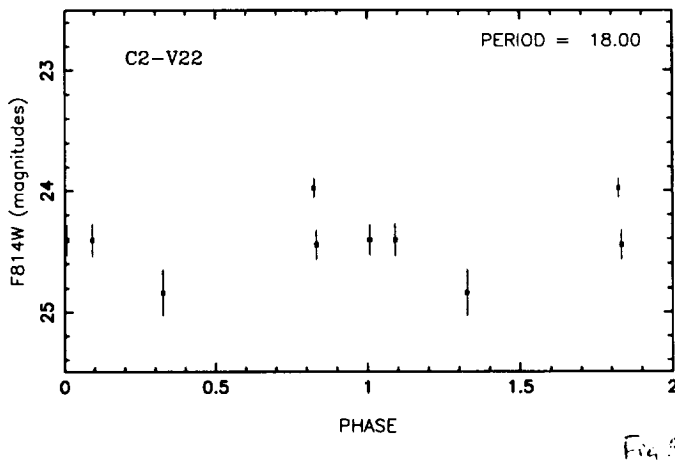
C2-V22
PERIOD = 18.00
F814W (magnitudes)
PHASE

Fig 5.7

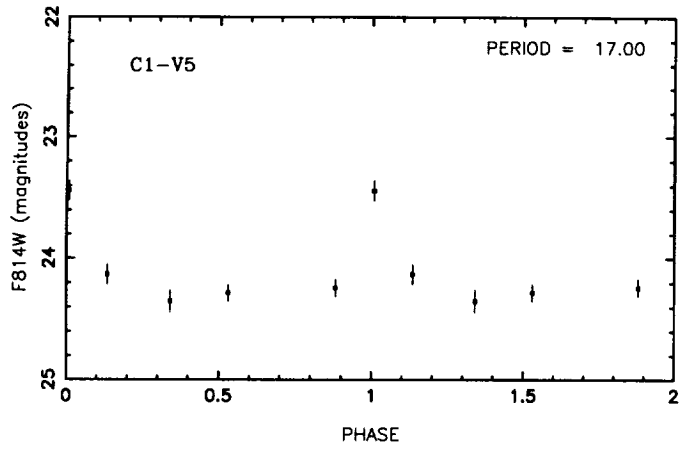
C1-V5
PERIOD = 17.00
F814W (magnitudes)
PHASE

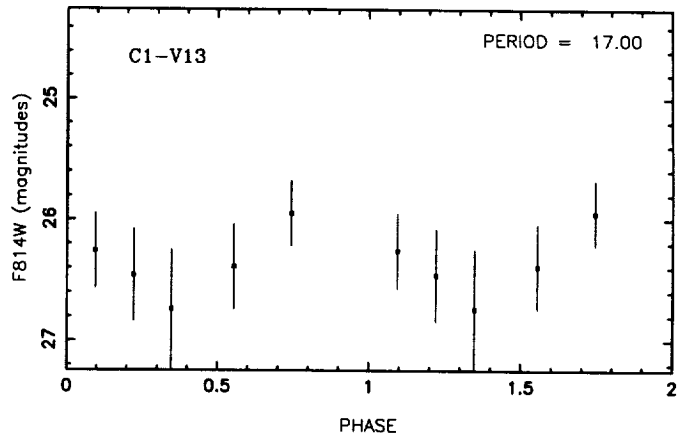
C1-V13
PERIOD = 17.00
F814W (magnitudes)
PHASE

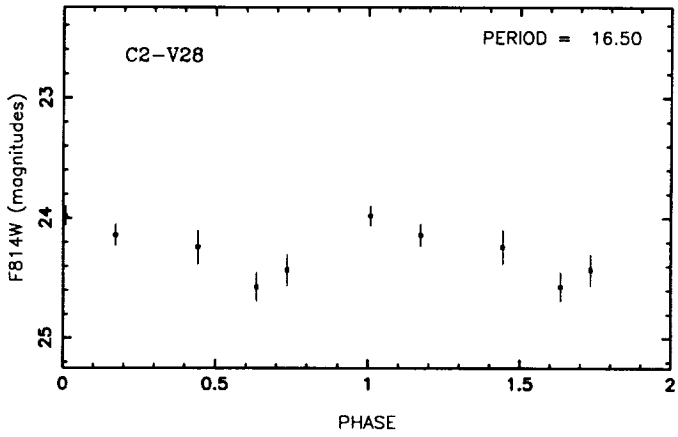
C2-V28
PERIOD = 16.50
F814W (magnitudes)
PHASE

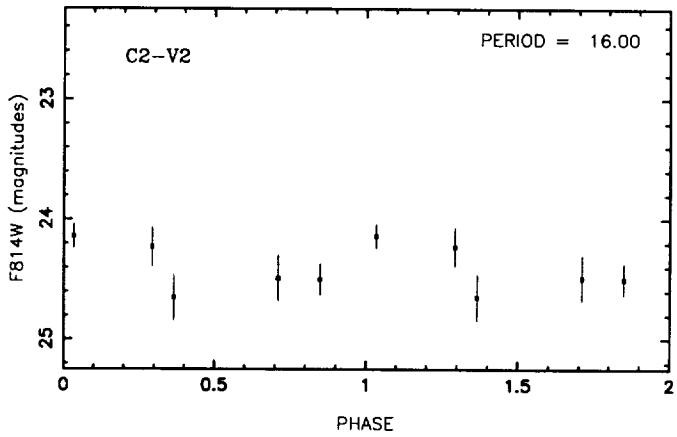
C2-V2
PERIOD = 16.00
F814W (magnitudes)
PHASE

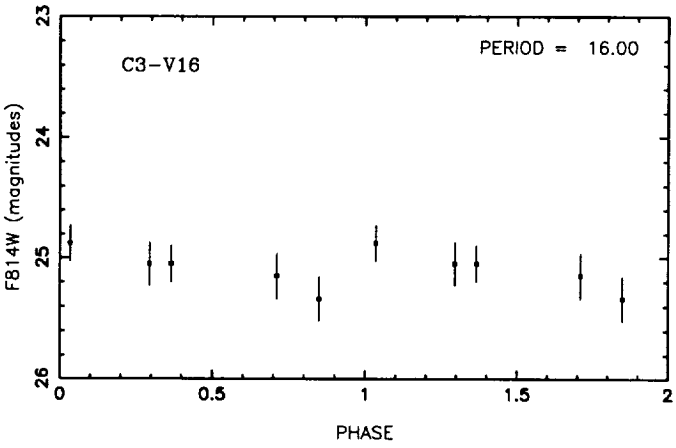
C3-V16
PERIOD = 16.00
F814W (magnitudes)
PHASE

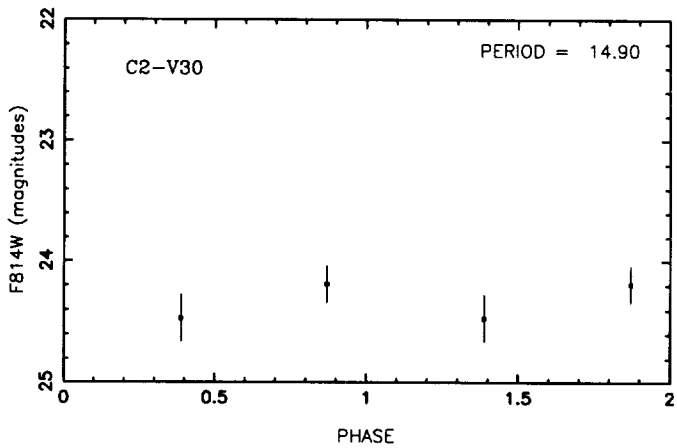
C2-V30
PERIOD = 14.90
F814W (magnitudes)
PHASE

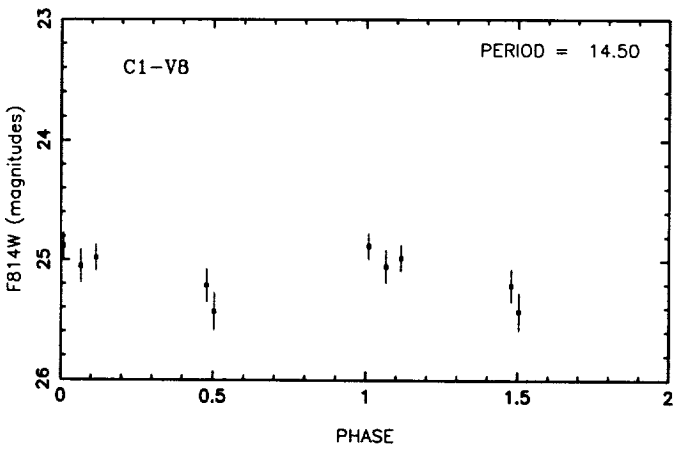
C1-V8
PERIOD = 14.50
F814W (magnitudes)
PHASE

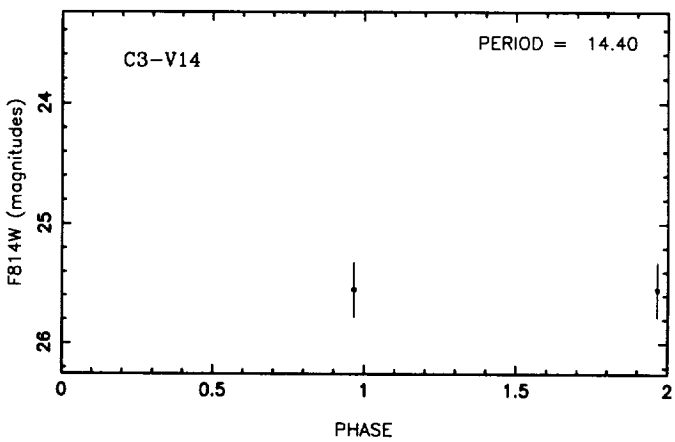
C3-V14
PERIOD = 14.40
F814W (magnitudes)
PHASE

Fig. 5.8

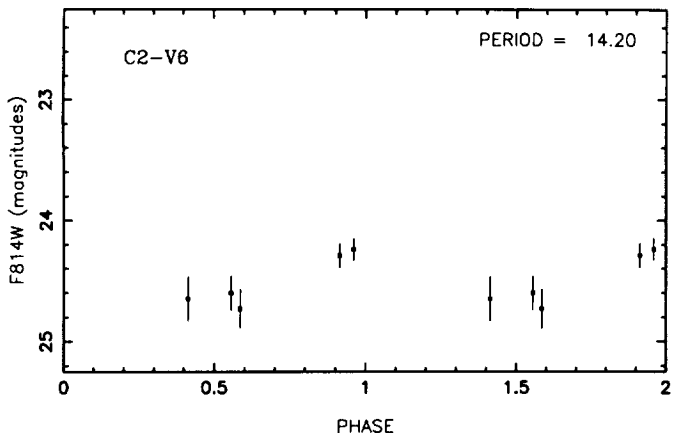
C2-V6
PERIOD = 14.20
F814W (magnitudes)
PHASE

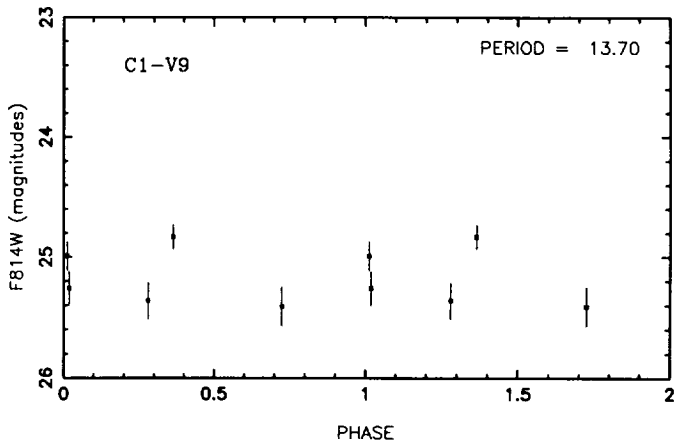
C1-V9
PERIOD = 13.70
F814W (magnitudes)
PHASE

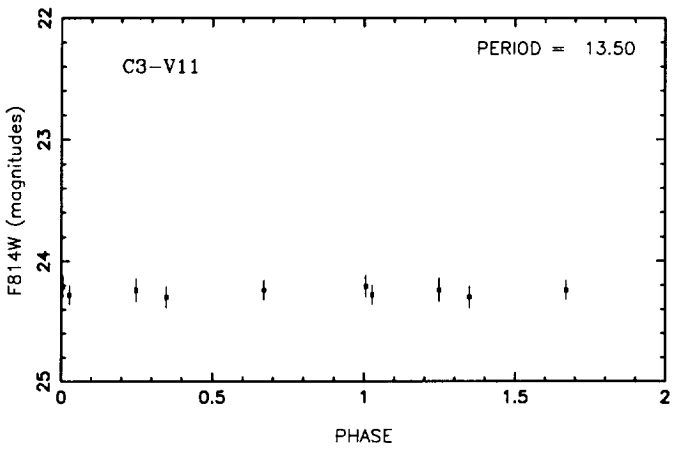
C3-V11
PERIOD = 13.50
F814W (magnitudes)
PHASE

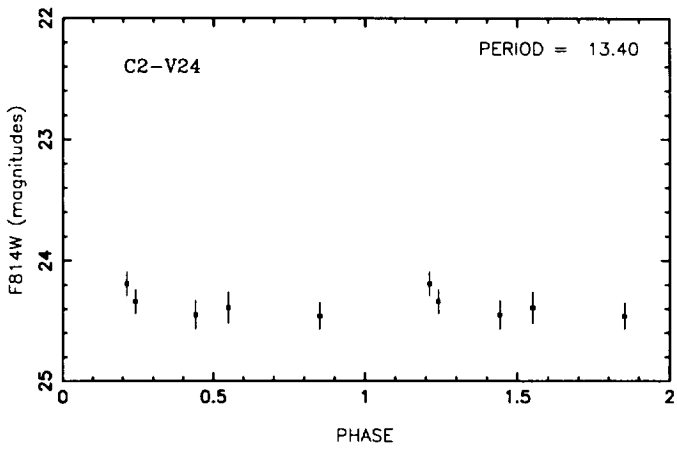
C2-V24
PERIOD = 13.40
F814W (magnitudes)
PHASE

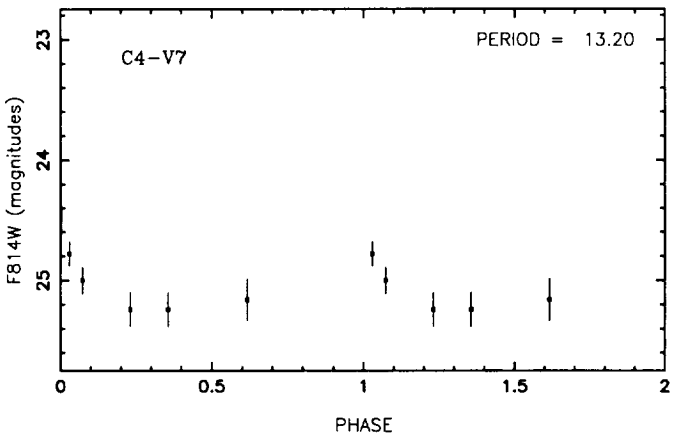
C4-V7
PERIOD = 13.20
F814W (magnitudes)
PHASE

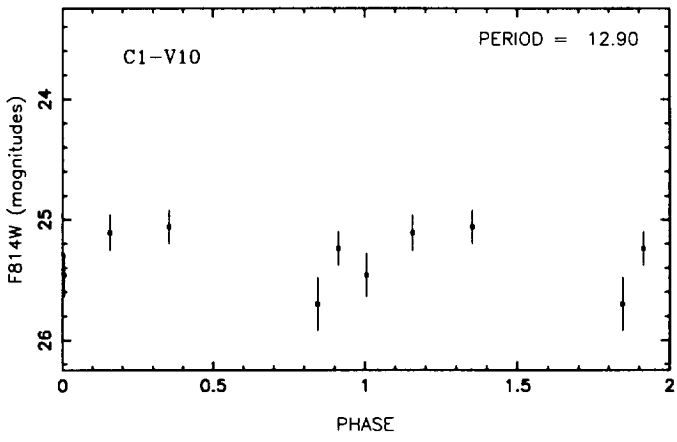
C1-V10
PERIOD = 12.90
F814W (magnitudes)
PHASE

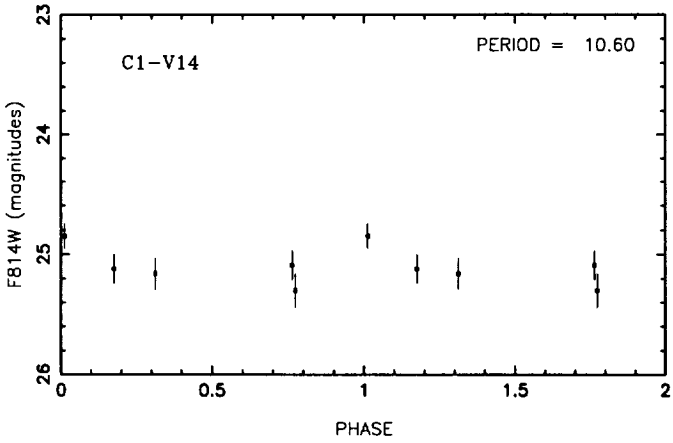
C1-V14
PERIOD = 10.60
F814W (magnitudes)
PHASE

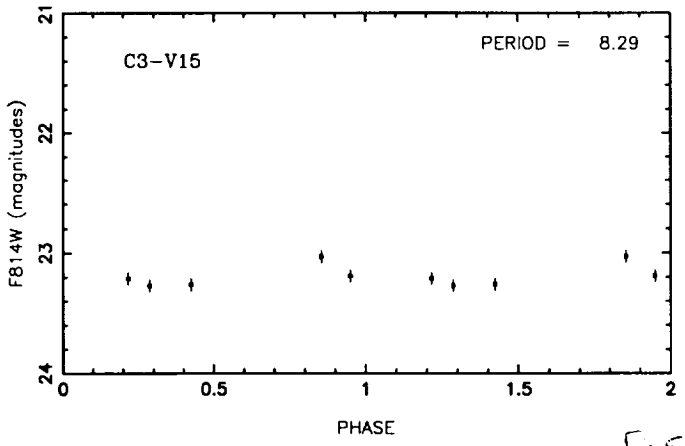
C3-V15
PERIOD = 8.29
F814W (magnitudes)
PHASE

Fig 5.9

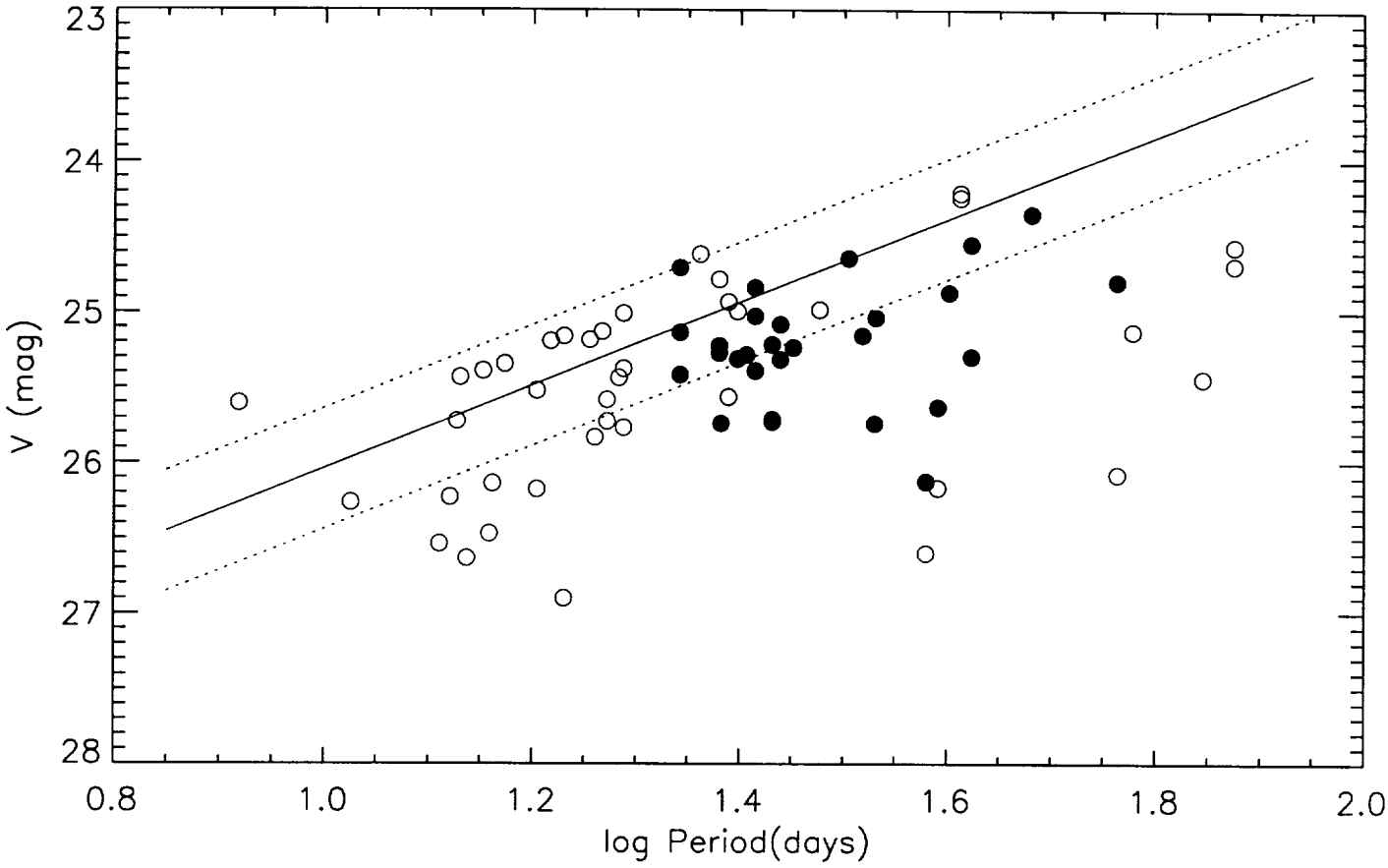
23
24
25
26
27
28
V (mag)
0.8
1.0
1.2
1.4
1.6
1.8
2.0
log Period(days)

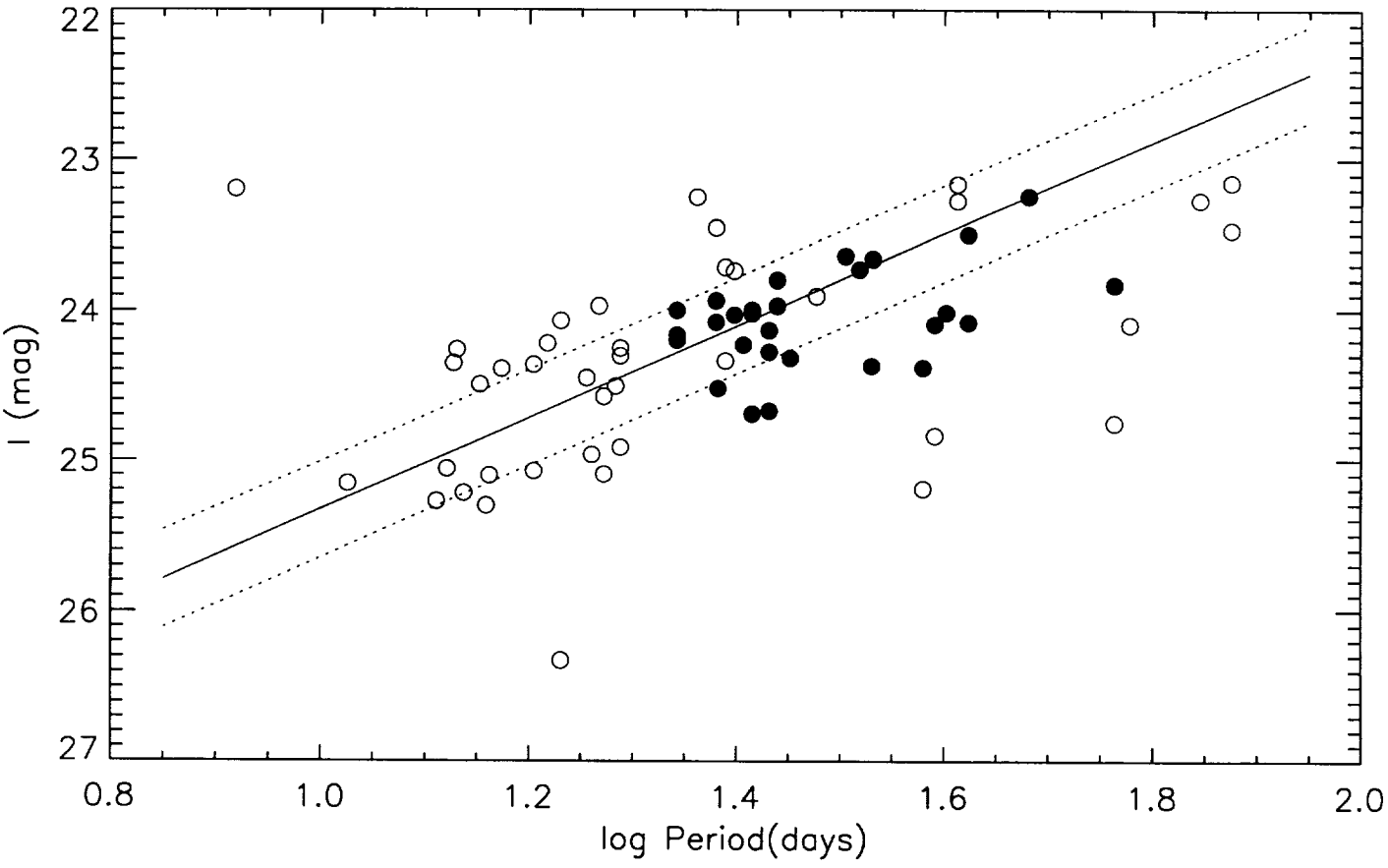
22
23
24
25
26
27
I (mag)
0.8
1.0
1.2
1.4
1.6
1.8
2.0
log Period(days)

Fig 6

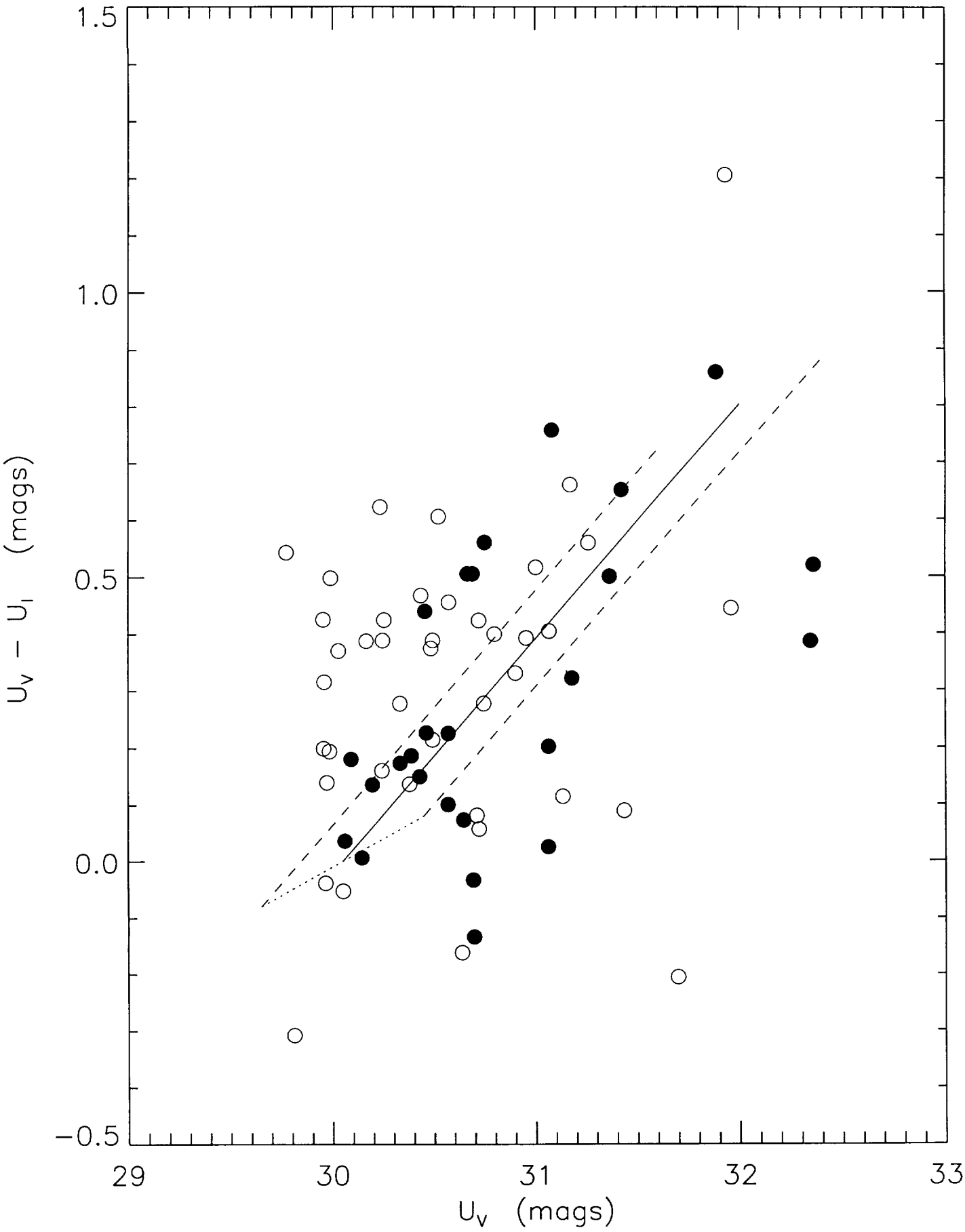

Fig 7

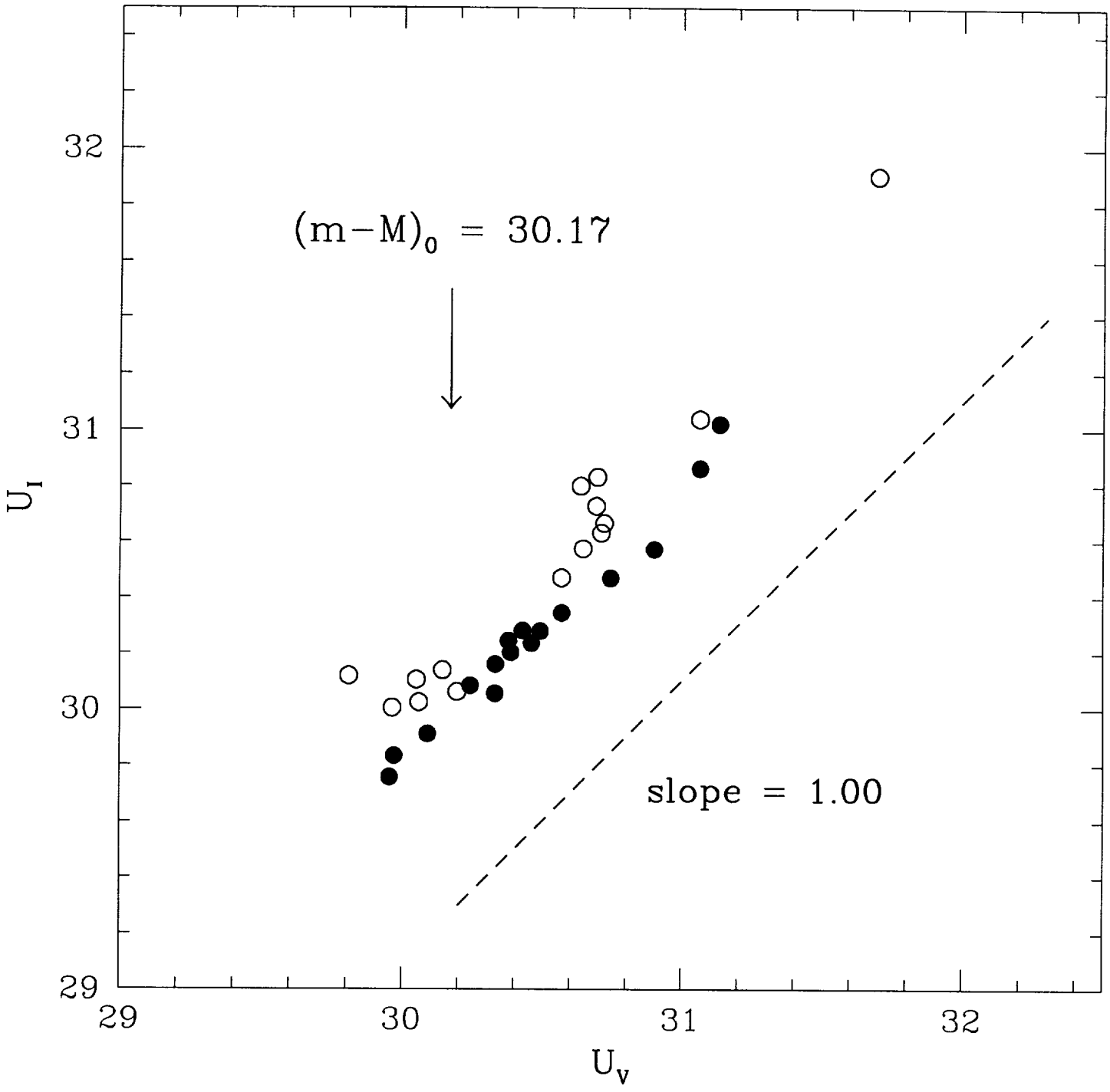

Fig 8

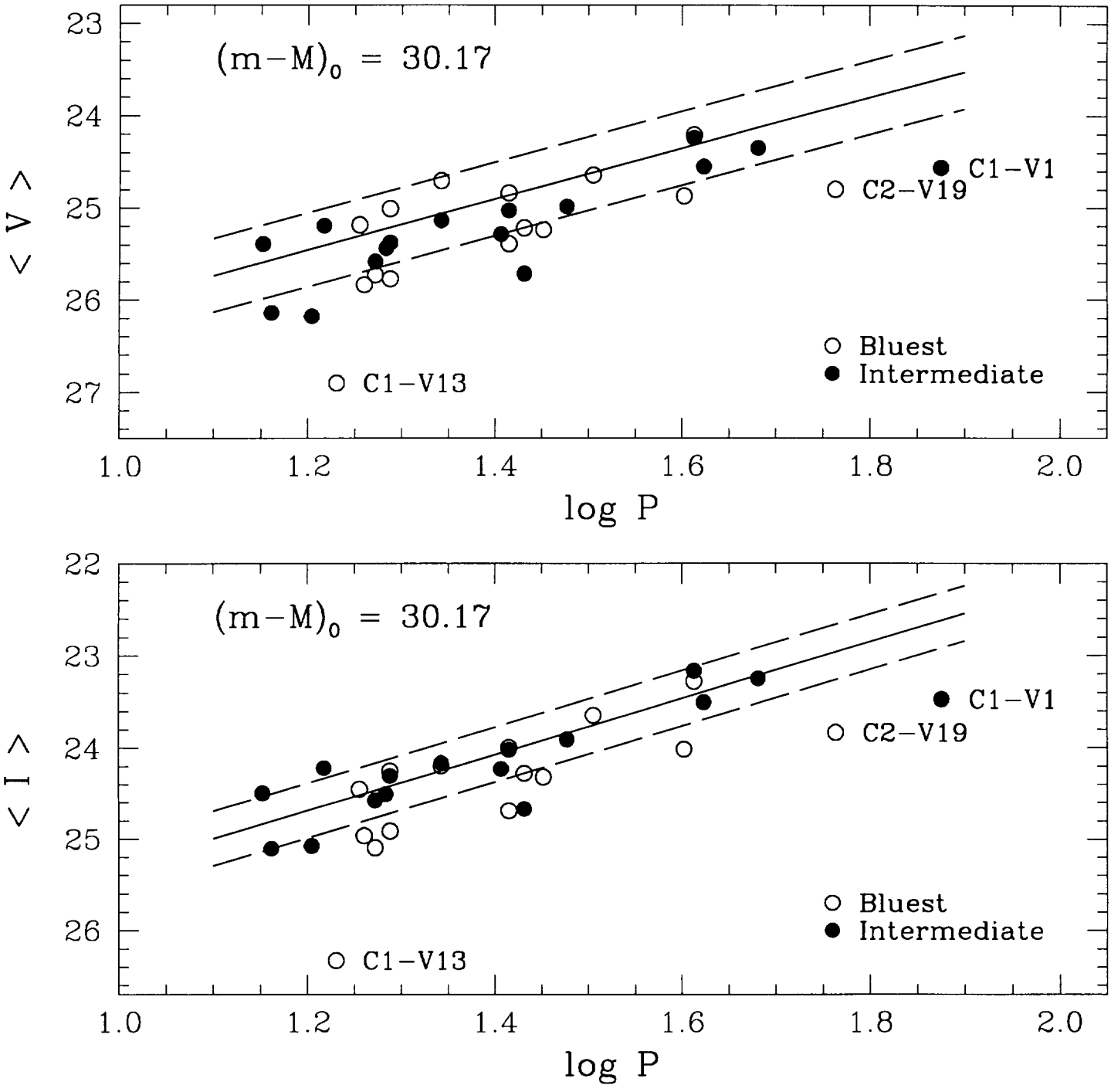
(m−M)$_0$ = 30.17
C1−V1
C2−V19
C1−V13
Bluest
Intermediate
< V >
log P
(m−M)$_0$ = 30.17
C1−V1
C2−V19
C1−V13
Bluest
Intermediate
< I >
log P

Fig 9

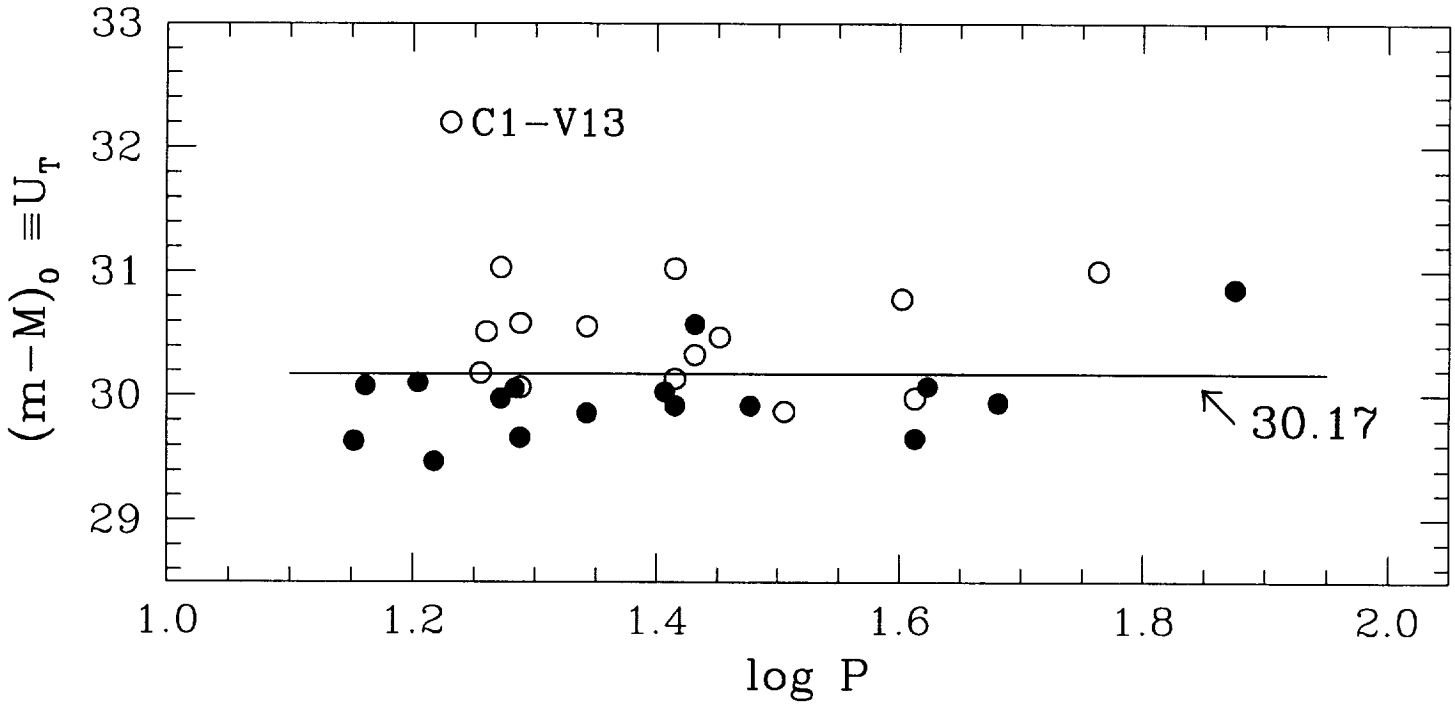

Fig 10

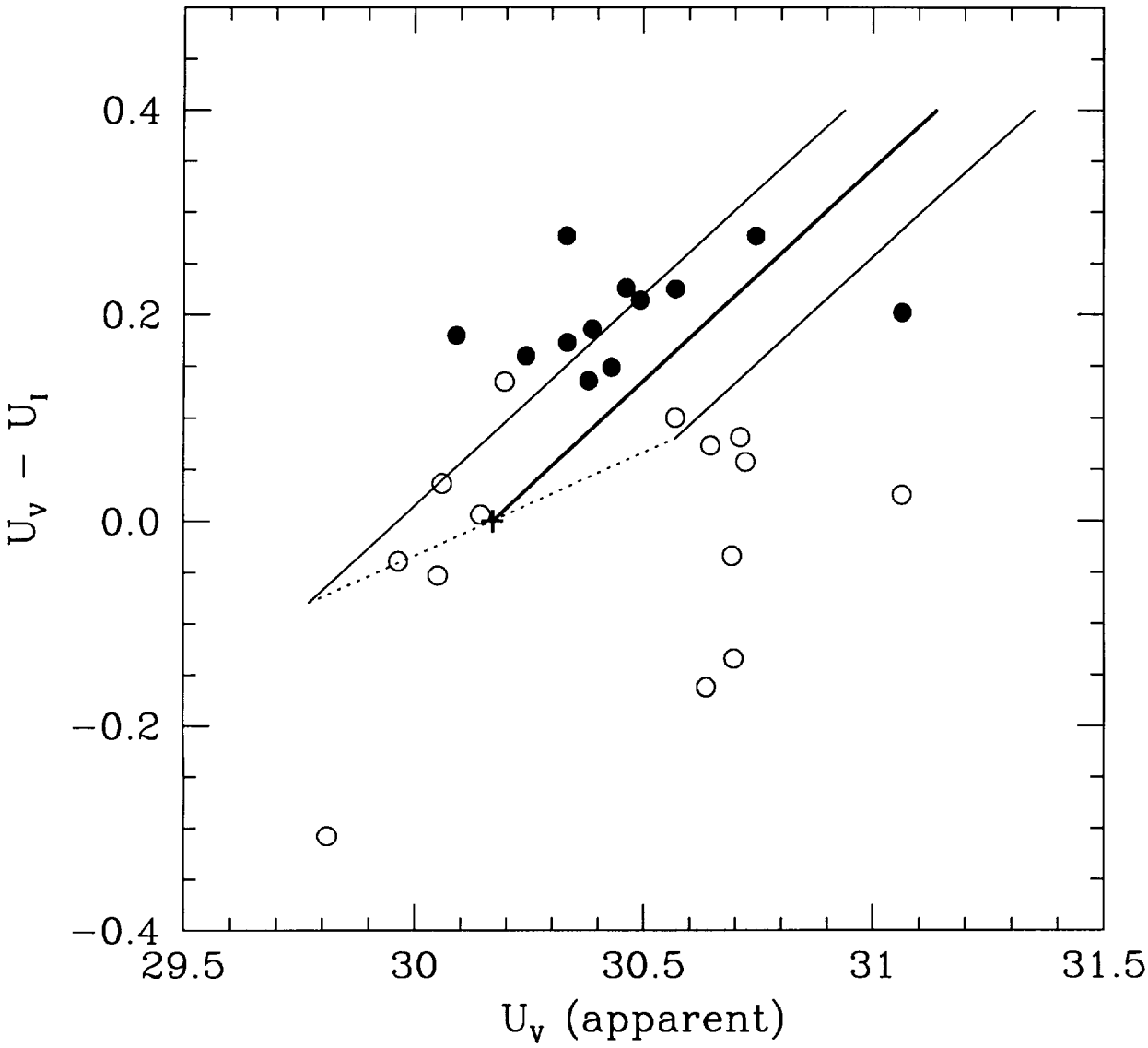

Fig 11

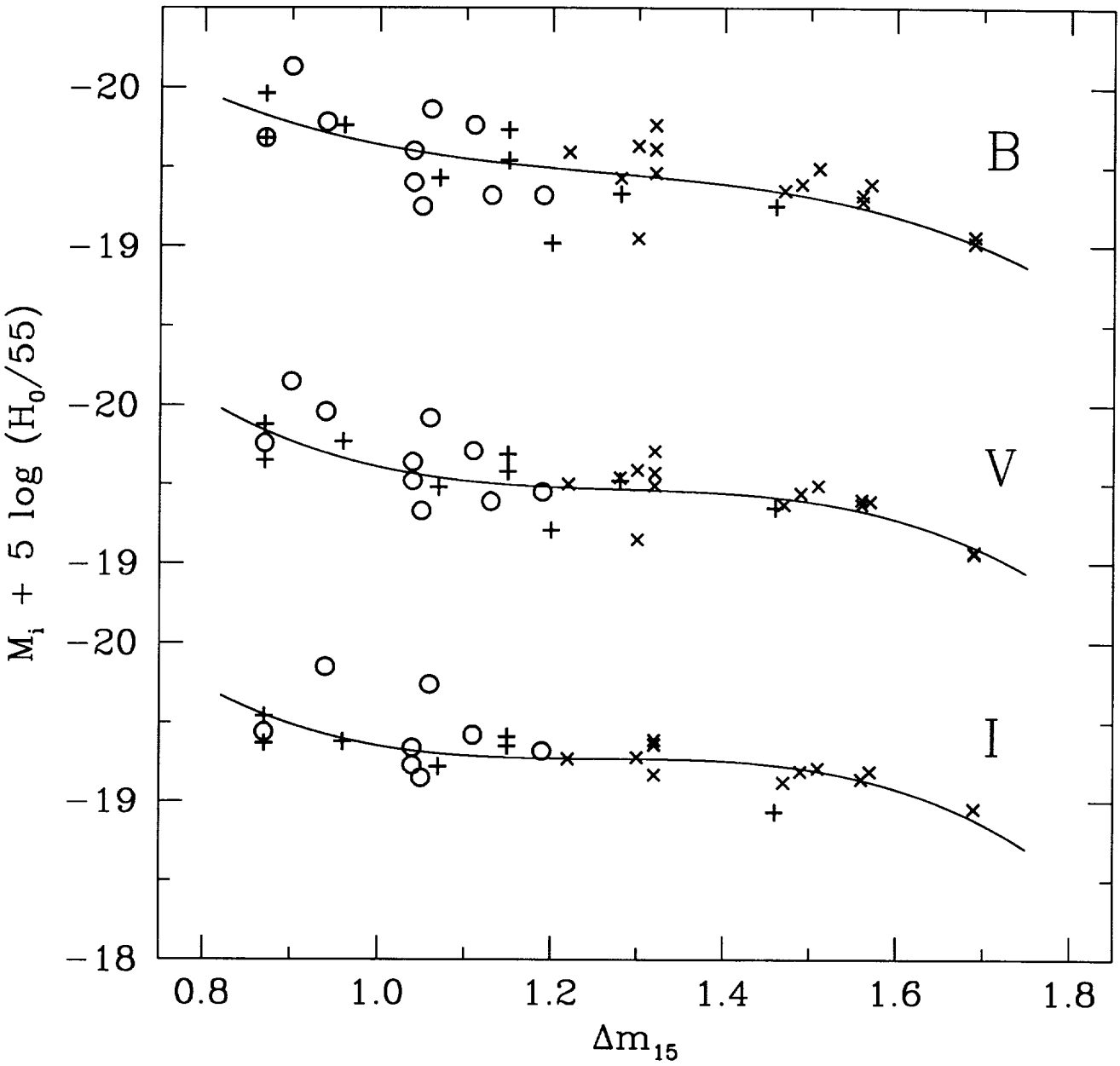

Fig 12

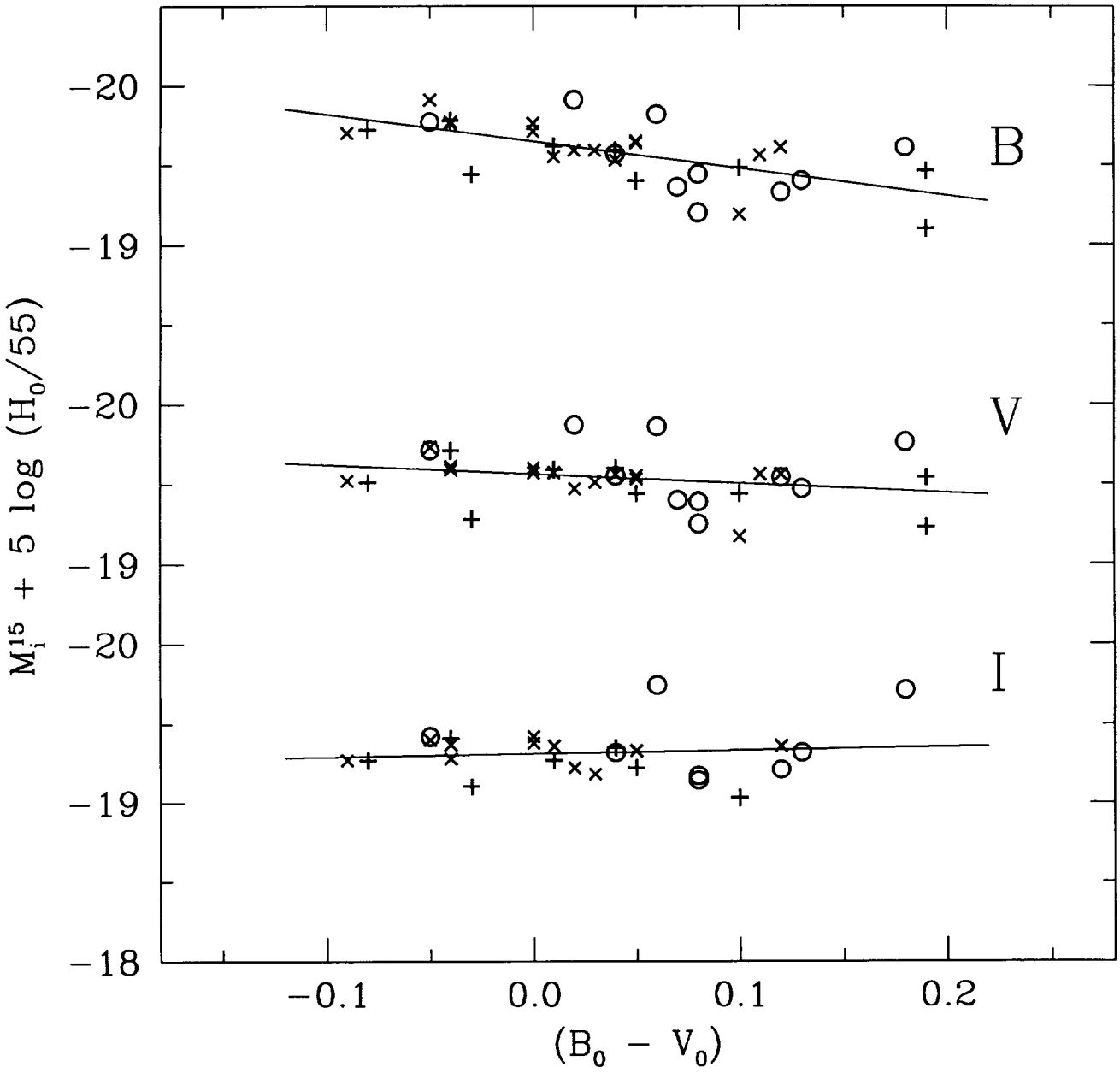

Fig13

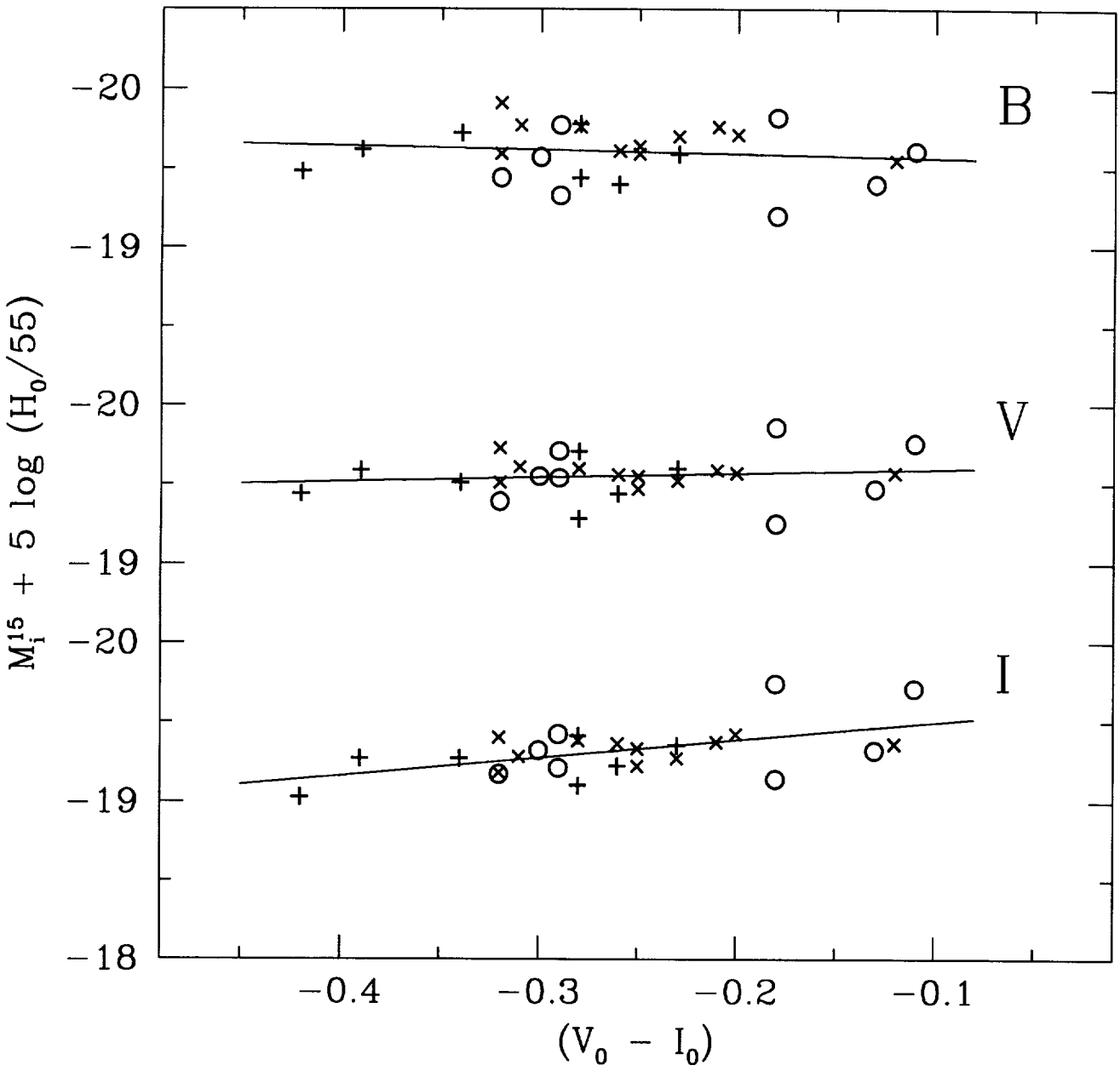

Fig 14